REPORT DOCUMENTATION PAGE

Form Approved
OMB No. 0704-0188

1. AGENCY USE ONLY (Leave Blank)	2. REPORT DATE	3. REPORT TYPE AND DATES COVERED
	1995	Final

4. TITLE AND SUBTITLE
A Study in the Interfacial Stability of Ti/Al203, Ti3Al/Al203 and TiAl/Al203 Composite Materials

5. FUNDING NUMBERS

6. AUTHORS
Joel Alan DeKock

AFRL-SR-BL-TR-98-

7. PERFORMING ORGANIZATION NAME(S) AND ADDRESS(ES)
University of Wisconsin - Madison

0009

N

9. SPONSORING/MONITORING AGENCY NAME(S) AND ADDRESS(ES)
AFOSR/NI
110 Duncan Avenue, Room B-115
Bolling Air Force Base, DC 20332-8080

10. SPONSORING/MONITORING AGENCY REPORT NUMBER

11. SUPPLEMENTARY NOTES

12a. DISTRIBUTION AVAILABILITY STATEMENT
Approved for Public Release

12b. DISTRIBUTION CODE

13. ABSTRACT *(Maximum 200 words)*
See attached.

19980115 226

14. SUBJECT TERMS

15. NUMBER OF PAGES

16. PRICE CODE

17. SECURITY CLASSIFICATION OF REPORT	18. SECURITY CLASSIFICATION OF THIS PAGE	19. SECURITY CLASSIFICATION OF ABSTRACT	20. LIMITATION OF ABSTRACT
Unclassified	Unclassified	Unclassified	UL

A STUDY OF THE INTERFACIAL STABILITY OF Ti/Al_2O_3, Ti_3Al/Al_2O_3 AND $TiAl/Al_2O_3$ COMPOSITE MATERIALS

by

Joel Alan DeKock

A dissertation submitted in partial fulfillment of the requirements for the degree of

Doctor of Philosophy
(Metallurgical Engineering)

at the

UNIVERSITY OF WISCONSIN - MADISON

1995

TABLE OF CONTENTS

ACKOWLEDGMENTS

The author expresses his sincere appreciation to Professor Y. Austin Chang, for the liberty, patience and support he extended throughout the course of this investigation.

Foremost, I thank my dear wife Nina for her support and patience which extends beyond reason, I dedicate this work to you and our son Walter. I also thank my colleagues at the UW-Madison, Chuck Florey, Bill Whealon, Dave Slezewski, Robert Kao and Ann Bolcavage, for their contributions to this work and my general self over the years.

The author wishes to acknowledge the financial support of ARPA through ONR Contract No. N-000-14-92-1863, and the USAF through UES for the Fellowship grant which permitted my return to school. He also wishes to thank Mr. W. Barker of ARPA for his interest in this work.

ABSTRACT

This thesis is a study of the interfacial stability of the Ti-Base metal matrix composites Ti/Al_2O_3, Ti_3Al/Al_2O_3 and $TiAl/Al_2O_3$. Interfacial stability is discussed in view of the importance of thermodynamics and kinetics as the primary considerations which govern the type of stability observed. From a thermodynamics approach, the application of phase equilibrium diagrams is essential in the design of composite systems. A classification system, with reference to phase equilibrium, is used to describe the type of interfacial stability observed for the composites studied. In addition, electron-probe microanalysis, atom-probe field ion microscopy and X-ray diffraction results are used to establish Ti-Al-O phase relations for the temperature range 900-to-1250°C. The kinetics of interfacial stability is discussed with particular attention given to the kinetic considerations; diffusion path, phase formation sequence, steady-state layer growth and interface morphology. Kinetic results in the form of parabolic growth constants and calculated interdiffusion coefficients are presented.

Each of the composite systems studied exhibited some degree of interfacial instability. The composite systems Ti/Al_2O_3 and Ti_3Al/Al_2O_3 exhibited Class III type interfaces, characterized by the diffusion paths β-Ti|α-Ti|Ti_3Al|TiAl|Al_2O_3 and Ti_3Al|TiAl|Al_2O_3, respectively. The $TiAl/Al_2O_3$ system exhibited a Class II type interface, characterized by mutual solubility at the interface. The interfacial reactions observed between the Ti-Base matrices and Al_2O_3 show a strong parabolic rate tendency, indicating diffusion control of reactions at the interfaces. These results are consistent over the entire 900-to-1250°C temperature range studied.

1.0 INTRODUCTION

The idea of combining two or more materials to produce a single composite material is not new. Knowingly, or not, man and animals have used mud/grass composites to build shelters throughout time. Today's common composite vary greatly, from the concrete we use for highways and buildings to the polymer/boron composites used in many of our sporting goods. The majority of these more common composites are best suited for use at relatively low temperatures. A need for light weight metallic materials, which are suited for applications wherein temperatures as high as 1000°C are reached, has been the motivation in the development of a class of materials know as metal matrix composites (MMC's).

In developing viable composites, attention must be given to the properties required of the individual materials which make up a composite system. A number of basic quantities are seen as indicators of the properties demanded of high temperature materials. These properties include high specific strength, high specific stiffness, low creep and low thermal expansion. The basic quantities which have been found to aid in choosing materials which may have these properties are melting temperature, specific gravity and elastic modules. In general, as the melting temperature of material increases, strength and stiffness tend to increase, whereas creep and thermal expansion tend to decrease. Since weight is an important factor, specific gravity is a major consideration. Since both the melting temperature and the specific gravity of materials are readily available, it is possible to evaluate the relative potential of a material for high-temperature use by considering the ratio melting temperature:specific gravity (T_m/ρ). Table 1 lists the melting temperature vs. specific gravity ratio of various high temperature materials and that of several Ti-base

MMC's. Ductility and oxidation resistance are also properties required of high-temperature materials. However, there are no simple indicators available to estimate these properties.

High Temperature Material	T_m/ρ [K·cm^3/gm]
Cobalt-Base Superalloys (S-816,V-36, Haynes Alloy 21™ and Mar M 302)	172 - 195
Heat Resistant Alloys (HA, HC, HD, HE, HF, HH, HI, HK and HL)	213 - 235
High Temperature Steels (1415 NW, 1430 MV and 17-22 AS)	220 - 225
Nickel-Base Superalloys (Inconel 751™, Udimet 700™, Hastelloy X™ and Rene-41)	186-202
Ti-Base/Al2O3 Composites* (Ti 99.0, Ti-5Al-2.5Sn, Ti-6Al-4V and Ti-8Mn)	393 - 448

Table 1. T_m/ρ for various high temperature materials. *Based on T_m of matrix and Al_2O_3 volume fraction of 0.30.

Metal matrix composites have the potential to compete with monolithic materials, such as the nickel-base superalloys, as high-temperature structural materials. In competing with monolithic materials, composites must be economical in addition to being mechanically competitive. Since MMC's are more expensive to prepare and process than monolithic materials, they have received major consideration for applications where the cost of the material is less of a factor than its potential performance, such as aerospace applications. Much of the recent research into developing light-weight high temperature MMC's has considered the utilization of SiC or Al_2O_3 fibers as reinforcements. Although both of these reinforcement materials are attractive, tow-base Al_2O_3 fibers are the least expensive reinforcement currently available.

One area of study that has often been overlooked in the many mechanical evaluations of composite materials is the chemical compatibility between the various materials used to fabricate a composite . Whether a material is utilized as a matrix or reinforcement, its compatibility at the interface between it and the other matrix or reinforcement materials can significantly affect the mechanical properties of a composite material. If the interfaces in composite materials are not stable, it is reasonable to assume that the mechanical properties of the composite will change also. This study is concerned with the chemical stability of interfaces in MMC's, and in particular the interfacial stability between Ti-base matrices and Al_2O_3 reinforcements.

The physical and chemical properties of potential matrix and reinforcement materials are fairly well established. However, how these materials will behave at an interface in composite form has not been studied extensively. Interactions between the matrix and the reinforcement materials in a composite will occur at the interfaces between the two, and can determine if a composite will be able to function successfully at high temperatures. The importance of the interfaces to the ability of composites to function at high temperatures has lead to this investigation of the thermodynamic and kinetic stabilities of these interfaces. This is the general theme of this work.

1.1 INTERFACE: A DEFINITION

To study the thermodynamic stability of interfaces in a composite, it is necessary to first establish a working definition for the interface. In 1968, Salkind [68Sal] came to the conclusion that "a precise definition of the interface is beyond our present knowledge." At that point in time, a useful composite interface implied an interface between two phases which wet each other. In 1974, Metcalfe [74Met] summarized much of the work in the

area of metal matrix composites and proposed the following definition for a composite interface, which is adopted for this study.

"An interface is the region of significantly changed chemical composition that constitutes the bond between the matrix and the reinforcement for the transfer of loads between these members of the composite structure."

Metcalfe points out that the use of the phrase "significantly changed chemical composition" in this definition excludes random fluctuations in compositions but includes all systematic changes required from thermodynamics (e.g. solution, segregation, adsorption and reaction). This study considers those interfaces that are formed as a result of the synthesis of composites in the solid state.

1.2 INTERFACE CONSIDERATIONS

From this definition for the interface it is now know what an interface is, and what its role is. To systematically approach this study of composite interfaces from a chemical stability point of view, the following three interface considerations are addressed. First, a classification system is introduced to identify clearly the types of stability exhibited at composite interfaces. Second, a system to evaluate the stability of composite interfaces is presented to help understand why a given class of interface is observed in a particular composite. Third, motivated primarily by the desire to design stable interfaces in composites, a brief discussion of the control of interfacial stability is presented.

1.2.1 Classification of Composite Interfaces

In an examination into the different types of interfaces observed in metal matrix composites, Petrasek and Weeton [64Pet] noted three interface types. These interfaces included: those interfaces which exhibited recrystallization at the periphery of the reinforcement, those interfaces where a new phase(s) formed at the interface, and those interfaces where mutual solution occurs between the matrix and the filament. Metcalfe [74Met] expanded on the results of Petrasek and Weeton, and formally proposed the following system for the classification of interfaces in metal matrix composites.

Class I: Filament (reinforcement) and matrix are mutually non-reactive and insoluble.
Class II: Filament (reinforcement) and matrix are mutually non-reactive, but soluble.
Class III: Filament (reinforcement) and matrix are reactive, and form a new compound(s) at the interface.

Although it was not explicitly stated by Metcalfe, it is assumed that a Class III interface may also exhibit solubility in the matrix or reinforcement. This classification system is useful for this study because it describes all interfaces characteristic of metal matrix composites, and it does so in a manner which is consistent with thermodynamic phase equilibrium.

From a thermodynamics approach, this classification system can be illustrated using the hypothetical binary phase equilibrium diagram shown in Fig. 1. It is assumed that the materials (A), (AB) and (B) are initially single phase materials when used in the synthesis of the hypothetical composites which follow. A Class I type composite interface is illustrated by a composite of materials (A) and (AB), of compositions 1 and 2

respectively. This composite will exhibit Class I interfaces only at temperature T_I, since this is the only temperature at which these materials are stable thermodynamically. At T_I, this composite exhibits local equilibrium at the interface between the phases (A) and (AB), since the compositions of (A) and (AB) are representative of two-phase equilibrium at T_I. Therefore, there would be no driving force to cause this system to react chemically at the interface.

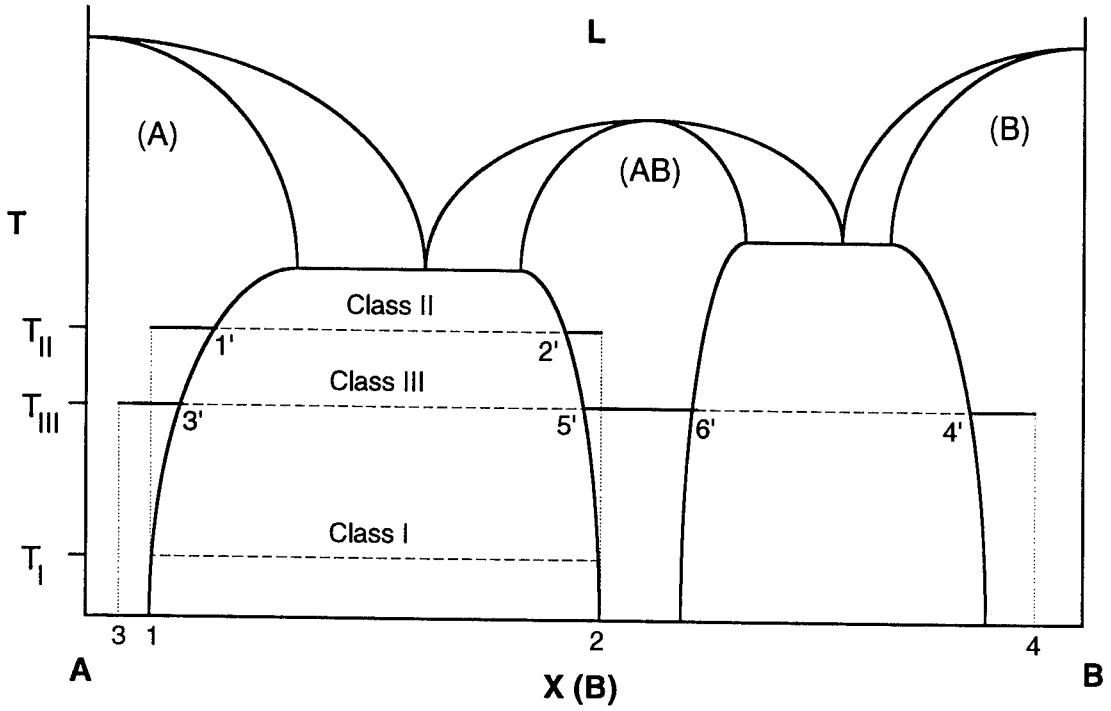

Figure 1. Hypothetical A-B binary phase equilibria diagram.

If this same composite system is heated to the temperature T_{II}, this system will no longer exhibit Class I type interfaces, but will instead exhibit Class II type interfaces. This is a result of phases (A) and (AB) not having compositions which are required of two-phase equilibrium at temperature T_{II}, and the system reacting accordingly in order to maintain local equilibrium at the interface. At temperature T_{II}, mutual solubility occurs

between phases (A) and (AB), of compositions 1 and 2 respectively. In order to maintain local equilibrium at the interface, phases (A) and (AB) will react such that their compositions at the interface are maintained a 1' and 2', respectively. It is noteworthy to point out that this mutual solubility will continue until phases (A) and (AB) are homogeneous solutions of compositions 1' and 2', respectively, and at a rate which is dependent upon the kinetics of this reaction. A Class III composite interface is characteristic of the reaction which would occur between phases (A) and (B), of Fig. 1. If a composite of phases (A) and (B), of compositions 3 and 4 respectively, is heated to temperature T_{III}, the system will react at the interface to form the phase (AB). The phase (AB) will exhibit a concentration gradient across its width in order to maintain local equilibrium at both the (A)|(AB) and (AB)|(B) interfaces, with the compositions of the phases on either side of these interfaces being 3'|5' and 6'|4', respectively. If this system is maintained at T_{III}, this composite of Class III type interfaces will continue to react until equilibrium is attained throughout the system. Although this illustration of the three classes of interfaces in composites was presented using a binary system, a similar approach can be used for ternary and higher-order systems.

Before proceeding with a discussion of the evaluation of interface stability, it is necessary to mention what is considered a 'stable' or 'steady-state' interface in this study. Thermodynamics defines what will be the equilibrium state of a system at a given pressure, temperature and composition. Kinetics describes how a system responds in order to attain thermodynamic equilibrium. From the viewpoint of this study, a 'stable' interface can be classified according to the classification system presented above, and a 'steady-state' interface is one which shows no change in classification, configuration of phases and interfacial composition with time at constant temperature.

1.2.2 Evaluation of Interfacial Stability

The evaluation of interfacial stability could be limited to identifying to which class an interface belongs. However, this would limit our understanding of why these different classes exist and how they develop, and would ignore the important thermodynamic and kinetic information which an interface can provide. From the preceding discussion of interface classification, it is clear that from an engineering point of view only Class II and Class III interfaces are likely to exist in metal matrix composites. Composites which would exhibit only Class I interfaces belong to a very restrictive class of composites, in that the materials necessary to produce such composite materials must exhibit two-phase equilibria over a wide range of temperatures and at fixed stoichiometry. This would essentially require the use of intermetallic compounds, which generally have very poor low-temperature engineering properties.

The evaluation of Class II and Class III interfaces can be accomplished successfully by identifying the phases which form at the matrix/reinforcement interface, measuring the steady-state rate at which these phases grow, and by determining the composition distribution across the interface. Knowing the composition distribution across the interface, or what would be a series of interfaces for Class III, provides thermodynamic data useful in establishing phase relations and phase solubility limits. Whereas, phase growth and composition data can be used to identify the kinetic process which controls the rate of the reaction between the matrix and the reinforcement. This kinetic data may be useful in estimating the expected service life of a composite material.

The kinetics of reactions between two solid materials can be dependent upon a combination of the two kinetic processes: interface reaction kinetics, and diffusion reaction kinetics. Usually only one of these kinetic processes will control the rate at which the steady-state reaction occurs at Class II and Class III interfaces. The first kinetic process, interface reaction kinetics, involves the rearrangement of the atoms at an interface for the growth of a new phase and may involve a reaction barrier of some type. Whereas the second kinetic process, diffusion reaction kinetics, involves the diffusion of matter, where the diffusion flux slows down with increasing layer thickness. The determination of which of these processes is rate limiting for a steady-state reaction can be accomplished by determining the change in reaction product (layer) width with time, and the composition of the phases adjacent to the interface. If an interfacial reaction barrier controls the kinetics of a reaction, layer thickness will increase linearly with time and the compositions adjacent to the interfaces will not correspond to those required for local thermodynamic equilibrium. If diffusion controls the kinetics of a reaction, layer thickness will increase proportionally to the square root of time, and the compositions adjacent to the interfaces will represent local thermodynamic equilibrium.

It is typical for solid-state reactions to be diffusion controlled, and thus exhibit layer growth which is a function of the square root of time. Therefore, diffusion controlled kinetic growth at an interface can be confirmed by a plot of W vs. $(t)^{1/2}$, where W is the layer thickness and t is time. Pieraggi [87Pie] points out that this is the preferred method of plotting parabolic type growth because it permits the direct determination of the parabolic growth constant. In addition, knowing that an interfacial reaction is diffusion controlled allows us to use diffusion theory to determine the rate

controlling step in the diffusion process. It will be shown in a latter section of this paper that the rate controlling step can be identified by determining the interdiffusion process.

The evaluation of Class II and Class III interfaces in the manner presented here is important because it enables one to identify what the reaction rate controlling process is in the steady-state growth of the interfaces. If the reaction at an interface is found to be diffusion controlled, it is possible to use the information gathered during the evaluation of an interface to establish thermodynamic phase equilibria, and to determine the necessary kinetic information needed to describe the diffusion process.

1.2.3 Control of Interfacial Reactions

Because of the importance of the interface between the matrix and the reinforcement materials in MMC's, it is desirable to control any reaction which may occur at the interface. One extreme in controlling interfacial reactions is to design composites with Class I interfaces. However, it was pointed out earlier that a non-reactive composite of this type is not practical. A second extreme in controlling interfacial reactions is to limit the use composites with Class II and Class III interfaces at lower temperatures, since it is well known that the kinetics of a reaction tends to slow with decreasing temperature. This extreme is contradictory to the need for metal matrix composites which can be used at high temperatures. Current practice in the design of composites which exhibit controll of interfacial reactions, is to use reinforcements which have been coated to prevent interaction between the matrix and the reinforcement. Such coatings are intended to serve as either inert barriers or barriers to diffusion. The inherent difficulties in this practice are the determination of coatings which are either thermodynamically or kinetically stable with

both the matrix and reinforcement, and the ability to produce a continuous coating free of defects.

The study of interfacial reaction control is a significant and complex area of study which is not discussed in any more detail here. A recent paper by Chang et al. [94Cha] illustrates the difficulty in identifying coating schemes for Ti-base/Al_2O_3 composites. It should be apparent that without thorough knowledge of the phase equilibria of ternary and higher order system, the current practice in controlling interfacial reactions is a trial and error process.

1.3 SCOPE OF THIS STUDY

The scope of this study is to evaluate the matrix/reinforcement interfacial stability of the metal matrix composites Ti/Al_2O_3, α_2-Ti_3Al/Al_2O_3 and γ-TiAl/Al_2O_3, over the temperature range 900-1250°C. The evaluation of these composite materials will include the classification of the steady-state interface type observed, the determination of the reaction rate for the interface class observed and the presentation of a theory explaining the steady-state diffusion controlled growth of the Class III interfaces observed in Ti/Al_2O_3 composites. In addition, Ti-Al-O ternary isothermal phase equilibrium are estimated for the temperature range 900-1250°C.

This study uses bulk-type diffusion couple samples of Ti/Al_2O_3, α_2-Ti_3Al/Al_2O_3 and γ-TiAl/Al_2O_3 to evaluate the interfacial stability of composites of these types. The diffusion couples are analyzed using the techniques of metallography and electron-probe microanalysis (EPMA) in order to obtain the necessary data to perform the evaluation described above. Other analytical procedures, including X-Ray Diffraction, Atom-Probe

Field Ion Microscopy and LECO Oxygen Determination, were also employed where necessary. In addition to these analytical techniques, diffusion theory is used to evaluate diffusion controlled reactions at the interface, where possible.

2.0 THERMODYNAMIC CONSIDERATIONS

The knowledge of thermodynamic phase equilibrium is extremely important in understanding the interfacial stability between the matrix and the reinforcement in metal matrix composites. Perhaps the best way to identify viable composite materials is to consult the phase diagram of the system in question. However, such phase equilibrium diagrams are rarely available for ternary, or higher order systems. Because ternary phase equilibria are not well established for the system Ti-Al-O, it is necessary to evaluate both the available constituent binary and ternary phase equilibium diagrams for this system and results from interfacial reactions in order to estimate phase equilibria at the ternary level. This section looks at the thermodynamic data available which can be used to understand the interfacial stability of Ti/Al_2O_3, α_2-Ti_3Al/Al_2O_3 and γ-$TiAl/Al_2O_3$ composite materials, and to estimate phase equilibria for the Ti-Al-O system in the 900-1250° temperature range.

2.1 Al-O BINARY PHASE EQUILIBRIA

The study of phase equilibria for the binary system Al-O has been summarized by Wriedt [85Wri]. The phase equilibria diagram presented by Wriedt is shown in Fig. 2. The crystal structure data for the phases in the Al-O system is given in Tab. 2. The phases of engineering importance in this system are fcc-(Al) and α-Al_2O_3. Fcc-(Al) is a terminal solid solution with negligible oxygen solubility. It is believed that a eutectic reaction occurs at 660°C and 3×10^{-8} at.% O. Pure Al melts at 660.452°C. Trigonal α-Al_2O_3 (α-alumina, sapphire, or corundum) is one of several identified polymorphs of the same composition. α-Al_2O_3 is the more stable form of alumina, and is stable to its melting point of 2054°C. α-alumina is the only form of alumina considered in this study.

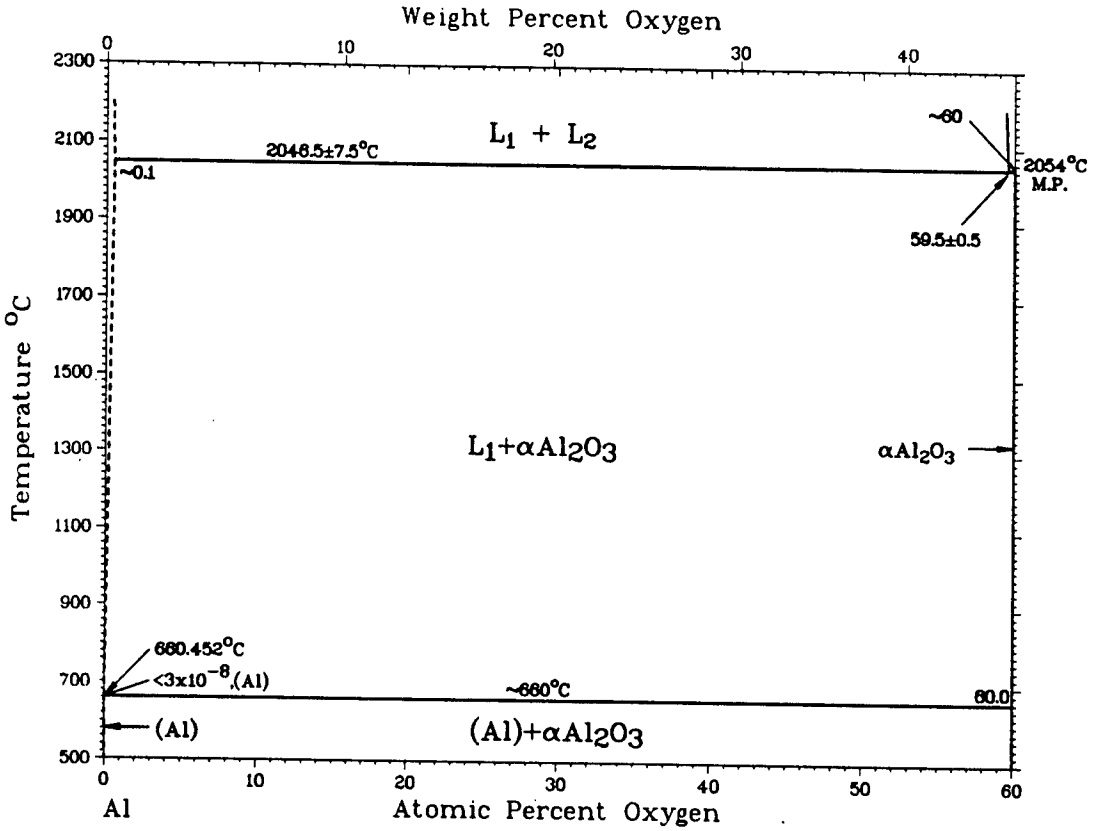

Figure 2. Al-O binary phase equilibrium diagram (from Wriedt [85Wri]).

2.2 Ti-O BINARY PHASE EQUILIBRIA

The study of phase equilibria for the binary system Ti-O has been summarized by Murray and Wriedt [87Mur]. The phase equilibrium diagram presented by Murray and Wriedt is shown in Fig. 3. The crystal structure data for the phases in the Al-O system is given in Tab. 2. The phases of engineering importance in this system are β-Ti and α-Ti, both of which exhibit extensive solubility of oxygen. Pure titanium is polymorphic, transforming from α-Ti to β-Ti upon heating at 882°C. β-Ti is stable to the melting point of titanium which is 1670°C. Oxygen has a maximum solubility in α-Ti of ~32 at.% in the range 600-940°C, and is an α-Ti stabilizer. TiO is of some interest in this study due to its

reported existence by Tressler et al. [73Tre] in Ti/Al_2O_3 diffusion couples. TiO is stable in a number of structures which have a wide range of stoichiometries. The β form of TiO is stable over the temperature range 900-1250°C.

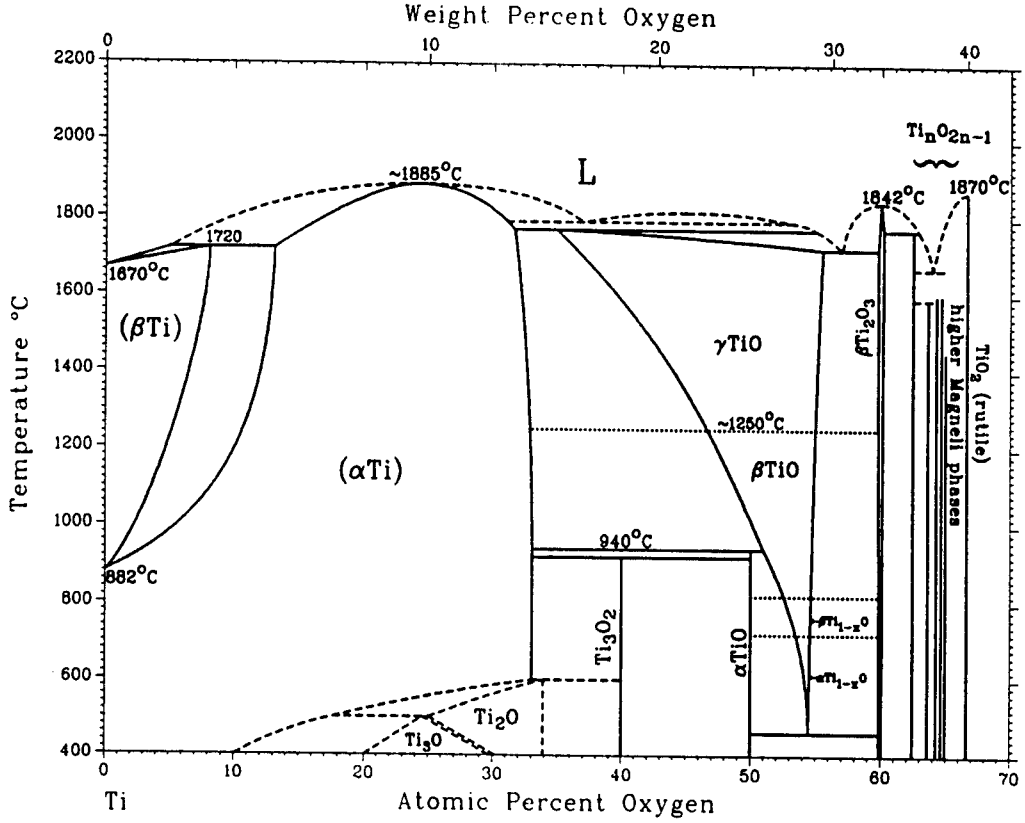

Figure 3. Ti-O binary phase equilibrium diagram (from Murray and Wriedt [87Mur]).

2.3 Ti-Al BINARY PHASE EQUILIBRIA

A considerable amount of work has been done on the determination of phase equilibria for the Ti-Al binary system. As a result, much of the phase equilibria is well established, except in the composition range 35 -to- 65 at.% Al above 1250°C. Due to discrepancies in this region, there are two versions of the Ti-Al phase diagram. One version [52Bum, 79Col, 86Mur] predicts β-Ti to be in equilibrium with γ-TiAl, whereas

the second version [61Enc, 87Val, 89Hua] predicts α-Ti to be in equilibrium with γ-TiAl. Recent work by Kattner et al. [92Kat] also predicts α-Ti to be in equilibrium with γ-TiAl, and is the version accepted for this study. The phase equilibrium diagram presented by Kattner et al. is shown in Fig. 4. The crystal structure data for the phases in the Ti-Al system is given in Tab. 2.

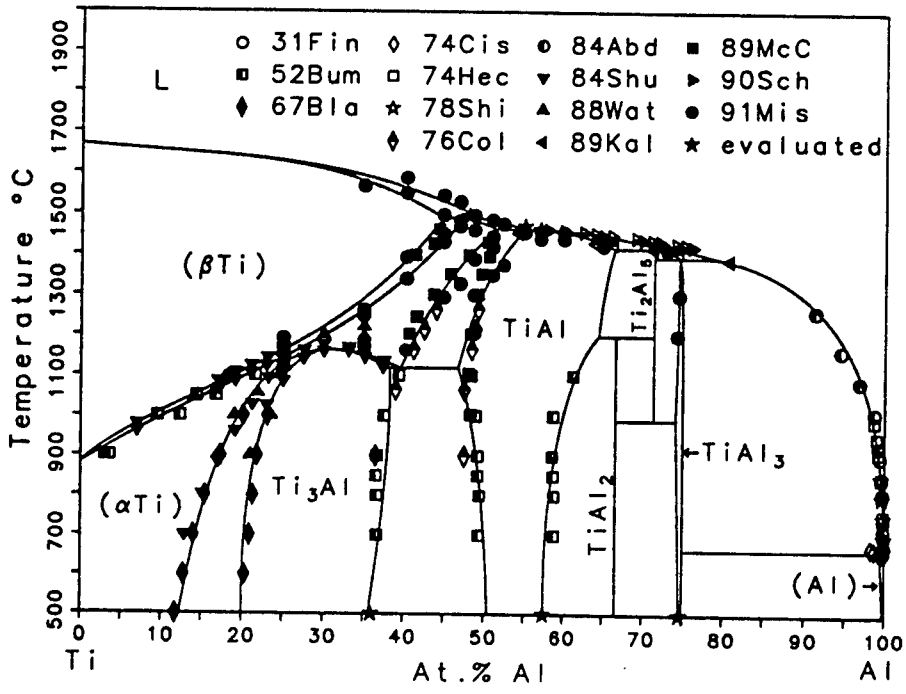

Figure 4. Ti-Al binary phase equlibrium diagram (from Kattner et al.[92Kat]).

The phases of engineering importance in this system are the disordered phases β-Ti and α-Ti, and the ordered intermetallic phases α_2-Ti_3Al and γ-TiAl. As shown by the phase diagram of Fig. 4., all four of these phases exhibit a relatively large range of stoichiometry. A notable feature of the Ti-Al diagram is the stabilizing effect of aluminum

on the α-Ti phase field. β-Ti exhibits a maximum solubility of ~45 at.% Al at 1490°C. α-Ti exhibits a maximum solubility of ~51 at.% Al at 1462°C, and decomposes peritectically at ~47 at.% Al. γ_2-Ti_3Al is stable to 1164°C, transforming from the ordered DO_{19} (hcp) structure to a disordered hcp structure at ~31 at.% Al. The γ-TiAl phase has the $L1_0$ (bct) structure, and has the highest temperature stability of any intermetallic phase in the Ti-Al system. γ-TiAl decomposes peritectically at ~55 at.% Al.

The intermetallic phases α_2-Ti_3Al and γ-TiAl are potential matrix materials for high-temperature metal matrix composites. Binary phase stability data, such as that given here, is important in the choosing of a proper matrix material for composites. For example, knowing that α_2-Ti_3Al has a maximum stability temperature of 1164°C, is a good indication that composites of this matrix material must be utilized well below this temperature. However, a composite utilizing γ-TiAl could possibly be used in excess of 1164°C.

2.4 Ti-Al-O TERNARY PHASE EQUILIBRIA

Several versions of Ti-Al-O phase equilibrium are available in the literature. The early versions presented Tressler et al. [73Tre] and DeKock et al. [90DeK] show major discrepancies in construction from later versions presented by van Loo et al. [92Li] and Zhang et al. [92Zha], and thus are probably in error. The versions by Tressler et al. estimated Ti-Al-O phase equilibria at 871°C based upon their experimental results, which may not have attained equilibrium. The version by DeKock et al. estimated Ti-Al-O phase equilibria at 1100°C based upon their calculated results, for which the thermodynamic data available is believed to be in error. The more recent versions of Ti-Al-O phase equilibrium by Li et al. and Zhang et al. are in good agreement with versions

of each other. Figure 5 shows the version by Li et al., and is based upon their results from diffusion couple samples. Although it is incomplete, Fig. 5 does represent the phase relationships of interest in this study of Ti/Al_2O_3, α_2-Ti_3Al/Al_2O_3 and γ-TiAl/Al_2O_3 metal matrix composites at 1100°C. It is important to mention that a ternary phase $Al_2Ti_7O_{15}$ is reported in the literature [88Rem], and noted in Tab. 2, but it does not influence on the phase relationships presented in Fig. 5.

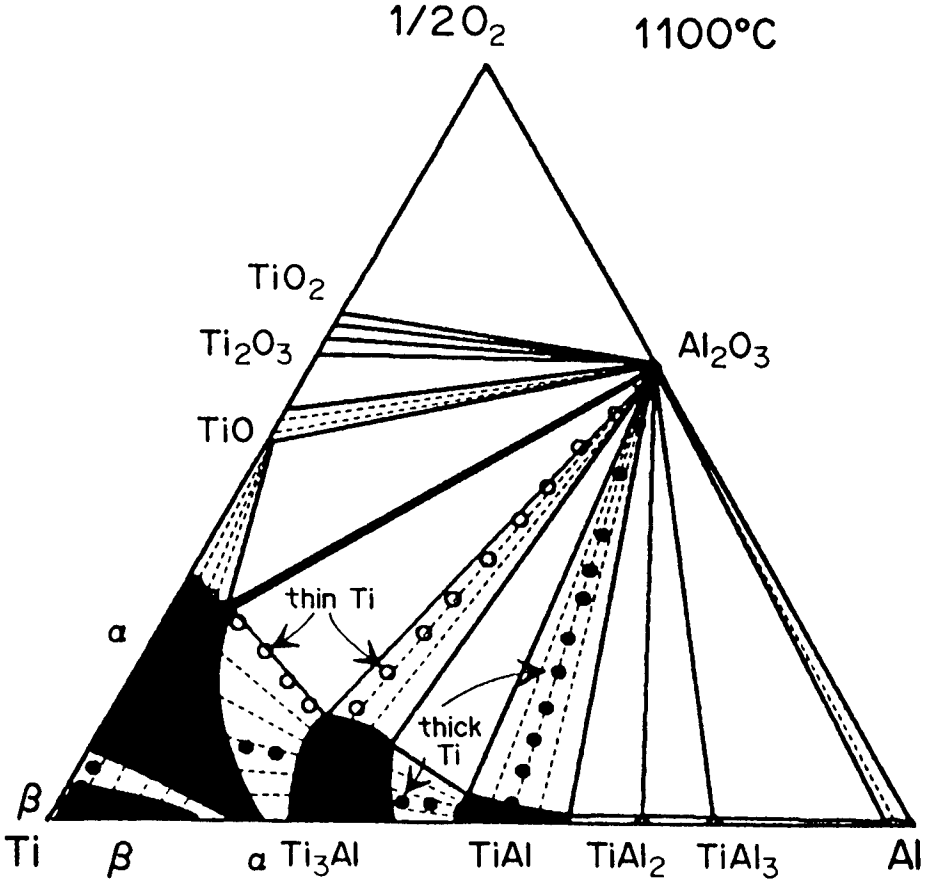

Figure 5. Ti-Al-O ternary phase equilibrium at 1100°C (from Li et al.).

Figure 5 is an important result for the determination of viable metal matrix composites based upon the Ti-Al-O system. Possible matrix materials which are thermodynamically stable with respect to Al_2O_3 at 1100°C are α-Ti, α_2-Ti_3Al and γ-

TiAl. However, the ternary solubility limits for these phases needs to be determined in order to avoid excessive interaction between these matrices and Al_2O_3. The results of this study should help to estimate more precisely what these solubility limits are.

System	Phase	Structure	Lattice Parameters (a, b, c in Å)	Reference
Al-O	(Al)	A1	a=4.0496	[85Wri]
	α-Al_2O_3	$D5_1$	a=5.1272, α=55°16.7'	[85Wri]
Ti-O	(β-Ti)	A2	-----	[87Mur]
	(α-Ti)	A3	-----	[87Mur]
	Ti_3O	$P31_c$	a=5.1411, c=9.5334	[87Mur]
	Ti_2O	P3m1	a=2.9593, c=4.8454	[87Mur]
	Ti_3O_2	P6/mmm	a=4.9915, c=2.8794	[87Mur]
	γ-TiO	B1	-----	[87Mur]
	β-TiO	(cubic)	12.54	[87Mur]
	α-TiO	A2/m	a=5.855, b=9.340, c=4.142, β=107.53°	[87Mur]
	β-Ti_2O_3	$D5_1$	-----	[87Mur]
	TiO_2 (rutile)	C4	a=4.594, b=2.959	[87Mur]
Ti-Al	α_2-Ti_3Al	DO_{19}	-----	[86Mur]
	γ-TiAl	$L1_0$	-----	[86Mur]
	Ti_2Al_5	-----	-----	[86Mur]
	$TiAl_2$	-----	-----	[86Mur]
	$TiAl_3$	DO_{22}	-----	[86Mur]
Ti-Al-O	$Al_2Ti_7O_{15}$	C2/m	a=17.67, b=2.973, c=9.358, β=98.66°	[88Rem]

Table 2. Crystal structure data for the systems Al-O, Ti-O, Ti-Al and Ti-Al-O.

3.0 KINETIC CONSIDERATIONS

If it can be shown that diffusion kinetics controls the rate of the interaction between the matrix and the reinforcement in a composite, then diffusion theory may be used to aid in identifying the rate controlling step in the diffusion process. The rate controlling step is identified by determining the diffusion behavior of each element at the interface of Ti/Al_2O_3, α_2-Ti_3Al/Al_2O_3 and γ-TiAl/Al_2O_3 composites. This section looks at the important kinetic considerations which must be understood in order explain why a given class of interface is observed in a specific composite material. The kinetic considerations discussed include the topics: 1) Diffusion path, 2) Phase formation sequence, 3) Steady-state layer growth, 4) Interface morphology and 5) Interdiffusion in Ti-Al-O composites.

3.1 DIFFUSION PATH

In simple terms for a given diffusion couple which has been annealed at a given temperature, a diffusion path maps the compositions and or phases which are in equilibrium. From the discussion of Class III type interfaces, it was shown that a composite of materials (A) and (B) would react to form a new phase (AB) between phases (A) and (B). For this composite the diffusion path is (A)|(AB)|(B).

To illustrate the complexity of the diffusion path in ternary systems, consider the hypothetical ternary system M-Al-O shown in Fig. 6. Although it is obvious that only one diffusion path is possible for binary couples, the same observation is not so obvious for a ternary couple. For example, consider the diffusion couple M/Al_2O_3 shown as a dashed line in Fig. 6. In keeping with the principle of mass balance, two of the several possible

diffusion paths are:

1) $M|M_3Al|MO|Al_2O_3$

2) $M|MO|MAl|Al_2O_3$.

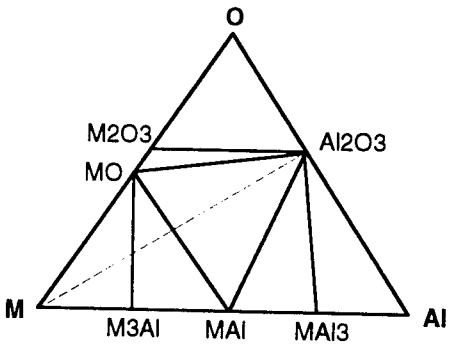

Figure 6. Hypothetical M-Al-O ternary isotherm.

Kirkaldy and Brown [63Kir] have developed a set of rules for the construction of diffusion paths on a ternary isothermal section. According to these rules, a specific ternary diffusion couple has only one diffusion path and that path can be determined if the kinetic and thermodynamic data are available. Experiments by van Loo and co-workers [80Lah, 83Vos, 84van] on metal/oxide and metal/sulfide systems have shown that these rules are effective in predicting diffusion paths. However, since kinetic data is not available for the Ti-Al-O system, it is necessary to determine diffusion paths experimentally.

It is important in the discussion of diffusion paths to mention that non-planar interfaces and two-phase regions are possible within multiphase ternary diffusion couples. This is a result of an additional thermodynamic degree of freedom from the Gibbs phase rule. Kirkaldy and Brown [63Kir] have taken this additional degree of freedom into account, and have developed the concept of a 'virtual' path to predict whether a diffusion

path will exhibit planar or non-planar interfaces, and/or two-phase regions. Clark [63Cla], utilizing the rules of Kirkaldy and Brown, conventionalized the illustration of diffusion paths on ternary isothermal diagrams.

Kinetic data is not available to predict the diffusion paths for Ti/Al_2O_3, α_2-Ti_3Al/Al_2O_3 and γ-$TiAl/Al_2O_3$ composites. However, knowing that there is only one diffusion path for each of these composites, and that this diffusion path may exhibit non-planar interfaces or two-phase regions, is important. The concept of a diffusion path is useful in understanding interfacial reaction kinetics.

3.2 PHASE FORMATION SEQUENCE

The diffusion path represented by a Class II or Class III composite interface is a kinetically stable arrangement of phases which is unique to a specific composite at constant temperature and pressure. Since the diffusion paths of Class II interfaces do not contain any matrix/reinforcement reaction product phases, this discussion of the sequence in which phases form is restricted to Class III interfaces. Although it may not be possible to precisely determine the phase formation sequence for a given system, Lin et al. [89Lin] have suggested some general considerations to follow when predicting the sequence in which phases form. Lin et al. [89Lin] and Schulz et al. [90Sch] have applied these ideas with some success on metal/GaAs systems.

To illustrate the methodology presented by Lin et al. [89Lin], we shall apply their method to the development of a phase sequence at the interface of a Ti/Al_2O_3 composite at 1100°C. From Fig. 5 it is clear that pure Ti and Al_2O_3 are not in equilibrium at 1100° C. Therefore, when a Ti/Al_2O_3 composite is heated to 1100°C the Ti matrix and the

Al_2O_3 reinforcement should react to produce a Class III interface. Since there is negligible solubility of Ti in Al_2O_3, this reaction may start with the dissolution of Al_2O_3 into the Ti matrix as elemental Al and O. The first phase to form in sequence is usually a ternary compound or a binary phase with extensive ternary solubility, and in this system that would be the α-Ti phase. At this point, the sequence β-Ti|α-Ti|Al_2O_3 is a possible steady-state sequence as indicated by Fig. 5. However, experience has shown that the steady-state diffusion path is actually β-Ti|α-Ti|α_2-Ti_3Al|γ-TiAl|Al_2O_3, thus the diffusion path β-Ti|α-Ti|Al_2O_3 is not kinetically favored. Continuing with the suggestions of Lin et al. [89Lin], to determine the next phase in the sequence it is necessary to note which of the remaining phases of Fig. 5 are favored thermodynamically and also have a composition close to that found at the interface α-Ti|Al_2O_3. The composition requirement is a kinetic consideration which takes in account the time necessary to redistribute the elements to nucleate the next phase. The phases TiO, Ti_2O_3, α_2-Ti_3Al, γ-TiAl, $TiAl_2$ and $TiAl_3$ all need to be considered. Excluding those phases which exhibit negligible solubility of either Al or O, leaves either α_2-Ti_3Al or γ-TiAl as the most likely phase to form next in our sequence. Since the γ-TiAl phase has a composition nearer to that of the α-Ti|Al_2O_3, it should be the next phase to form in sequence, leaving the α_2-Ti_3Al phase to be the last phase to form.

This illustration of the process in which a given sequence of phases may form ignores the possibility that other phases might form and be consumed during an initial transient period. If it had not been known that the γ-TiAl and α_2-Ti_3Al phases must be present in the sequence, it would have been logical to stop with the diffusion path β-Ti|α-Ti|Al_2O_3. It is not known if this is the actual phase formation sequence in achieving the

steady-state diffusion path observed at the interface of a Ti/Al_2O_3 composite. However, the methodology used here helps to identify a probable formation sequence.

3.3 STEADY-STATE LAYER GROWTH

To understand how diffusion controls the steady-state layer growth of Class III interfaces it is necessary to evaluate the interdiffusion behavior at the composite interfaces. Towards this goal, it is important to present some of the formalism for ternary diffusion in addition to presenting the means by which necessary quantities can be determined from C(X) plots. Ultimately, by making certain assumptions and by identifying the needed diffusion quantities, an argument can be presented which identifies how and why the steady-state reaction at Ti/Al_2O_3 interfaces is observed, and the rate at which this reaction continues. Three assumptions which are made at this time are: semi-infinite diffusion couples can be used to approximate the interfacial interaction between the matrix and reinforcement materials, the formation of phases in Class III interfaces occurs at an interface, and the partial molar volume change for the diffusing species is negligible upon mixing. The first two assumptions are straight forward, but the third assumption is made because it is necessary to estimate a mass balance in this analysis. Molar volume is assumed constant since such data is not available for the system studied.

The two most important relationships in the study of diffusion are Fick's first law for flux and Fick's second law for diffusion. In their general form for binary diffusion these equations are, respectively,

$$J1 = -D1\frac{\partial C1}{\partial X} \qquad (3.1)$$

$$\frac{\partial C}{\partial t} = \frac{\partial}{\partial X}\left[D \frac{\partial C}{\partial X} \right]. \qquad (3.2)$$

Onsager [31Ons, 45Ons] extended the first of Fick's laws for flux in multi-component systems, describing the interdiffusion flux ($\tilde{J}_i$) as a linear function of chemical potential gradients. Because chemical potential gradients are not convenient for the analysis of experimental results, Onsager's expressions for $\tilde{J}_i$ are transformed to functions of composition gradients. Therefore, the generalized form of Fick's first law for flux in ternary systems are,

$$\tilde{J}1 = -\tilde{D}11\frac{\partial C1}{\partial X} - \tilde{D}12\frac{\partial C2}{\partial X} \qquad (3.3)$$

$$\tilde{J}2 = -\tilde{D}21\frac{\partial C1}{\partial X} - \tilde{D}22\frac{\partial C2}{\partial X} \qquad (3.4)$$

where $\tilde{D}11$ and $\tilde{D}22$ describe the effect of the concentration gradient of a given component on its own flux, and $\tilde{D}12$ and $\tilde{D}21$ describe the effect of interaction between components. The subscripts 1 and 2 refer to specific elements of a ternary system. C_1 and C_2 are the concentration variables, and **X** is the distance variable. If composition at some point is changing with time, C(X,t), Fick's first law is not a convenient for to use to describe diffusion. In these cases Fick's second law is a more useful equation, but it is first necessary to define continuity of mass in order to solve for Fick's second law. Equation (3.5) is referred to as the continuity equation and is a statement for the conservation of mass

$$J1 - J2 = \Delta X\frac{\partial C}{\partial t} = -\Delta X\frac{\partial J}{\partial X} \qquad (3.5)$$

in a diffusion reaction. Given a volume element $1*\Delta X$ in a diffusion couple, the net increase in matter in the element can be described by any part of equation (3.5). Combining equations (3.3) and (3.4) with the continuity equation results in the following general forms of Fick's second law for ternary diffusion,

$$\frac{\partial C1}{\partial t}+\frac{\partial \tilde{J}1}{\partial X}=0 \tag{3.6}$$

$$\frac{\partial C2}{\partial t}+\frac{\partial \tilde{J}2}{\partial X}=0 \tag{3.7}$$

where t is the time variable. If the composition dependency of $\tilde{D}ij$ is neglected equations (3.6) and (3.7) yield the following expression for Fick's second law;

$$\frac{\partial C1}{\partial t}=\tilde{D}11\frac{\partial^2 C1}{\partial X^2}+\tilde{D}12\frac{\partial^2 C2}{\partial X^2} \tag{3.8}$$

$$\frac{\partial C2}{\partial t}=\tilde{D}21\frac{\partial^2 C1}{\partial X^2}+\tilde{D}22\frac{\partial^2 C2}{\partial X^2} \tag{3.9}$$

with the parametric solutions to these equations being of the form,

$$C1=C1(\lambda) \tag{3.10}$$

$$C2=C2(\lambda) \tag{3.11}$$

where $\lambda = X/\sqrt{t}$, provided that the boundary conditions of a semi-infinite couple are maintained. These equations result in the two following conclusions of importance to steady-state layer growth: 1) There exists a unique solution for a given set of boundary conditions, such that only one diffusion path exists for a given time and temperature, and 2) Since the interfacial compositions of a phase are fixed due to thermodynamics, and since $C(\lambda)$, the growth of a phase will vary with the square root of time. From equation (3.8) and (3.9) for diffusion in ternary system, it is clear that in order to fully describe diffusion in an n-component system, it is necessary to know or determine $(n-1)*2$ independent diffusion coefficients for each phase in a diffusion couple. Kirkaldy and Young [87Kir] discuss a number of studies that report data for such ternary interdiffusion coefficients, but the Ti-Al-O system is not one of them. To determine these coefficients, $(n-1)*2$ unique couples would be required to determine the interdiffusion coefficients needed for a single phase. A monumental task which is not within the scope of this study.

Equations (3.8) and (3.9) for ternary diffusion in a single phase have been extended for multiphase diffusion couples by Kirkaldy [57Kir, 58Kir, 58Kir2, 58Kir3, 62Kir], and he has applied these solutions to two-phase couples. Others who have applied the Fick's laws solutions to multiphase couples include Dayananda and co-workers [85Day, 89Day], Jan et al. [91Jan] and Zhang et al. [92Zha]. If the data were available for the Ti-Al-O system, one could use the data to calculate values of interest to identify both a rate-controlling step in the diffusion process and the change in layer thickness with time.

Because there is a lack of data necessary to describe interfacial instability in Ti-base/Al_2O_3 composites using Fick's laws, an experimental approach is taken to provide

the information needed. This experimental approach involves the determination of the interdiffusion flux values for n-component systems from diffusion couple concentration profiles. This approach in the study of isothermal diffusion in multi-component systems was presented by Dayananda and co-worker [79Day, 83Day], and is an extension of the more common Boltzmann-Matano analysis method for variable D's first used by Matano [33Mat].

During isothermal diffusion the concentration profile will develop parabollically with time (t), and the concentration (C_i) at any section in the diffusion zone will be a function of the Boltzmann parameter λ ,

$$\lambda = \frac{(X - X_o)}{\sqrt{t}} \tag{3.12}$$

where X is distance and X_o is the position of the Matano plane (mass balance plane) as shown in Fig. 7.

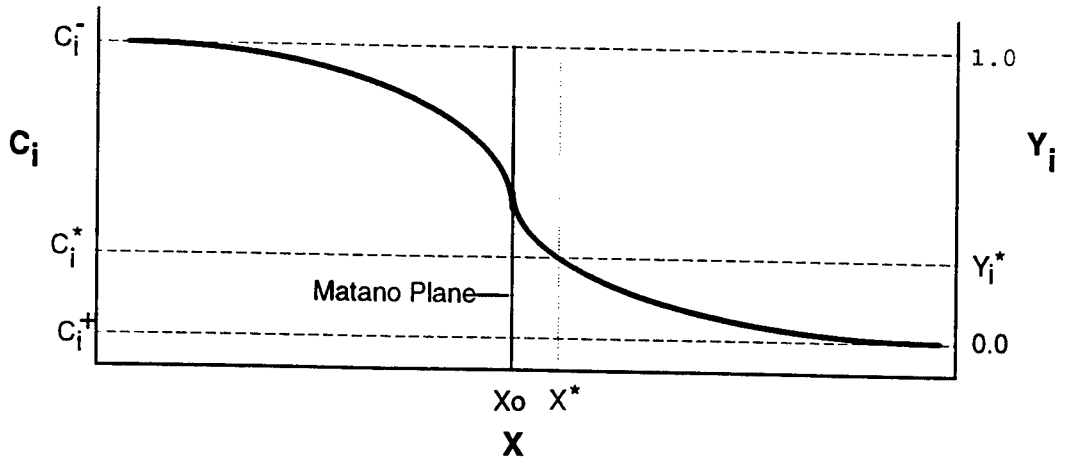

Figure 7. Concentration profile for a hypothetical diffusion couple.

A relative concentration variable $Y_i(X,t)$ for component i is defined as,

$$Y_i(X,t) = \frac{C_i(X,t) - C_i^+}{C_i^- - C_i^+} \qquad (i = 1, 2, ..., n) \qquad (3.13)$$

The common Boltzmann-Matano solution for interdiffusion flux ($\tilde{J}_i$) is,

$$\tilde{J}_i(X^*) = \frac{1}{2t} \int_{C_i^-}^{C_i(X^*)} (X - Xo)\,dC_i \qquad (i = 1, 2, ..., n) \qquad (3.14)$$

where the Matano plane location (Xo) is based upon the mass balance expression,

$$\int_{C_i^-}^{C_i^+} (X - Xo)\,dC_i = 0 \qquad (i = 1, 2, ..., n) \qquad (3.15)$$

Equations (3.14) and (3.15) can be expressed in terms of Y_i as,

$$\tilde{J}_i(X^*) = \frac{\Delta C_i}{2t}\left[(X^* - Xo)Y_i^* + \int_{X^*}^{+\infty} (Y_i)\,dX\right] \qquad (i = 1, 2, ..., n) \qquad (3.16)$$

$$\int_0^1 (X^* - Xo)\,dY_i \qquad (i = 1, 2, ..., n) \qquad (3.17)$$

where $\Delta C_i = C_i^- - C_i^+$. The location of the Matano plane, which can be determined by applying equation (3.17), can not be identified directly from diffusion data and is not necessary in the determination of $\tilde{J}_i$ if equation (3.16) is expanded to read,

$$\tilde{J}_i(X^*) = \frac{\Delta C_i}{2t}\left[Y_i^* \int_{-\infty}^{X^*} (1-Y_i)dX + (1-Y_i^*) \int_{X^*}^{+\infty} (Y_i)dX \right] \qquad (3.18)$$

Equation (3.18) is a very useful expression in that it does not require knowledge of the Matano plane in determining interdiffusion flux for the individual components, and it is ideally suited for diffusion couples with maximums or minimums in their concentration profiles. Although the equations presented here were developed for single phase couples, they can also be applied to multiphase couples provided the interfaces are planar and the molar volumes of the elements show negligible change. Dayananda and co-workers [65Day, 68Day,72Car, 76Moy, 77Sis, 79Che, 89Day) have used equation (3.18) to determine interdiffusion data for a number of substitutional systems. This same solution is used in this study to calculate the diffusion quantities useful in characterizing the instability observed in Ti-base/Al_2O_3 diffusion couples. In addition to interdiffusion flux, lattice flux and intrinsic flux are estimated in order to describe the diffusion reaction at the γ-TiAl|α_2-Ti_3Al interface of these composites. In addition to determining interdiffusion coefficient data which can be used to calculate steady-state growth, this study identifies the parabolic constants for growth of each phase in Ti/Al_2O_3 and α_2-Ti_3Al/Al_2O_3 couples from the observed layer growth with time.

From the work of Darken [48Dar] on the determination of intrinsic diffusion coefficients, it is known that interdiffusion flux ($\tilde{J}_i$) is the sum of the two contributing fluxes, lattice flux ($J_{i,Lat}$) and intrinsic flux ($J_{i,Intr}$). Darken was able to separate these to contributing fluxes by determining the velocity (V_{Lat}) at which a marked plane translates relative to the laboratory frame of reference. This translation of a lattice plane results in a

flux relative to the reference, which differs from the intrinsic flux across this same plane as a result of a composition gradient. In equation form, this separation is expressed as,

$$\tilde{J}i = Ji,lat + Ji,Intr = Vlat * Ci,lat + Ji,Intr \qquad (3.19)$$

Since $\tilde{J}i$ is available from equation (3.18) and C_i from the EPMA data, determination of $J_{i,Intr}$ requires knowledge of V_{Lat}. Similar to Darken's analysis in which inert markers were found to translate with a plane of fixed composition and used to determine V_{Lat}, this study uses the interfaces between phases to determine lattice velocities. This is done because thermodynamics requires that local equilibrium be maintain at planar interfaces in semi-infinite diffusion couples and because it is not possible place enough markers in multiphase couples to duplicate Darken's methodology. By making the assumption that the planes of fixed composition in the immediate vicinity of the interface translate at the same velocity as the interface, $J_{i,Intr}$ can be estimated at these locations for each interface. Calculation of $J_{i,Intr}$ at the interfaces is useful in making relative comparison of fluxes into the interface. Since it is assumed that the reactions in the formation of phases occur at the interfaces, such comparisons of flux are capable identifying the rate controlling step. Because it is assume that partial molar volume for each diffusing species remains constant, the mass balance plane calculated by equation (3.15) will a have zero velocity relative to a laboratory reference (or the ends of the couple), and can be used to determine the velocity of each interface. In this study, velocity is estimated by equation (3.20).

$$Vlat = Vinterface = (Xinterface - Xo)/2t \qquad (3.20)$$

For composites which exhibit instability in the form of Class III interfaces, the rate at which reaction occurs is important from both thermal processing and high-temperature lifetime points of view. Typical of diffusion controlled reactions, the rate reaction is inversely proportion to the extent of the reaction. With respect to the growth of a product phase for a Class III interface, the phase will grow at the rate,

$$\frac{dW}{dt} = \frac{const.}{W} \tag{3.21}$$

Integration of equation (3.21) yields the following expression for the parabolic growth of a phase at constant temperature,

$$W = Wo + K\sqrt{t} \tag{3.22}$$

where W is the width of the phase, W_o is the initial phase width, K is the parabolic growth constant and t is time. Interfaces which have more than one phase in the diffusion path can be evaluated by determining K for each phase or the overall reaction. Furthermore, by determining K at a series of temperature it is possible to estimate an activation energy, Q, and the pre-exponential constant K_o, if K can be expressed by the Arrhenius equation,

$$K = Ko * e^{(-Q/RT)} \tag{3.23}$$

Given the assumption that growth is diffusion controlled, equation (3.23) can provide reasonable estimates of K for use in predicting the extent of an interfacial reaction during the thermal processing or the use of a composite.

3.4 INTERFACE MORPHOLOGY

The addition of one degree of freedom available in going from a binary to a ternary system permits the existence of stable non-planar or aggregate interface morphologies between two phases in diffusion couples. Wagner [56Wag] established the criterion for determining the stability of a planar interface by studying the oxidation of noble metal alloys. Wagner's criterion has been applied metal/metal-oxide and metal/metal-sulfide by Rapp and co-workers[73Rap, 73Yur, 79Sha], and by van Loo and co-workers [80Lah, 83Vos, 84van].

The stability of a planar interface is dependent upon the magnitudes of individual fluxes on either side of an interface in a particular system. To illustrate the criterion for a planar interface, consider the hypothetical isothermal diffusion couple **AB/C** in Fig. 8. **A**, **B** and **C** represent metals, and it is assumed that alloys of these metals exhibit some solubility. The following two initial assumptions are made: 1) Tentatively, a wavy interface exists between phases, and 2) One metal is relatively immobile compared to the others. In this case **A** is assumed to have low mobility. With these assumptions, two cases are possible based upon the relative mobility's of **B** and **C**. In the first case, Fig. 8(a), if the mobility of **B** is greater that of **C**, then the growth of the phases $\mathbf{BC_3}$ and **AC** will occur at the $\mathbf{BC_3|C}$ and **AB|AC** interfaces, respectively. The bold arrows in figures 8(a) and 8(b) indicate a moving interface, which is referred to as a growth front. The growth of $\mathbf{BC_3}$ and **AC** are controlled by the diffusion of **B** and **C**, respectively. Since the flux of **B** arriving at position **I** exceeds that at position **II**, the growth front $\mathbf{BC_3|C}$ will become planar with time. Likewise, since the flux of **C** arriving at **III** exceeds that at **IV**, the **AB|AC** growth front will be planar, In the second case, Fig. 8(b), if the mobility of **C** is greater than that of **B**, then the growth of phases $\mathbf{BC_3}$ and **AC** will occur at the $\mathbf{AC|BC_3}$

and **AB|AC** interfaces, respectively. Since the flux of **C** arriving at position **V** is greater than at position **VI**, the growth front **AB|AC** will be planar. However, since the flux of **B** arriving at position **VII** is greater than that at position **VIII**, and since **C** is high in mobility, the reaction $B+3C \Leftrightarrow BC_3$ will occur at **VII** at a higher rate than at **VIII**. This will cause the growth front $AC|BC_3$ to become non-planar with time. It is seen here, that the rate controlling step in the growth of the phase BC_3 is the relatively slow diffusion of **B**. It is evident from this discussion that knowledge of the relative mobility of the elements is important in understanding and prediction interface morphology in ternary and higher order systems.

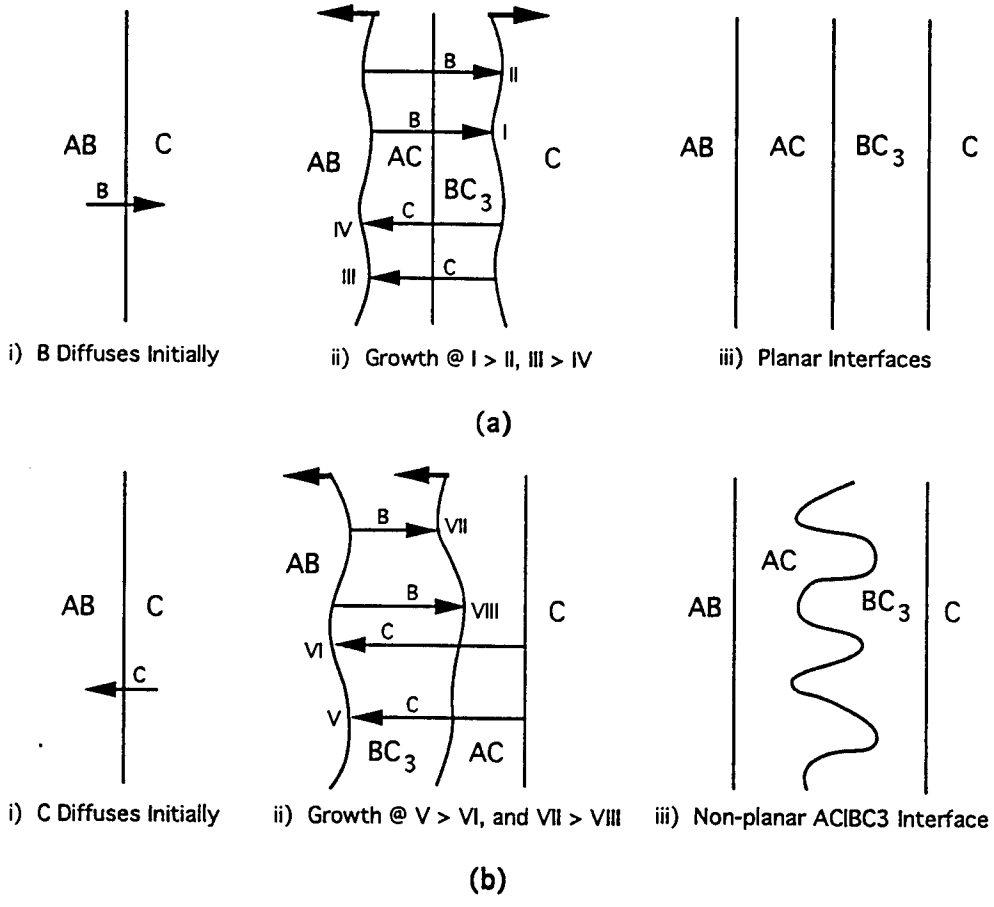

Figure 8. Criteria for planar and non-planar interfaces.

3.5 INTERDIFFUSION IN TI-AL-O COMPOSITES

No diffusion studies of the systems Ti/Al_2O_3, α_2-Ti_3Al/Al_2O_3 or γ-TiAl/Al_2O_3 were found in the literature. Studies of the O diffusion in Ti, and the interdiffusion between Ti and Al are available in the literature, and are discussed below. To simplify this discussion of interdiffusion in these composite systems, interdiffusion of O in Ti and (Ti,Al) alloys is discussed separately from the interdiffusion of Ti and Al .

3.5.1 Interdiffusion of Oxygen

A number of studies [68Sok, 69Sok, 70Ros, 70Tik, 71Zho] report on the diffusion of O in α-Ti and β-Ti, but no reports were found on the diffusion of O in (Ti,Al) alloys. These studies confirm that O diffuses interstitially in α-Ti and β-Ti, which was expected since the atomic radii ratios O:Ti and O:Al are 0.33 and 0.34, respectively. The activation energies for the diffusion of O are reported to be in the range 48-52 Kcal/mole for α-Ti, and 36-58.8 Kcal/mole for β-Ti. Since no information is available for the diffusion of O in (Ti,Al) alloys, it is assumed that the diffusion mechanism in these alloys will be interstitial diffusion. This assumption is based on the large difference in atomic radii between O and both Ti and Al, and on the fact that the crystal structures of α_2-Ti_3Al and γ-TiAl closely resemble those of α-Ti and β-Ti, respectively.

3.5.2 Ti and Al Interdiffusion

Studies of interdiffusion between Ti and Al were reported by Pouliquen et al. [72Pou] and by van Loo and Rieck [73van, 73van2]. Pouliquen et al. report that, in the temperature range 590-648°C, the growth kinetics of the phase Al_3Ti is diffusion controlled, and report the interdiffusion coefficient in Ti_3Al to be 0.066×10^{-10} -to- 0.9×10^{-10} cm^2/sec over this same temperature range. The studies by van Loo and Rieck

report that Ti is the most mobile element in the phase α_2-Ti_3Al at temperatures between 768-865°C, and that Al is the most mobile element in the Al-richer phases at temperature between 784-972°C. In addition, the results of van Loo and Rieck show that the ratio D_{Ti}:D_{Al} in the phases α_2-Ti_3Al and γ-TiAl to be in the range 10 -to- 0.1, indicating a substitutional diffusion mechanism between the two. The substitutional mechanism for these elements could be one, or a combination, of the three mechanisms: vacancy diffusion, interstitialcy diffusion, and exchange diffusion. Determination of the actual mechanism(s) is not in the scope of this study.

4.0 EXPERIMENTAL PROCEDURE

If the necessary thermodynamic and kinetic data were available for the Ti-Al-O system one could theoretically evaluate the interfacial stability of Ti/Al_2O_3, α_2-Ti_3Al/Al_2O_3 and γ-TiAl/Al_2O_3 composites. Such data would allow one to identify the compositions which are required for interfacial stability, or the reaction products and the rate of reaction for composite systems if stability is not possible . Since little or none of this information was available at the onset of this study, it was necessary to evaluate these composite systems by using experimental approach. In order to study these systems in a way that would provide both the thermodynamic and kinetic data necessary for future studies, an approach utilizing both diffusion couple samples and phase equilibria samples was chosen. Prior to discussing in detail the samples used in this study, the materials used in preparing the samples, the processes used to prepare the samples and the analysis methods used to evaluate the sample will be treated first.

4.1 MATERIALS

The basic materials used in the preparation of the samples for this study are given in Tab. 3. The use of powdered materials was avoided in effort to minimize any oxygen additions due to surface oxides on the basic materials. No effort was made to remove pre-existing oxides from these basic materials prior to their use. The diffusion couple materials Ti, α_2-Ti_3Al and γ-TiAl were ground and polished to a 1 μm surface quality prior to being bonded to Al_2O_3.

Material	Grade	Form	Source
Ti Granules	99.9%	-15 mesh	Johnson Matthey Co., Ward Hill, MA
Ti Rod	99.99%	6.35 mm dia.	Johnson Matthey Co., Ward Hill, MA
Ti Plate	99.7%	3.175 mm	Johnson Matthey Co., Ward Hill, MA
Al Shot	99.999%	4-8 mm	Johnson Matthey Co., Ward Hill, MA
Al_2O_3	Optical Grade	0.125"x1.0" dia. Disk	Crystal Systems Inc., Salem, MA
Sapphire	80-50 Polish	Random Orientation	
Al_2O_3 Disk	High Alumina	0.093"x1.25" dia.	Ceramicon Designs Ltd., Golden, CO
Al_2O_3 Pellets	99%	3.2 mm	Alfa Products, Danvers, MA
Y_2O_3 Coating	Type "YV"	Suspension	ZYP Coatings, Oak Ridge, TN
Ta Foil	99.95%	0.025 mm	Johnson Matthey Co., Ward Hill, MA

Table 3. Basic materials used in this study.

4.2 PROCESSING

Sample processing incorporates a wide range of steps, from the preparation of the basic materials to the analysis of a finished sample. To be as brief as possible, only those steps that are important in the preparation of composite materials or those of technical merit are covered here. Sample processing is readily divided into two general categories, which are: 1) The preparation of samples for analysis, and 2) The analysis of samples. Within each of these categories are methods which were either adopted from others or developed along the way.

4.2.1 Sample Preparation

The significant steps in the preparation of samples for this study included: 1) Weighing, 2) Sectioning, 3) Grinding/Polishing, 4) Alloying, 5) Couple Bonding, and 6) Heat Treatment.

4.2.1.1 Weighing

The weighing of materials is fundamental to any experimental study. For this study, measurement were made using a Mettler Balance, Model AE200, capable of 0.1 mg precision. The samples which required the weighing of basic materials for alloy preparation were the diffusion couple alloys α_2-Ti_3Al and γ-TiAl, and the phase equlibria alloys α_2-Ti_3Al(O) and γ-TiAl(O).

4.2.1.2 Sectioning

Because of the wide range in properties exhibited by Ti, (Ti,Al,O) alloys and Al_2O_3, the only means available to section these materials was by using a slow-speed saw equipped with a diamond wafering blade. All cutting operations in study were performed on a Beuhler Isomet Saw, using a Norton Diamond Wheel (M4D150-N100M99-1/8). In addition to being capable of cutting a wide variety of materials, diamond wafering blades were found to cut composites without producing relief between the metal matrix and the Al_2O_3 reinforcement, and did not fracture or distort the materials being cut. Best cutting results were achieved at mid-speed and at a modest load. Excessive loads frequently resulted in seizing of blade in the sample, and damage to the saw.

4.2.1.3 Grinding and Polishing

For grinding and polishing, and to facilitate electron-probe microanalysis (EPMA), samples were mounted using Konductomet mounting material in a 1" diameter mounting press, both from Beuhler Ltd., Lake Bluff, IL. If possible, numerous samples were mounted in a singe mount. Since samples were ground and polished by hand, several samples in a mount helped to maintain planar and relief-free surfaces. The grinding and polishing process was performed using, in order, 400, 600, 1000 and 1500 grit SiC paper, followed by a 1 μm diamond polish using a nylon clothe. Best results were obtained if the grinding and polishing time was kept to a minimum.

4.2.1.4 Alloying

The preparation of alloys for this study involved arc-melting of each weighed sample, followed by homogenization. Arc-melting was performed using a Centorr Arc - Melt Furnace, Suncook, N.H. equipped with a Miller 1000 Amp power supply, a water-cooled copper hearth plate connected to a Fisher Scientific Isotemp Refreigerated Circulator and a Centorr Getter Furnace. The important parameters or aspects of this process were as follows: 1) the melting chamber is evacuated to 50×10^{-3} torr after loading samples, 2) the chamber is back-filled with 'gettered' Ar to a pressure of -2 psi gauge. Centorr reports an increase in Ar purity by one '9' using the Ti charged getter furnace operating at 800°C. This would provide a melting atmosphere of 99.999 % Ar, given an initial gas purity of 99.998 %, 3) the Cu hearth plate is maintained at 15°C, 4) a Ti getter is melted before melting each sample. This is done to scavenge addition oxygen from the atmosphere in the chamber, and 5) each sample is melted, and turned over, a minimum of four times, to ensure thorough mixing of the alloying materials.

Homogenization of alloy samples was performed in a resistance type furnace, fitted with a closed-end Alumina furnace tube. The open end of the furnace tube was fitted with a cap that was connected to both a Ti charged getter furnace and a vacuum roughing pump. The getter furnace was custom made for the purification of Ar and operated at 800 °C. Within the furnace tube there was a static Ar atmosphere of 99.998% purity or better. This system was designed to prevent continuously passing freshly purified Ar over the sample. The static atmosphere was maintain at a slight positive pressure by using a glycerin filled air lock. All samples were coated with Y_2O_3 and placed in an Alumina boat for homogenization. Next to the sample boat was another boat, towards the open-end of the tube, filled with Ti as an oxygen getter. This furnace maintained temperature of the sample to within ±15°C of the set-point temperature. Heating and cooling, to and from the set-point temperature, was done at the rates 10 °C/min and 5 °C/min, respectively. The furnace tube was evacuated to an estimated 10^{-2} torr and back-filled with gettered Ar, three times, at the start of a homogenization cycle.

3.2.1.5 Couple Bonding

Two distinct methods were used for the bonding of diffusion couples prior to heat treatment. The Ti/Al_2O_3 couples were bonded using a custom made hot-pressing furnace. This furnace provided for the application of a uni-axial load to the sample via. a graphite ram and an externally applied hydraulic load. The furnace was equipped with resistance type elements operating in a vacuum chamber maintained at a vacuum in the 10^{-5} torr range. The following parameters were used for hot-press bonding: 1) load sample as shown in Fig. 9, and evacuate chamber, 2) heat to 1050°C at 10°C/min., 3) hold at 1050°C for 6 hours. For the first hour at 1050°C, a sample load of 300 psi was applied. This load is applied to ensure good contact for bonding. The load was removed after the

first hour to avoid plastic deformation of the Ti plate, 4) cool to room temperature at 5° C/min., and 5) back-fill chamber and remove sample. The basic materials used were Ti (plate) cut 1" square, Al_2O_3 (sapphire) disc and Al_2O_3 (high alumina) disc. This process prepared a large sample which was then sectioned into smaller samples.

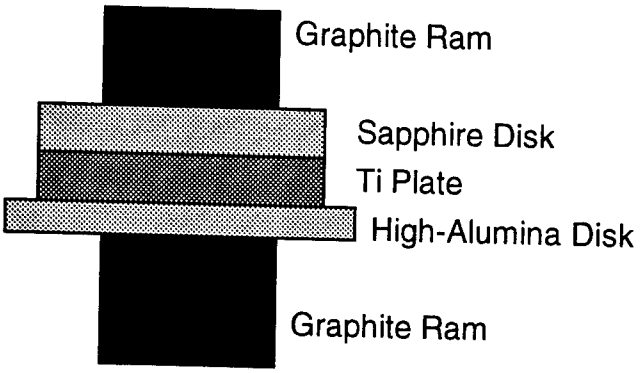

Figure 9. Bonding arrangement of Ti/Al_2O_3 samples.

The α_2-Ti_3Al/Al_2O_3 and γ-$TiAl/Al_2O_3$ diffusion couples were bonded using an Eagle Hot Isostatic Press (HIP), International Pressure Service, Inc. (IPS). This method, using the process parameters given in Tab. 4, was found to successful after failing to achieve bonding via. hot pressing of these materials. HIP bonding differs significantly from Hot Pressing in that the sample experiences a hydrostatic load. The fluid medium used was 99.998 % Ar. HIP processing requires the samples to be enclosed in an evacuated envelop that will collapse onto the sample at the temperature and pressure used for bonding. In this case, Pyrex tubing was used to envelope the samples at 10^{-3} torr, with each sample being prepared in the same manner as described in the following section (Heat Treatment). After bonding, all materials used in enveloping were tediously removed prior to heat treatment.

Segment	1	2	3	4	5	6	7	8	9	10
Profile 1 (Temp., °C)	15	15	15	15	15	700	1100	1100	10	10
Profile 2 (Pres., Ksi)	3	3	3	3	3	3	25	25	0	3
Time (hr:min:sec)	1:00	15:00	0:02	0:40	0:01	1:00:00	2:00:00	8:00:00	1:00:00	0:05
Event*	---	1	3	2	3	5	4, 5	5	5	---
Next Seg.	2	3	4	2	6	7	8	9	10	10
Recycles	0	0	0	2	0	0	0	0	0	0

*Event	1	2	3	4	5
Process	Vacuum	Vent	Gas	Compressor	Furnace

Table 4. Hot isostatic pressing parameters.

4.2.1.6 Heat Treatment

All samples in this study were heat-treated in Lindberg 1500°C tube type furnaces, equipped with Globar elements and controlled with an Omega Model 9000 controller. Using solid-state switches, these furnaces maintained temperature at better than ± 5°C. To monitor accuracy of temperature, a thermocouple was placed inside the tube in the vicinity of the sample(s) being treated. Because the furnace tube was open to the atmosphere, all samples were individually encapsulated in quartz tubing to prevent reaction with air. At the end of heat treatment, samples were quenched in water. The fragile nature of the diffusion couples did not permit breaking of the quartz tube during quenching, but for all other samples the tubes were broken.

The encapsulation of samples in quartz tubing was a very important procedure in this study. Not only did the samples need protection from reaction with the air, but they also had to be kept from reacting the quartz container. This was accomplished as shown in Fig. 10. Individual samples were painted with Y_2O_3 coating, wrapped in Ta foil and then inserted into a quartz tube which was closed at one end. Prior to sealing of the tube, samples were dried in a vacuum oven at ~100°C and a vacuum of 30 inches Hg for at least one hour. Sealing of the quartz capsules was performed using a custom built sealing system, equipped with a roughing pump, both mechanical and thermocouple vacuum gauges, and valve connections for optional N_2 or Ar back-filling. A natural gas/oxygen torch was used to seal the capsules. All Ti/Al_2O_3 samples were sealed in 6 mm ID × 8 mm OD quartz tubing at ~30×10^{-3} torr. The α_2-Ti_3Al/Al_2O_3, γ-$TiAl/Al_2O_3$ and phase equilibria samples required larger diameter tubing that could not be sealed without first back-filling with 99.998 % Ar. In these cases a vacuum of 15 inches Hg was used for 17 mm ID × 19 mm OD quartz tubing. If these larger capsules had not been backed filled prior to sealing, they would either collapse non-uniformly and lose its vacuum during sealing or, if it did seal, it might fracture due to stress while heating of the sample for heat treatment.

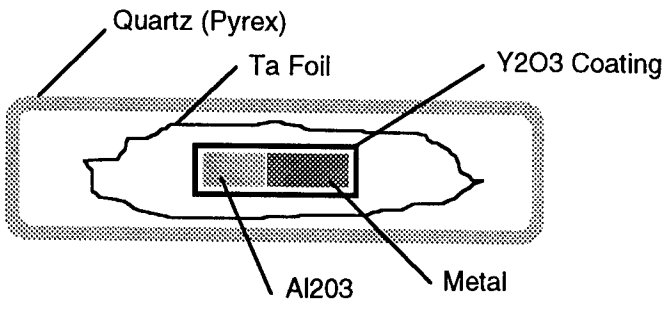

Figure 10. Sample capsules for heat treatment and HIP bonding.

4.2 SAMPLE ANALYSIS

Two analysis techniques were relied upon extensively to aid in characterizing the stability of interface for the composite systems studied. These techniques were Metallography and Electron-Probe Microanalysis (EPMA). To evaluate phase equilibrium samples the techniques X-Ray Diffraction (XRD), Atom Probe Field Ion Microscopy (APFIM) and Oxygen Determination were used .

4.2.1 Metallography

The use of metallography in metallurgical studies is valuable and common. In this study, metallography of both diffusion couples and phase equilibria samples was used to identify the class of interface common to a particular composite (diffusion couple), the extent of reaction at a given temperature and time, or to monitor the homogenization or heat treatment of equilibrium samples.

Sample preparation for metallography was accomplished by surface preparation (Grinding and Polishing) followed by etching. The etchant used in this study consisted of an aqueous solution containing 10% HF (48% ACS) and 10% HNO_3. All diffusion couples were sectioned, after mounting, to expose the core of the sample for analysis. Only bright field micrographs were taken, and the most common magnification used was nominally 200X. Magnification correction was found to be necessary, and was done using a 0.01 mm standard.

Evaluation of the extent of reaction, by measuring the width of reaction layers, was performed using metallographic images of the samples. Variations along the length of the interfaces between reaction layers could be averaged out, thus providing a better estimate

than that provided by a single EPMA trace. For the most part, measurements of phase widths were obtain by this method.

4.2.2 Electron-Probe Microanalysis

EPMA analysis was performed on the diffusion couples to obtain composition data for both the estimation of phase equilibrium boundaries and the reaction kinetics analysis. Some imaging was also done during EPMA. Secondary-electron (SE) and or backscatter-electron (BSE) images were taken of a number of samples. Analysis was performed at the University of Wisconsin-Madison or at Sandia National Laboratories, Albuquerque, N.M.

An Applied Research Laboratories (ARL) microprobe was used for analysis at UW-Madison. The standards used for analysis included: Ti (99.99%) for the determination of titanium, Al (99.999%) for the determination of aluminum, and Al_2O_3 (sapphire) for the determination of oxygen. Not all samples were analyzed quantitatively for oxygen content, since it was determined that oxygen determination by the difference method provided the same level of accuracy as did quantitative analysis. The energy levels and the diffracting crystals used were: 1) Ti-Kα_1, LiF(200) for titanium, 2) Al-Kα_1, ADP(101) for aluminum and 3) O-Mα_1, W-synthetic for oxygen. ZAF correction program was used to calculate compositions from the counts data. The microprobe was operated at 15 KeV. Composition data was obtained by a trace of the beam across the reaction zone, perpendicular to the observed interfaces. Composition was determined at steps of 1 -to- 5 microns. Because the beam affected area in the sample was estimated to be 5 μm in diameter, 2 μm steps were most commonly used. Larger steps were used when little variation in composition occurred over large distances.

A JEOL 8600 microprobe was used for analysis at Sandia National Laboratories, by their staff. The standards used for analysis were of the same as those used at UW-Madison, except Al_2O_3 was not used. Oxygen was estimated by the difference method. The operating voltage was 15 KeV. The procedure followed was similar to that used at UW-Madison, except steps of 1 μm were used because of the speed at which the JEOL could operate. SE and BSE images were taken of each sample analyzed on the JEOL.

The preparation of samples for EPMA involved surface preparation to 1 μm, followed by the application of a carbon coating. The carbon coating was necessary due to the non-conductive nature of Al_2O_3. The samples were mounted in Kunductomet to provide conduction from the sample to the holding block.

4.2.3 X-Ray Diffraction Analysis

XRD was used for structure identification of the α_2-$Ti_3Al(O)$ phase equilibrium samples. The analysis was performed in the XRD Laboratory at the Department of Materials Science & Engineering, UW-Madison. The -200 mesh powder samples were analyzed using a Philips Model PW1729 X-ray generator. For data acquisition and analysis, the XRD system was interfaced with a Dapple Systems computer control system.

Analysis concentrated on those peaks in the range 25 -to- 80° 2θ, at a rate of 0.02° 2θ/step and 0.5 sec./step. Divergence-limiting and receiving slits of 1.0° and 0.2°, respectively, were used. The X-ray source was Cu K_α=1.5405 Å, generated at 40 KeV and 30 mA.

4.2.4 Atom-Probe Field Ion Microscopy

APFIM was used for the determination of extent of oxygen solubility in the phase γ-TiAl at 1100°C. γ-TiAl(O) phase equilibrium samples, containing small fractions of Al_2O_3, were prepared for analysis at Oak Ridge National Laboratories, under the direction of Dr. M.K. Miller. Because this analysis was performed at ORNL, the specifics of the process are not available to report here. The samples were cut and polished to 1 mm × 1 mm × 1 cm at UW-Madison before being sent to ORNL.

4.2.5 Oxygen Determination

Oxygen analysis was performed on the γ-TiAl(O) phase equilibrium samples to check the overall oxygen content of these samples. The goal of this analysis was to evaluate the quality of the process used to prepare the γ-TiAl(O) and α_2-Ti_3Al(O) phase equilibrium samples. Equipment failure prohibited the analysis of the α_2-Ti_3Al(O) samples.

Oxygen determination was performed using a LECO Oxygen Determinator, Model RO-116, LECO Corporation, 3000 Lakeview Ave., St. Joseph, MI 49085. This determinator was available through Dr.Y.A. Chang, Department of Materials Science & Engineering, UW-Madison. The procedure followed during the analysis was that suggested for titanium metal by LECO. A LECO standard, Ti-0.1550 ± 0.005 wt.% O, was used to standardize the determinator.

4.3 SAMPLES

Diffusion couple and phase equilibrium were the two general types of samples used in this study. Diffusion couple samples were prepared to evaluate the stability of Ti-based composites utilizing Al_2O_3 reinforcement. Whereas, phase equilibrium samples were prepared to provide phase equilibrium data not provided by the diffusion couples. Combined, these two types of samples were intended to help estimate Ti-Al-O phase equilibium over the temperature range 900-1250°C and aid in understanding the instability of (Ti,Al)/Al_2O_3 composites.

4.3.1 Ti/Al_2O_3 Diffusion Couples

These samples were prepared by bonding Ti (plate) and Al_2O_3 (sapphire). The large Ti/Al_2O_3 bonded materials were sectioned into smaller diffusion couple samples measuring 0.125" square. After sectioning, samples were cleaned by gentle agitation in acetone. For heat treatment, the samples were coated with Y_2O_3, wrapped in Ta foil and sealed in quartz capsules. At the end of heat treatment, the sample capsules were removed from the furnace and quenched in water. Samples were heat-treated at the following temperatures and time periods: 1) 900°C for 50 -to- 400 hours, 2) 1000°C for 50 -to- 408 hours, 3) 1100°C for 50 -to- 312 hours, 4) 1144°C for 25 -to- 150 hours, 5) 1200°C for 25 -to- 154.5 hours, and 6) 1250°C for 10 -to- 70 hours.

4.3.2 α_2-Ti_3Al/Al_2O_3 Diffusion Couples

These samples were prepared by first arc-melting a binary α_2-Ti_3Al alloy of composition Ti-35 at.% Al. The alloy was cast into a rod shape measuring approximately 0.375" in diameter. The basic materials used for this alloy were Ti granules (99.9%) and Al shot (99.999%). Homogenization of the alloy was done at 1100°C for 141 hours. After homogenization, the ingot was sectioned into 0.125" thick disks for bonding to Al_2O_3 (sapphire). Bonding was accomplished by use of the HIP process. The α_2-Ti_3Al/Al_2O_3 couples were heat treated at 1100°C, in the same manor as the Ti/Al_2O_3 couples. The heat-treatment times used were 50, 100, 145 and 195 hours. Because of the difficulty in preparing these samples, no other temperatures were studied.

4.3.3 γ-$TiAl/Al_2O_3$ Diffusion Couples

These samples were prepared by first arc-melting a binary γ-TiAl alloy of composition Ti-50 at.% Al. The basic materials used for this alloy were Ti granules (99.9%) and Al shot (99.999%). The alloy was cast into a rod shape measuring approximately 0.375" in diameter. Homogenization of the alloy was done at 1100°C for 283 hours. After homogenization, the ingot was sectioned into 0.125" thick discs for bonding to Al_2O_3 (sapphire). Bonding was accomplished by use of the HIP process. The γ-$TiAl/Al_2O_3$ couples were heat-treated at 1100°C, in the same manor as the Ti/Al_2O_3 couples. The heat-treatment times used were 50, 100, 150, 200 and 250 hours. Like the α_2-Ti_3Al/Al_2O_3 couples, these samples were difficult to prepare and only the 1100°C temperature was studied.

4.3.4 α_2-Ti_3Al(O) Phase Equilibrium Samples

The existence of a reaction layer in Ti/Al_2O_3 diffusion couples at 1200 and 1250° C, with composition corresponding to the α_2-Ti_3Al phase, prompted the analysis of this group of samples. Binary Ti-Al phase equilibrium indicated that the critical temperature for α_2-Ti_3Al is 1164°C, above which the disordered phase α-Ti is stable. What effect soluble oxygen in the α_2-Ti_3Al phase has on increasing the stability temperature of this phase was investigated by these samples.

Three alloys were prepared in order to study the stability of the α_2-Ti_3Al(O) phase. These samples included: 1) Ti-34.5 at.% Al-3 at.% O, 2) Ti-31 at.% Al-8 at.% O, and 3) Ti-34 at.% Al. The basic materials used to prepare these samples were Ti granules (99.9), Al shot (99.999%) and Al_2O_3 pellets (99%). Each alloy was prepared by arc-melting. In an effort to prevent the loss or gain of oxygen during homogenization, these alloys were homogenized by encapsulating them in quartz tubing. The two oxygen containing samples were homogenized at 1100°C for 246 hours. The binary sample was homogenized at 1100°C for 290 hours. Following homogenization, samples of each composition were heat-treated by placing them in furnaces at 1200 and 1250°C. After 24 hours at temperature, the samples were removed from the furnaces and quenched in water. To obtain a rapid quench, the quartz tubes were broken. It is noteworthy to mention that the composition of these α_2-Ti_3Al(O) alloys was not checked to confirm success of their preparation. However, since these alloys were prepared in the same manner as the γ-TiAl(O) described in the following section, accuracy in composition is believed to be similar to that found for those alloys.

X-ray diffraction was used to identify the phase(s) present in each of the alloys quenched from 1200 and 1250°C. To accomplish this, each sample was powdered to a -200 mesh size. The powders were produced by mortar and pestle grinding at room temperature. The mortar and pestle were constructed of A2 alloy tool steel.

4.3.5 γ-TiAl(O) Phase Equilibrium Samples

These sample were prepared to identify the maximum solubility of oxygen in this phase. EPMA results of this phase in Ti/Al_2O_3 diffusion couples were not conclusive due a relatively large error in oxygen determination by that method. APFIM was identified as an analytical technique capable of much greater accuracy. These samples were prepared for analysis at Oak Ridge National Laboratories.

Three compositions of γ-TiAl(O) alloys were prepared: 1) Ti-49 at.% Al-2 at.% O, 2) Ti-49.5 at.% Al-1.0 at.% O, and 3) Ti-49.75 at.% Al-0.5 at.% O. The basic materials used to prepare these samples were Ti granules (99.9%), Al shot (99.999%) and Al2O3 pellets (99%). Alloying was accomplish by arc-melting. Annealing of these alloys was performed at 1100°C for 250 hours by encapsulating them in quartz tubing to prevent the loss or gain of oxygen. The samples were quenched in water from 1100°C by fracturing the quartz capsule.

Analysis of the γ-TiAl(O) samples for overall composition was not performed. However, determination of the oxygen content of the 1.0 and 0.5 at.% O samples was performed as a check of our ability to prepare samples of know oxygen content. If accuracy in oxygen could be attained, similar accuracy of Ti and Al content should follow.

To check the process used to prepare these oxygen containing samples, analysis of the 1.0 and 0.5 at.% O samples was performed using a LECO Oxygen Determinator. These samples were chosen because of the availability of a standard near these levels of oxygen. Analysis followed guidelines provided by LECO, using a Ti oxygen standard containing 0.1550 ± 0.005 wt.% O. During the set-up period, for analysis, five standard samples were analyzed at 0.1550 ± 0.010 wt.% O. The analysis of six samples at the 0.5 at.% O (0.2143 wt.% O) level gave the results 0.226 ± 0.008 wt.% O. The analysis of six samples at the 1.0 at.% O (0.4298 wt.% O) level gave the results 0.4511 ± 0.0411 wt.% O. A follow-up check of two standard samples gave an oxygen analysis of 0.166 ± 0.009 wt.% O. These results are significant because they show that each of these samples indicated a relative gain in oxygen content of less than 5.5 % during the processes of arc-melting and annealing. Further, these results imply that similar accuracy's in oxygen content may be attributed to those alloys not analyzed in this study, which include the 2 at.% O γ-TiAl(O) sample and all three of the α_2-Ti_3Al(O) phase equilibrium samples prepared for XRD analysis.

5.0 RESULTS AND DISCUSSION

In this study of the interfacial stability of Ti/Al_2O_3, α_2-Ti_3Al/Al_2O_3 and γ-$TiAl/Al_2O_3$ composites, two general areas were considered: 1) Thermodynamic Phase Equilibrium, and 2) Kinetics of Interfacial Instability. Together, these two topics areas compliment each other to indicate why stability may or may not exist and how the system reacts in the event of instability.

If available, thermodynamic phase equilibrium data is very useful in determining if a given composite system will exhibit interfacial stability. At the initiation of this study, phase equilibria for the Ti-Al-O system was not established in the temperature range 900 - to- 1250°C. Therefore, an experimental approach utilizing diffusion couple samples and phase equilibrium samples was chosen to establish Ti-Al-O phase relations in this temperature range.

Since a state of local thermodynamic equilibrium can exist at the interfaces which separate phases in a diffusion couple, thermodynamic data in the form of two-phase equilibrium compositions can be identified by analyzing the composition of each phase at the interface. In this study, this was done by EPMA. Although the vast majority of the samples in this study were of the diffusion couple type, phase equilibrium samples of α_2-Ti_3Al(O) and γ-TiAl(O) were prepared to answer questions presented by the diffusion couple results. Namely, the stabilizing effect of oxygen on α_2-Ti_3Al and the maximum solubility of oxygen in γ-TiAl.

Kinetic analysis of diffusion couples was performed for the Ti/Al_2O_3 and α_2-Ti_3Al/Al_2O_3 couples in this study. The analysis of these couples included the calculation of interdiffusion flux, interdiffusion coefficients and the parabolic growth of the layers observed in these couples. Interdiffusion flux and the parabolic growth data are used in this study to characterize the instability of Ti/Al_2O_3 and α_2-Ti_3Al/Al_2O_3 composite interfaces. Calculation of the interdiffusion coefficients was performed to provide that data for future studies. Since Ti/Al_2O_3 couples at 900 and 1000°C exhibit a non-planar type interface between the phases γ-TiAl(O) and α_2-Ti_3Al(O), this phenomena was analyzed and an explanation presented.

5.1 Ti/Al_2O_3 DIFFUSION COUPLES

Of the three types of diffusion couples studied, these couples were examined extensively. This system was of primary interest because of the high degree of interfacial instability observed and because it more nearly represents the α-Titanium and or β-Titanium alloys currently regarded as possible matrix materials. Although it is not likely that Ti-base/Al_2O_3 composites would be used at temperatures reaching 1250°C, the temperature range 900 -to- 1250°C was studied in order obtain both thermodynamic and kinetic data in a realistic period of time.

5.1.1 Thermodynamic Results

The establishment of local thermodynamic equilibrium at a planar interface between phases in diffusion couples makes it possible to estimate phase equilibria for the Ti-Al-O system. Figures 11,12,13,14,15 and 16 show the microstructure and composition profiles typical of Ti/Al_2O_3 couples at 900, 1000, 1100, 1144, 1200 and 1250°C, respectively. These results indicate that, at atmospheric pressure, Ti/Al_2O_3 couples are

reactive and the diffusion path β-Ti|α-Ti(O)|α_2-Ti_3Al(O)|γ-TiAl(O)|Al_2O_3 is typical for semi-infinite couples at these temperatures.

Although a planar interface represents a state of local thermodynamic equilibrium between two phases, the determination of what is or is not a planar interface is a clear-cut issue. Of all the interfaces present in the β-Ti|α-Ti(O)|α_2-Ti_3Al(O)|γ-TiAl(O)|Al_2O_3 diffusion path, the interface which is clearly non-planar is the α_2-Ti_3Al(O)|γ-TiAl(O) interface at 900 and 1000°C, as shown in Fig.'s 11 and 12. It can be argued that this same interface is not planar at 1100°C, but is considered planar given the initial microstructure of all samples shown in Fig. 17 and that significant improvement is seen at times greater than 100 hours at 1100°C.

Given that all interfaces are planar, except those noted, Tab. 5 lists the two-phase equilibrium compositions for all interfaces from the EPMA results provided in Appendix A. The error associated with all EPMA results is conservatively estimated at ± 1.0 at.% for titanium and aluminum and ± 2.5 at.% for oxygen. The results of Tab. 5 are instrumental in estimating Ti-Al-O phase equilibria, which in turn can be used to evaluate the interfacial stability of a Ti-base/Al_2O_3 composites. Gibbs isothermal diagrams will be presented in the conclusions, based upon these results and others to follow.

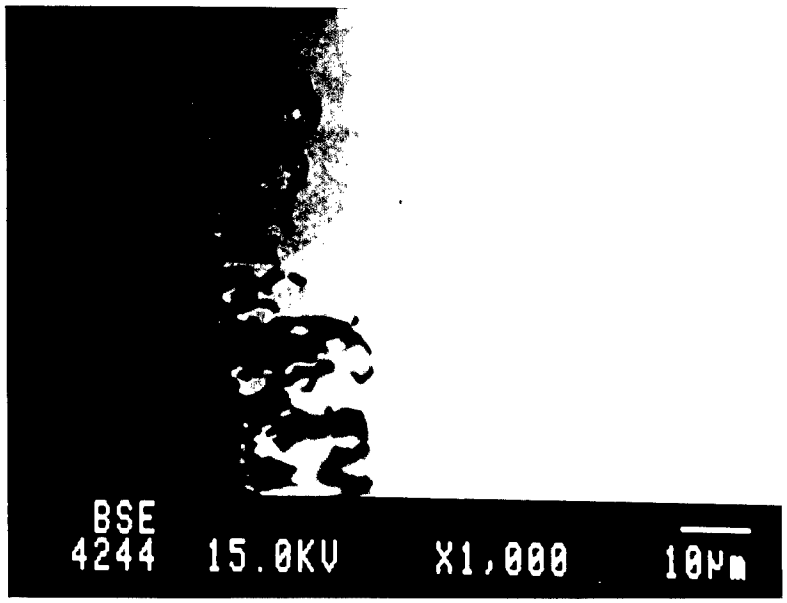

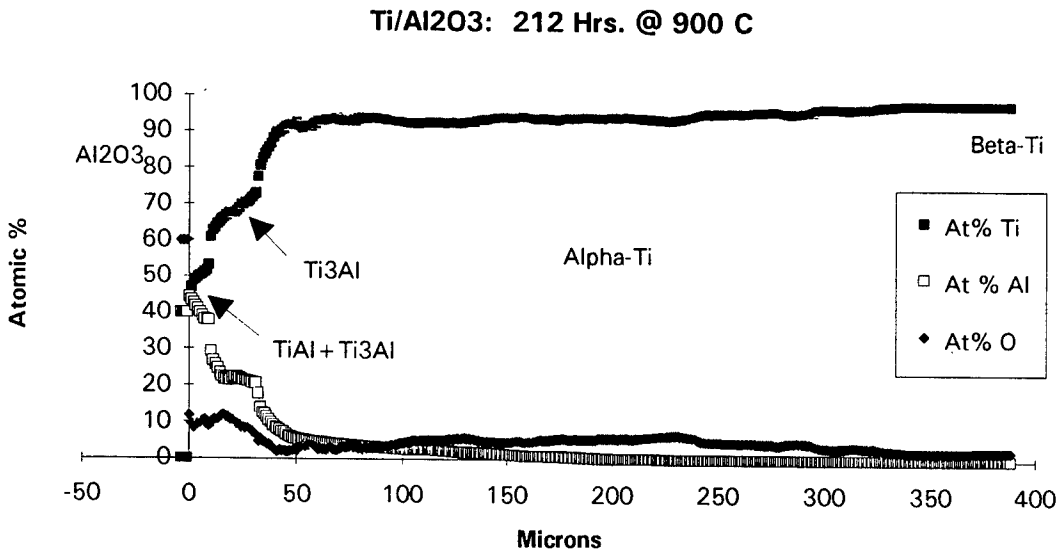

Figure 11. Ti/Al_2O_3 diffusion couple at 900°C for 212 hours. **Top:** BSE image showing the phases (left to right) Al_2O_3, γ-TiAl, α_2-Ti_3Al and α-Ti. β-Ti not shown because of high magnification. **Bottom:** EPMA results of analysis at Sandia National Laboratories.

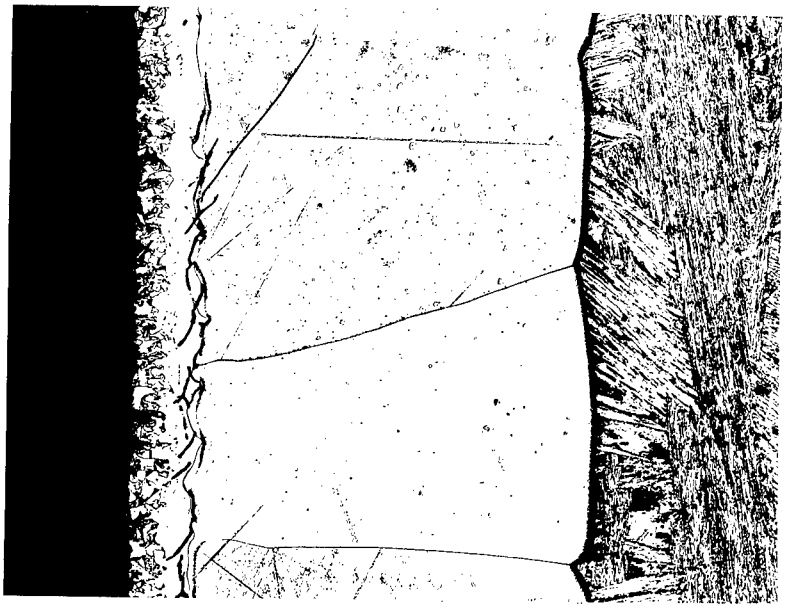

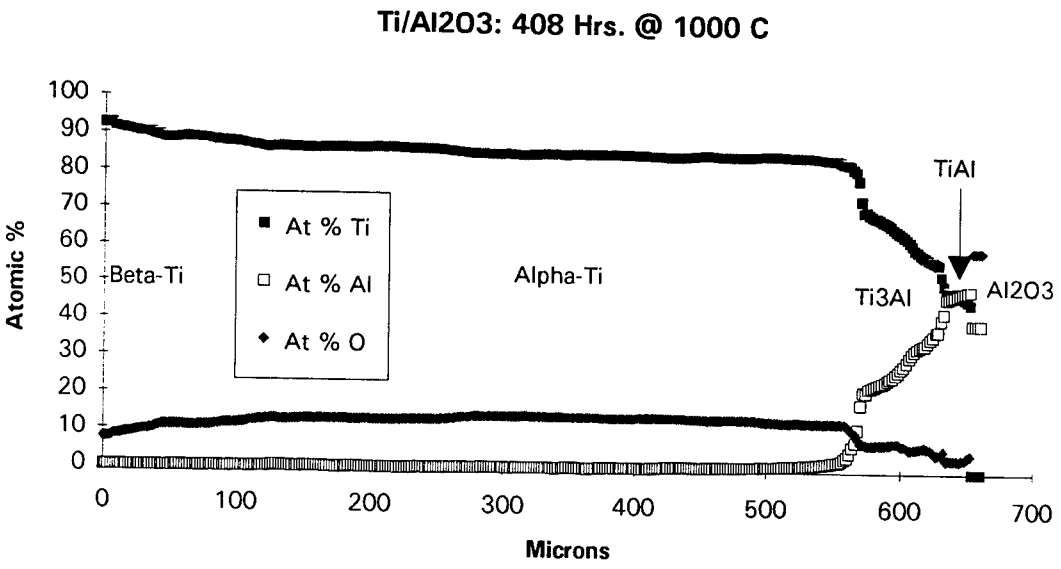

Figure 12. Ti/Al_2O_3 diffusion couple at 1000°C for 408 hours. **Top:** Optical micrograph (100X) showing the phases (left to right) Al_2O_3, γ-TiAl, α_2-Ti_3Al, α-Ti and β-Ti. **Bottom:** EPMA results of analysis at University of Wisconsin-Madison.

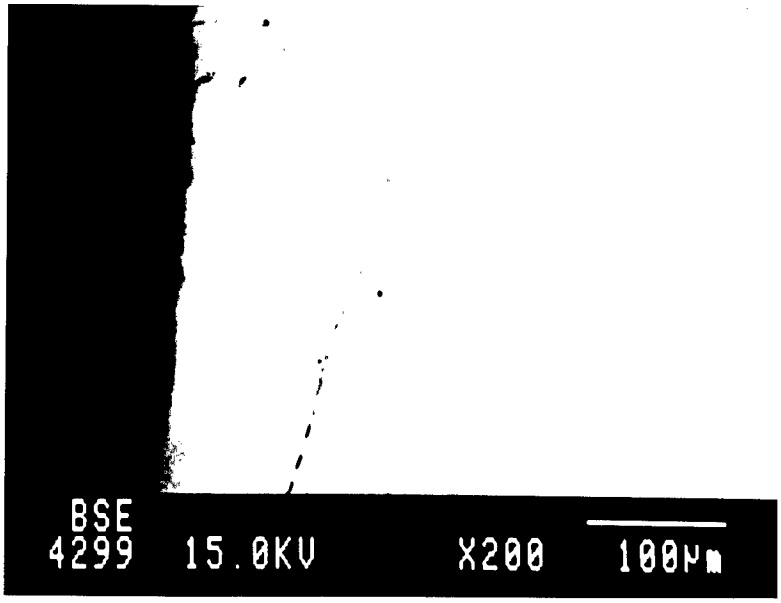

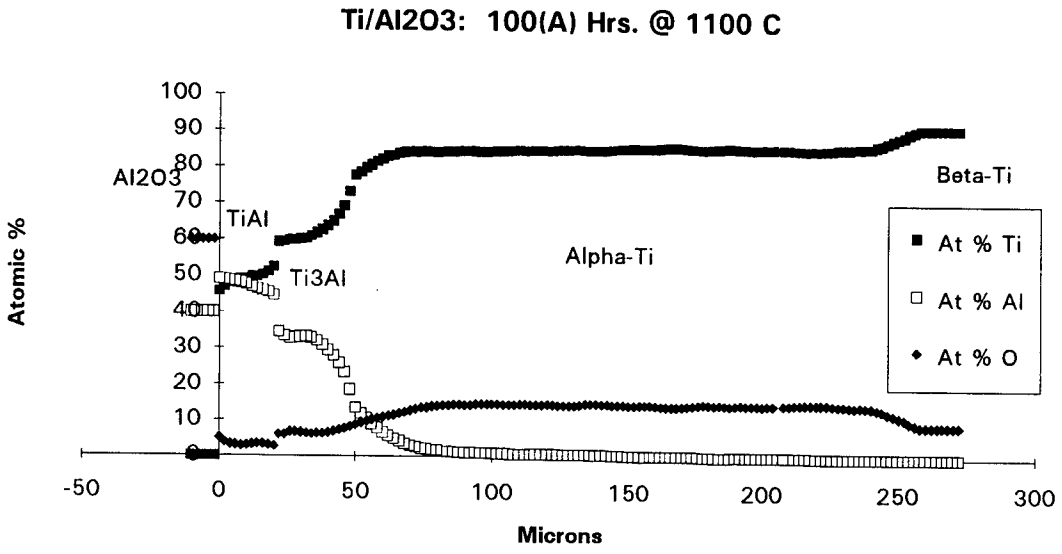

Figure 13. Ti/Al_2O_3 diffusion couple at 1100°C for 100 hours. **Top:** BSE image showing the phases (left to right) Al_2O_3, γ-TiAl, α_2-Ti_3Al, α-Ti and β-Ti. **Bottom:** EPMA results of analysis at Sandia National Laboratories.

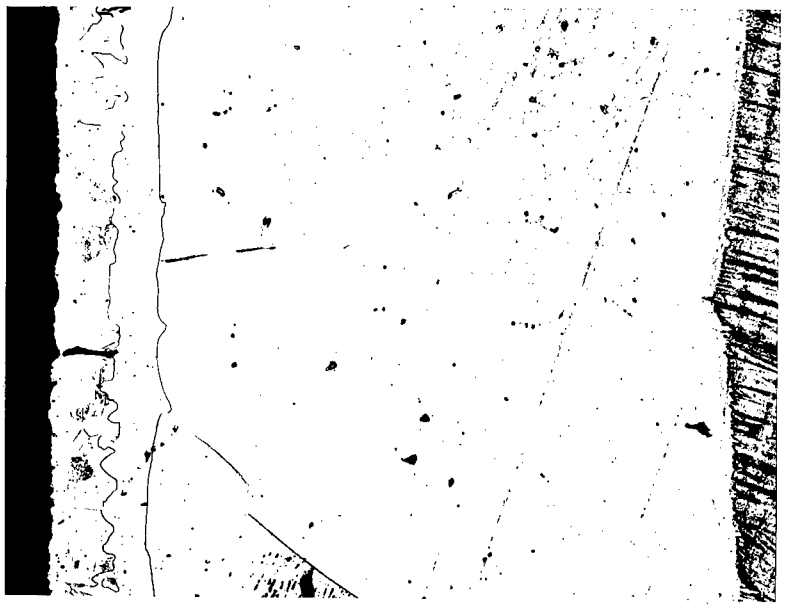

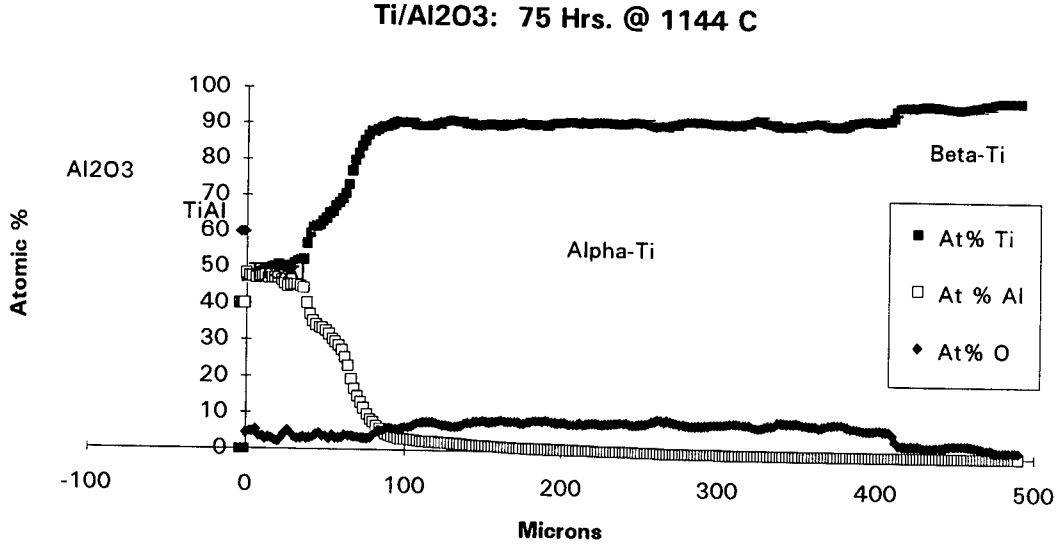

Figure 14. Ti/Al_2O_3 diffusion couple at 1144°C for 75 hours. **Top:** Optical micrograph (200X) showing the phases (left to right) Al_2O_3, γ-TiAl, α_2-Ti_3Al, α-Ti, and β-Ti. Dark region between Al_2O_3 and γ-TiAl due to separation at Al_2O_3 | Metal interface upon quenching. **Bottom:** EPMA results of analysis at Sandia National Laboratories.

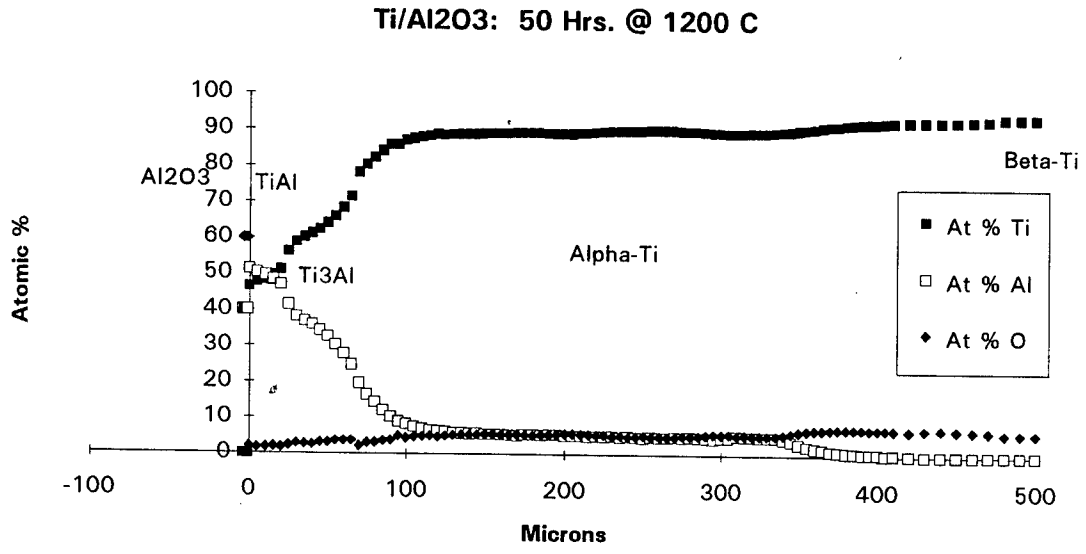

Figure 15. Ti/Al_2O_3 diffusion couple at 1200°C for 50 hours. **Top:** Optical micrograph (200X) showing the phases (left to right) Al_2O_3, γ-TiAl, α_2-Ti_3Al, α-Ti, and β-Ti. Dark region between Al_2O_3 and γ-TiAl due to separation at Al_2O_3 | Metal interface upon quenching. **Bottom:** EPMA results of analysis at University of Wisconsin-Madison.

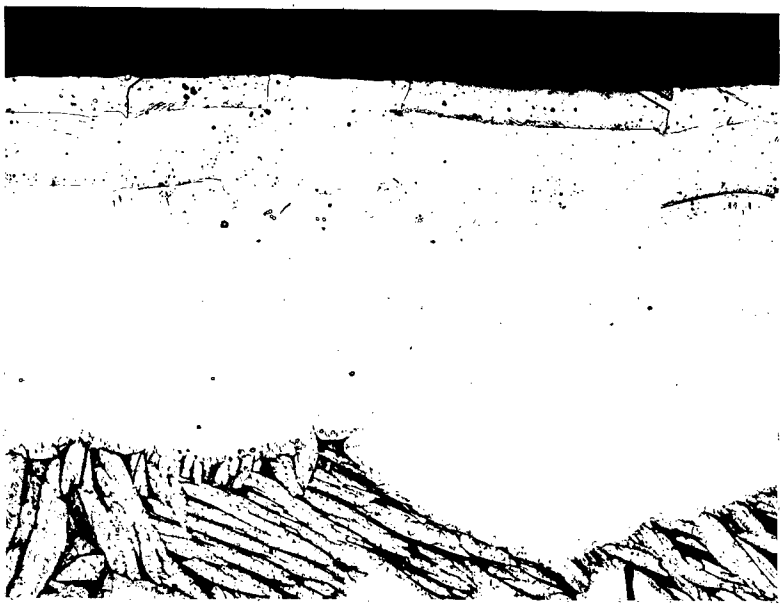

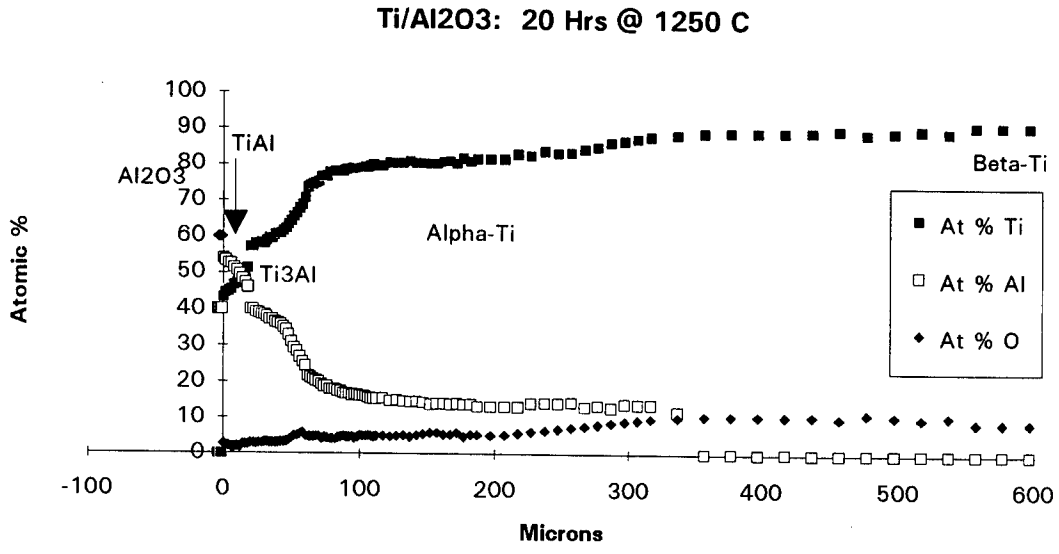

Figure 16. Ti/Al_2O_3 diffusion couple at 1250°C for 20 hours. **Top:** Optical micrograph (200X) showing the phases (top to bottom) Al_2O_3, γ-TiAl, α_2-Ti_3Al, α-Ti, and β-Ti. Dark region between Al_2O_3 and γ-TiAl due to separation at Al_2O_3 | Metal interface upon quenching. **Bottom:** EPMA results of analysis at University of Wisconsin-Madison.

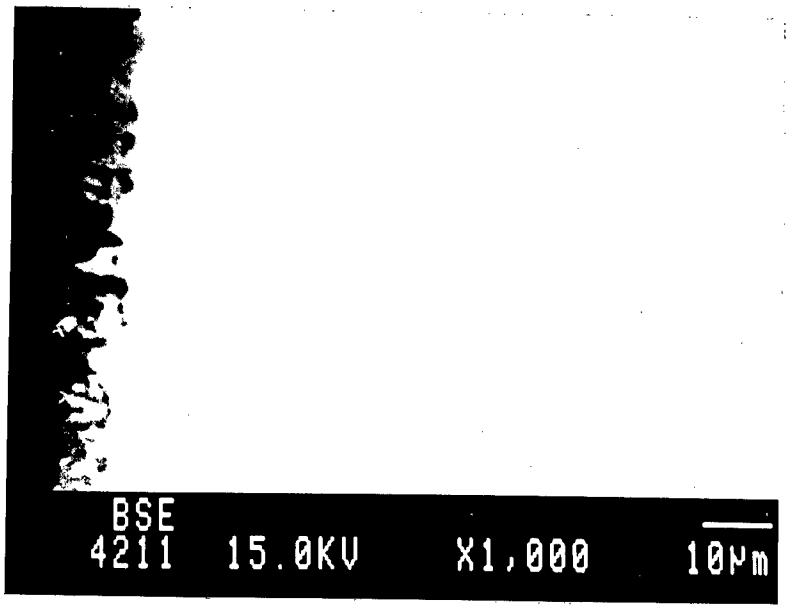

Figure 17. BSE image of microstructure after bonding, but prior to heat treatment. Phases shown include (left to right) Al_2O_3, γ-TiAl, α_2-Ti_3Al and α-Ti. The β-Ti region is not apparent due to slow cooling from 1050°C bonding temperature. Image shows non-planar γ-TiAl | α_2Ti_3Al interface.

Interface	$\gamma \mid Al2O3$	$\gamma \mid \alpha_2$	$\alpha_2 \mid \gamma$	$\alpha_2 \mid \alpha$	$\alpha \mid \alpha_2$	$\alpha \mid \beta$	$\beta \mid \alpha$
900°C/C_{Ti}	49.0 ± 2.2	---	---	74.0 ± 1.4	83.0 ± 2.2	96.0 ± 1.1	98.0 ± 1.1
C_{Al}	39.0 ± 4.1	---	---	18.0 ± 2.2	12.0 ± 3.2	0.0 ± 1.0	0.0 ± 1.0
C_O	12.0 ± 3.9	---	---	7.0 ± 2.7	6.0 ± 2.5	3.0 ± 2.5	2.0 ± 2.6
1000°C/C_{Ti}	50.0 ± 1.4	---	---	80.0 ± 3.2	89.0 ± 1.4	95.0 ± 1.4	96.0 ± 1.1
C_{Al}	46.0 ± 3.2	---	---	15.0 ± 3.2	7.0 ± 1.0	0.0 ± 1.0	0.0 ± 1.0
C_O	4.0 ± 4.7	---	---	5.0 ± 2.5	5.0 ± 2.7	5.0 ± 2.6	3.0 ± 2.6
1100°C/C_{Ti}	48.0 ± 2.2	52.0 ± 1.4	60.0 ± 1.4	71.0 ± 3.2	81.0 ± 4.1	93.0 ± 1.4	96.0 ± 1.4
C_{Al}	49.0 ± 1.4	45.0 ± 1.4	36.0 ± 1.4	23.0 ± 2.2	15.0 ± 3.2	1.0 ± 1.4	1.0 ± 1.4
C_O	4.0 ± 2.5	3.0 ± 2.5	4.0 ± 3.0	6.0 ± 3.2	5.0 ± 3.9	5.0 ± 2.7	3.0 ± 2.8
1144°C/C_{Ti}	46.9 ± 1.0	52.5 ± 1.2	60.0 ± 1.4	72.7 ± 1.1	78.3 ± 1.6	94.0 ± 1.4	96.8 ± 1.6
C_{Al}	49.3 ± 1.2	43.9 ± 1.5	36.4 ± 1.8	23.4 ± 1.5	18.4 ± 1.2	0.0 ± 1.0	0.0 ± 1.0
C_O	3.8 ± 2.6	3.7 ± 2.6	3.6 ± 2.7	3.9 ± 2.6	3.3 ± 2.6	5.9 ± 2.7	3.2 ± 2.8
1200°C/C_{Ti}	46.5 ± 1.0	50.8 ± 1.1	57.0 ± 1.6	74.1 ± 3.8	80.0 ± 2.8	---	---
C_{Al}	51.3 ± 1.0	46.9 ± 1.0	39.8 ± 2.5	21.9 ± 4.3	16.9 ± 4.1	---	---
C_O	2.3 ± 2.5	2.4 ± 2.6	3.2 ± 2.7	4.1 ± 2.5	3.2 ± 2.9	---	---
1250°C/C_{Ti}	43.3 ± 1.0	51.3 ± 1.0	57.1 ± 1.0	68.7 ± 1.0	73.6 ± 1.0	---	---
C_{Al}	53.9 ± 1.1	46.0 ± 1.0	40.0 ± 1.0	25.6 ± 1.0	21.6 ± 1.0	---	---
C_O	2.8 ± 2.5	2.7 ± 2.5	3.0 ± 2.5	5.7 ± 2.5	4.8 ± 2.5	---	---

Table 5. EPMA interface compositions from Ti/Al_2O_3 diffusion couple results (read: phase | neighboring phase). Compositions in atomic %.

5.1.2 Kinetics Results

The application of diffusion theory in evaluating the instability observed at $Ti|Al_2O_3$ interfaces requires that it be shown that diffusion is reaction controlling process. This is most readily done by demonstrating that the reaction between Ti and Al_2O_3 proceeds at a parabolic rate. Figures 18, 19, 20, 21, 22 and 23 show the growth rate for the reaction product phases γ-TiAl(O), α_2-Ti_3Al(O) and α-Ti(O) at 900, 1000, 1100, 1144, 1200 and 1250°C, respectively. These results were obtained by measuring the width of a phase (listed in Appendix B), W, using either optical micrographs or BSE images. Figures 18-23 show that at each temperature the phase growth is proportional to $\sqrt{t}$, indicating that diffusion is the rate controlling process in the reaction at $Ti|Al_2O_3$ interfaces. Although parabolic growth is observed, such plots are not an indicator of the rate controlling step in the reaction, nor the diffusion mechanism.

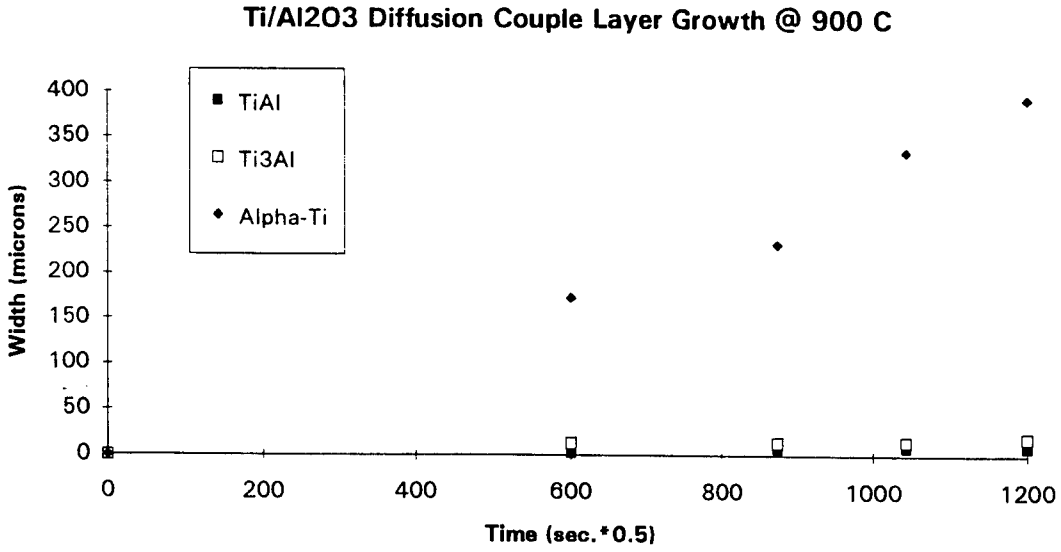

Figure 18. Growth of γ-TiAl(O), α_2-Ti_3Al(O) and α-Ti at 900°C. γ-TiAl(O): K= 8.37E-03 $\mu m/s^{-1/2}$, intercept= -0.82 μm, corr. coef.= 0.948. α_2-Ti_3Al(O): K= 1.48E-02 $\mu m/s^{-1/2}$, intercept= 1.21 μm, corr. coef.= 0.969. α-Ti: K= 3.21E-01 $\mu m/s^{-1/2}$, intercept= -12 μm, corr. coef.= 0.989.

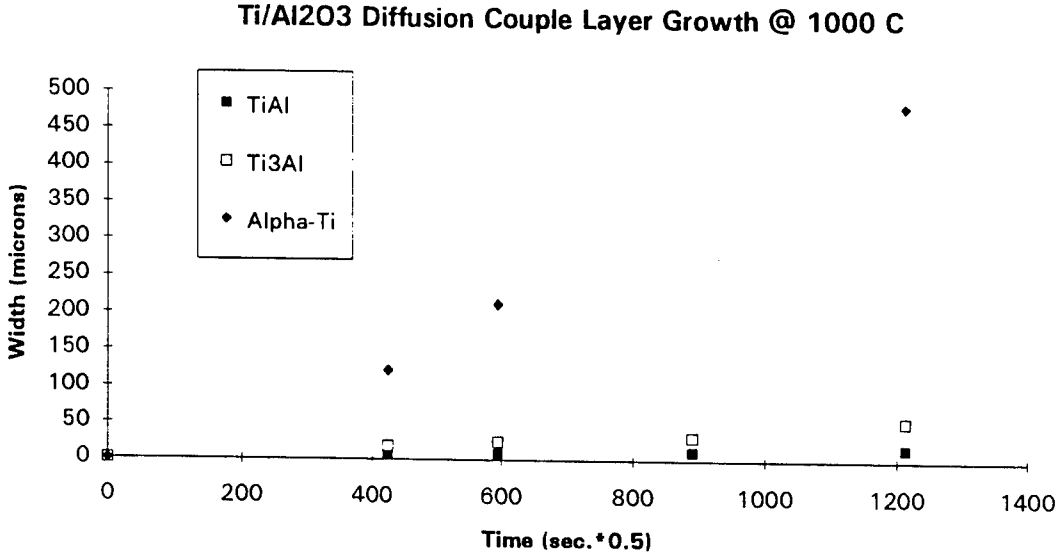

Figure 19. Growth of γ-TiAl(O), α_2-Ti_3Al(O) and α-Ti at 1000°C. γ-TiAl(O): K= 1.38E-02 μm/$s^{-1/2}$, intercept= 0.16 μm, corr. coef.= 0.998. α_2-Ti_3Al(O): K= 4.22E-02 μm/$s^{-1/2}$, intercept= -0.33 μm, corr. coef.= 0.987. α-Ti: K= 4.05E-01 μm/$s^{-1/2}$, intercept= -21.4 μm, corr. coef.= 0.994.

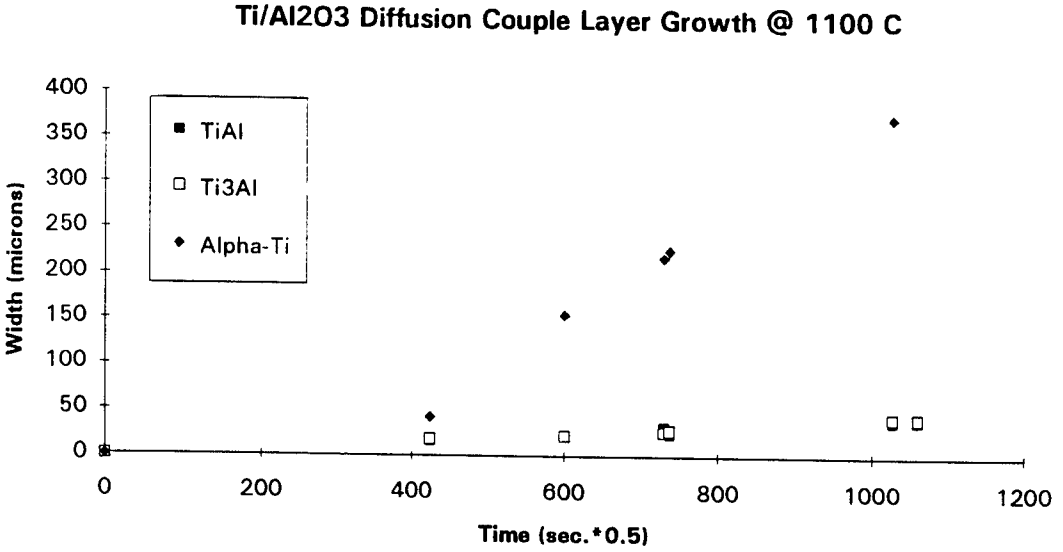

Figure 20. Growth of γ-TiAl(O), α_2-Ti_3Al(O) and α-Ti at 1100°C. γ-TiAl(O): K= 3.8E-02 μm/$s^{-1/2}$, intercept= -0.03 μm, corr. coef.= 0.984. α_2-Ti_3Al(O): K= 4.01E-02 μm/$s^{-1/2}$, intercept= -0.63μm, corr. coef.= 0.993. α-Ti: K= 3.71E-01 μm/$s^{-1/2}$, intercept= -48.3 μm, corr. coef.= 0.951.

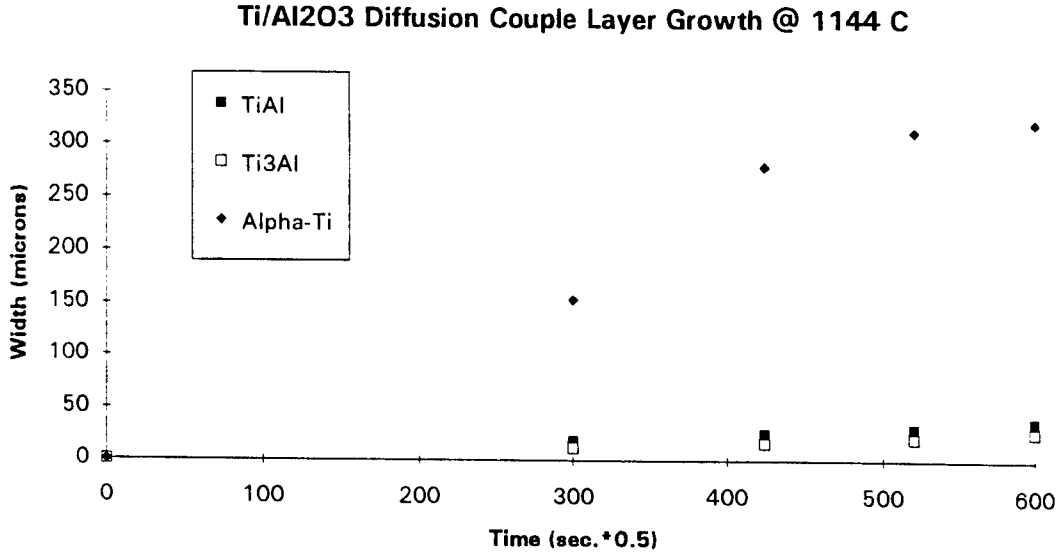

Figure 21. Growth of γ-TiAl(O), α_2-Ti_3Al(O) and α-Ti at 1144°C. γ-TiAl(O): K= 6.18E-02 μm/$s^{-1/2}$, intercept= 0.01 μm, corr. coef.= 0.999. α_2-Ti_3Al(O): K= 4.33E-02 μm/$s^{-1/2}$, intercept= -0.57 μm, corr. coef.= 0.995. α-Ti: K= 5.75E-01 μm/$s^{-1/2}$, intercept= 1.62 μm, corr. coef.= 0.984.

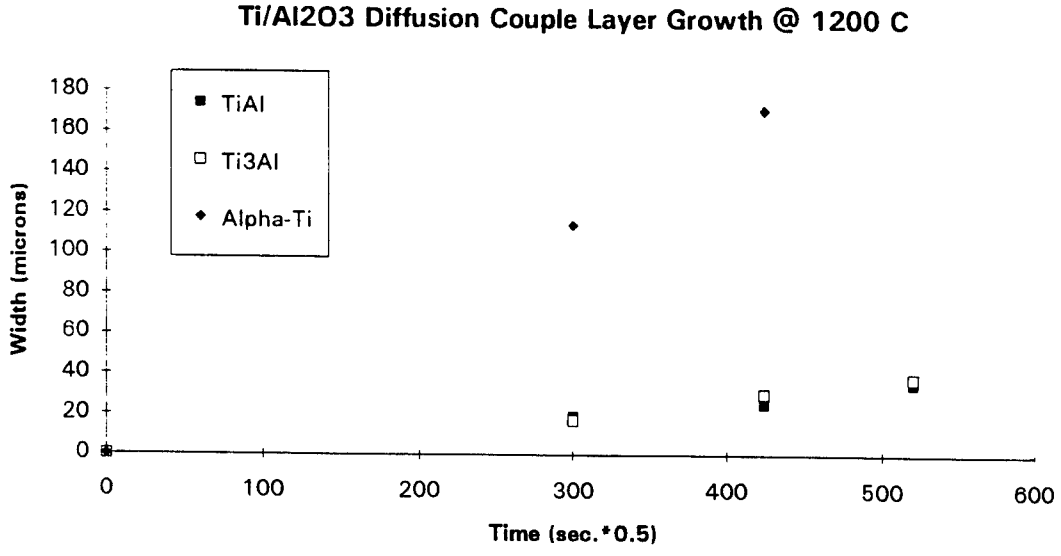

Figure 22. Growth of γ-TiAl(O), α_2-Ti_3Al(O) and α-Ti at 1200°C. γ-TiAl(O): K= 6.48E-02 μm/$s^{-1/2}$, intercept= -0.4 μm, corr. coef.= 0.994. α_2-Ti_3Al(O): K= 7.27E-02 μm/$s^{-1/2}$, intercept= -1.36 μm, corr. coef.= 0.990. α-Ti: K= 3.99E-01 μm/$s^{-1/2}$, intercept= -1.29 μm, corr. coef.= 0.999.

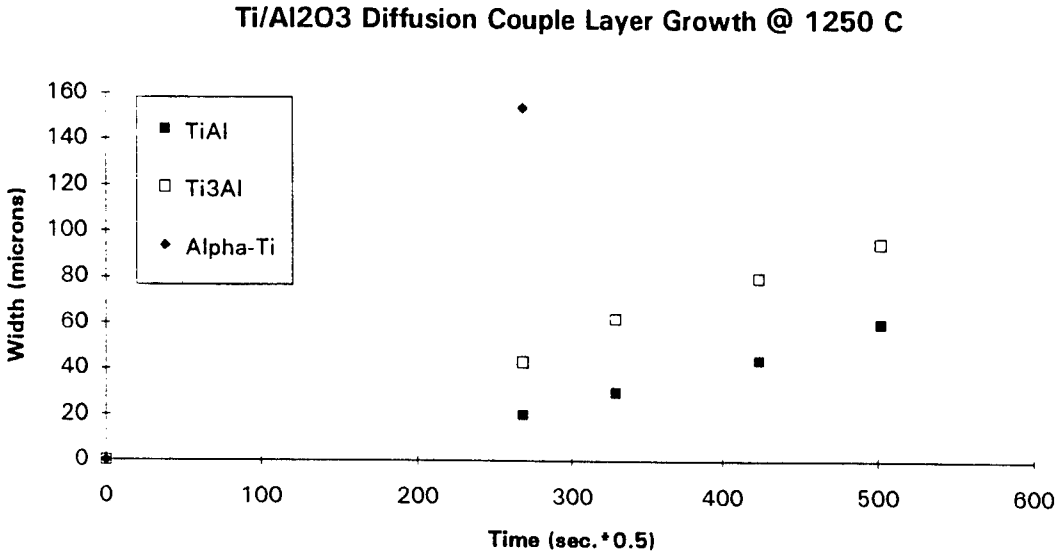

Figure 23. Growth of γ-TiAl(O), α_2-Ti_3Al(O) and α-Ti at 1250°C. γ-TiAl(O): K= 1.16E-01 μm/$s^{-1/2}$, intercept= -4.4 μm, corr. coef.= 0.972. α_2-Ti_3Al(O): K= 1.91E-01 μ m/$s^{-1/2}$, intercept= -2.15 μm, corr. coef.= 0.996. α-Ti: K= 5.75E-01 μm/$s^{-1/2}$, intercept= 0.0 μm, corr. coef.= 1.0.

From the discussion of interdiffusion in Ti-Al-O composites, Chap. 3, it is assumed that the mechanism by which Ti and Al diffuse is a substitutional one, whereas O diffuses by an interstitial mechanism. In diffusion controlled reactions, the reaction proceeds at a rate limited by the diffusion of the reactants. Since different elements diffuse at different rates, it is generally the slower diffusing species that controls the rate of a reaction. For the reaction observed in Ti/Al_2O_3, kinetic data is not available to explain the reaction creating the diffusion path β-Ti|α-Ti(O)|α_2-Ti_3Al(O)|γ-TiAl(O)|Al_2O_3 and thus must be determined. Although the determination of all the kinetic data necessary to prove certain the rate controlling step(s) in the reaction of Ti/Al_2O_3 couples is beyond the scope of this study a number of kinetic variables are calculated from the EPMA results in order to help understand the behavior of Ti/Al_2O_3 composites in the 900-1250°C temperature range. The variables include interdiffusion flux, intrinsic flux and interdiffusion coefficients.

The calculation of interdiffusion flux, $\tilde{J}$, was performed using the methodology present by Dayananda [79Day]. This method is a variation on the Boltzmann-Matano method and is ideally suited to calculation of $\tilde{J}$ from EPMA C(X) data. Figure 24 shows a typical plot of $\tilde{J}$ vs. X generated by this analysis. The results for all samples are given in Appendix C. Included in Fig. 24 is the summation of the individual $\tilde{J}$, and since it should equal zero, it is a good indicator of the quality of the EPMA data. Although different factors can contribute to poor results in the determination of $\tilde{J}$, and are given along with the EPMA results in Appendix C, the major factor is the high error associated with the analysis of oxygen by EPMA.

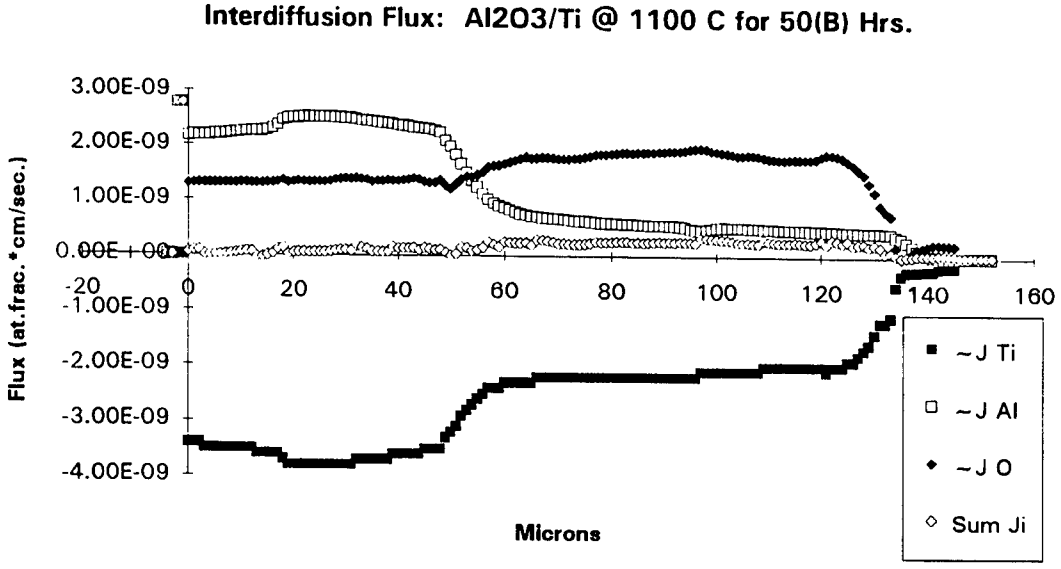

Figure 24. Calculated results for interdiffusion flux from EPMA results using the Boltzmann-Matano method.

Glover [92Glo] found that surface oxidation of samples prior to EPMA was a significant factor in oxygen determination, contributing as much as 3.0 at.% to standards of known oxygen analysis. Excess oxygen was not observed in analyzing TiO and Al_2O_3 standards but was observed when 99.99 % Ti was analyzed. This error in analysis of oxygen affects the calculation of $\tilde{J}$ by preventing the boundary value for C_O in the β-Ti phase from reaching $C_O(X=\infty) = 0$. Aside from the difficulties in accurately determining $\tilde{J}$, for Ti/Al_2O_3 couples, a noteworthy result of this calculation is that $|\tilde{J}_{Ti}|=|\tilde{J}_{Al}+\tilde{J}_O|$ and that the flux of Ti is counter to that of Al and O. Furthermore, comparison of the relative magnitudes for $\tilde{J}_{Ti}$, $\tilde{J}_{Al}$ and $\tilde{J}_O$ shows that Al is the slower diffusing species as measured from a laboratory reference. Intuitively, these results make sense in that $\tilde{J}_O$ should be greater than $\tilde{J}_{Al}$ given their different mechanism for diffusion, but these results do not directly indicate a rate controlling step in this diffusion reaction. In order to identify the rate controlling step requires knowledge of the intrinsic flux for Ti, Al and O, at the interfaces where it is assumed that the reactions occur in the formation of the phases γ-TiAl(O), α_2-Ti_3Al and α-Ti(O).

The determination of intrinsic flux values for the reaction observed in Ti/Al_2O_3 diffusion couples is not practical. Such a study would require knowledge of lattice translation within each phase of the reaction. Darken [48Dar] showed that intrinsic flux can be determined for binary single phase couples using inert markers to observe lattice motion, but no studies were found in the literature for ternary multi-phase couples. If a material could be identified as inert to Ti, Al and O and used in Ti/Al_2O_3 couples, such a marker would only provide intrinsic data in a single phase at the location of the marker. Therefore, such an analysis was only performed at the γ-TiAl(O)|α_2-Ti_3Al(O) interface in order to evaluate the non-planar nature of this interface below 1100°C. From the previous

discussion on interface morphology, the relative magnitudes for flux into an interface, in formation of a phase, is a determining factor in the type of interface morphology observed. Because of the lack of a marker at this interface, the interface itself was used as an indicator of lattice translation. Proof of the accuracy in using the interface as a marker is not provided since the intent of this analysis is only to obtain estimates for the intrinsic flux values for Ti and Al to the interface. Oxygen diffusion is not considered because its interstitial mechanism.

Determination of intrinsic flux at the γ-TiAl(O)|α_2-Ti_3Al(O) interface was performed for Ti/Al_2O_3 couples at 1100, 1144, 1200 and 1250°C. Because this interface is planar at these temperatures, and stability in composition and flux direction can be assumed. The results of this analysis are reflected in Fig. 25 which shows the dependency of the intrinsic flux ratio J_{Al}^{γ}: $J_{Ti}^{\alpha}2$, and the composition ratios C_{Al}^{γ}:C_{Ti}^{γ} and C_{Al}^{α} 2:$C_{Ti}^{\alpha}2$ on temperature. It is not known which phase forms at the γ-TiAl(O)|α_2-Ti_3Al(O) interface but these results indicate that the flux ratio is sufficient for the formation of either. Further, based on the criteria presented by Wagner [56Wag] that the flux of one component needs to be significantly greater than that of the other component ($J_A >> J_B$) in order for a non-planar interface to form, the ratio of J_{Al}^{γ}: $J_{Ti}^{\alpha}2$ shown in Fig. 25 is not significant enough to cause the non-planar morphology observed at 900 and 1000°C. Therefore, grain boundary diffusion can be assumed to be the cause of the is morphology.

The conclusion that grain boundary diffusion is resonsible for the morphology of the γ-TiAl|α_2-Ti_3Al interface observed at 900 and 1000°C is based upon an empirical rule

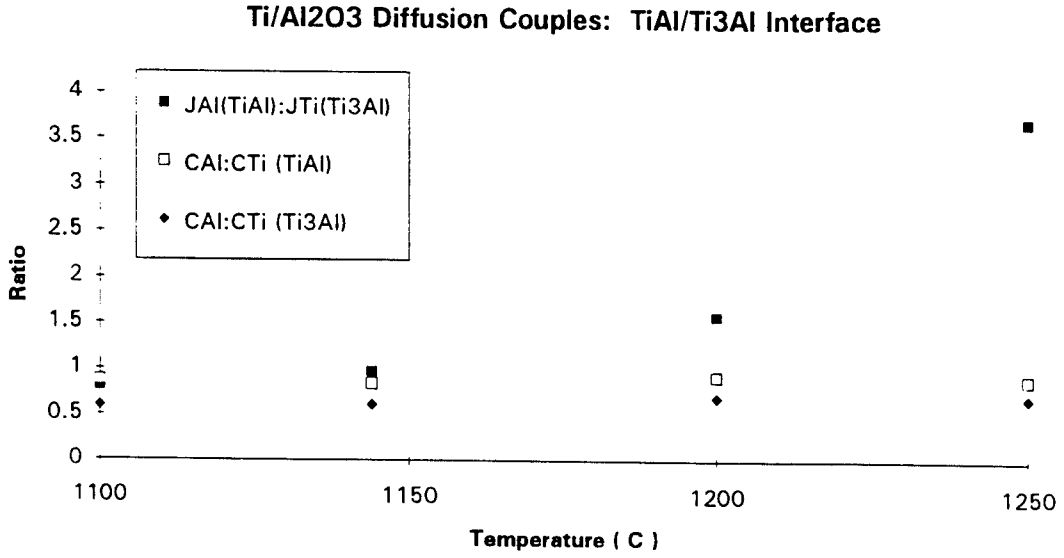

Figure 25. γ-TiAl | α_2-Ti_3Al interface results at 1100,1144, 1200 and 1250°C.

which predicts the domination of grain boundary diffusion over bulk diffusion below $0.7(T_m)$ for a given metal. Microstructural evidence for grain boundary diffusion in Figs. 11, 12 and 17 shows the γ-TiAl(O) phase to form into the metal from the Al_2O_3 along irregular networks. Broadening of the γ-TiAl(O) phase at the Al_2O_3 interface indicates the possibility of lateral diffusion away from grain boundaries. Since the initial grain size of the Ti-plate used to fabricated the Ti/Al_2O_3 couples is not known, it is not available as further microstructural evidence. The empirical rule presented was noted in the results of Hoffman and Turnbull [51Tur] in which poly-crystalline materials showed higher diffusivities at low temperature than did single-crystal materials. Convergence of the poly and single crystal results at ~$0.7(T_m)$ indicated this temperature to be the transition in dominance from grain-boundary diffusion to bulk diffusion. For titanium (T_m=1943 K) this transition would be expected to occur at ~1087°C, or just below 1100°C, which is the

temperature at which the γ-TiAl(O)|α_2-Ti_3Al(O) interface starts to show planar morphology.

Estimation of interdiffusion coefficients for Ti/Al_2O_3 couples was performed by two methods. In both methods composition dependency of the interdiffusion coefficient was significant but not taken into account. The interdiffusion coefficients reported are average values for the range of values calculated for each phase. The first method was a psuedo-binary estimation which neglected the presence of oxygen. The reasoning behind this approach was that a first order approximation for the coefficient $\tilde{D}$ could be determined and compared to existing Ti-Al binary data. Because of the low concentration level of oxygen compared to Ti and or Al, and because oxygen diffuses interstitially in (Ti,Al) alloys, oxygen was assumed to have a negligible effect on the interdiffusion of Ti and Al. In reducing the analysis to a binary problem, the Ti and Al composition data from EPMA were normalized with respect to (C_{Ti}+C_{Al}). This resulted in relatively small changes in the composition profiles and gradients for Ti and Al. The results of this analysis are shown in Tab. 6, and are consistent with the Ti-Al binary diffusion results available in the literature [73van, 85Hir, 93Meh].

Value\Phase	**γ-TiAl(O)**	**α_2-Ti_3Al(O)**	**α-Ti(O)**
$\tilde{D}o$ (cm^2/s)	6.62×10^{-4}	4.53×10^{-8}	1.62×10^{-2}
Q (KJ/mol)	177	77.8	195

Table 6. Psuedo-binary results for Ti/Al_2O_3 diffusion couples, Arrhenius function values.

The second method used to estimate the interdiffusion coefficient in Ti/Al_2O_3 couples was a ternary analysis which assumed little or no interaction between the diffusing species. Although this analysis is not comprehensive in that $\tilde{D}_{TiAl}$ and $\tilde{D}_{AlTi}$ are assumed to be negligible, it does estimate the primary coefficients $\tilde{D}_{TiTi}$ and $\tilde{D}_{AlAl}$. The results of this analysis are given in Appendix D, and summarized here in Tab. 7.

Since no sources of Ti-Al-O interdiffusion results are available in the literature, the accuracy of these results are not known. The error values reported in Tab. 7 are more of an indication of the composition dependency of $\tilde{D}_{ii}$ than a variance between samples. In comparison to the Ti-Al binary results available these results are also comparable. For γ-TiAl at 1144°C Hirano et al. [85 Hir] report a binary coefficient of $\sim 7 \times 10^{-11}$ cm^2/sec. For α_2-Ti_3Al at 1144°C Hirano et al. report a binary coefficient of $\sim 1 \times 10^{-10}$ cm^2/sec. Both of these reported values are within the range calculated for ternary coefficients, indicating that these results are acceptable. A noteworthy result of this analysis is that the activation energy for the interdiffusion of Al in each phase is nearly twice that of Ti, indicating a higher temperature dependency of $\tilde{D}_{AlAl}$. This result, together with the estimation of intrinsic flux at the γ-TiAl(O)|α_2-Ti_3Al(O) which showed Al to have a slightly higher flux than Ti, tend to indicate that Al may be more mobile than Ti in Ti/Al_2O_3 couples above 1100°C.

Temperature\Phase		γ-TiAl	α_2-Ti_3Al	α-Ti
1100°C	$\tilde{D}TiTi$	1.21±1.20 x 10^{-10} cm^2/s	8.06±11.4 x 10^{-11} cm^2/s	1.08±1.03 x 10^{-9} cm^2/s
	$\tilde{D}AlAl$	7.95±6.51 x 10^{-11} cm^2/s	3.70±4.05 x 10^{-11} cm^2/s	2.11±2.63 x 10^{-10} cm^2/s
1144°C	$\tilde{D}TiTi$	3.73±0.22 x 10^{-10} cm^2/s	1.32±0.93 x 10^{-10} cm^2/s	5.03±3.42 x 10^{-9} cm^2/s
	$\tilde{D}AlAl$	8.34±2.00 x 10^{-11} cm^2/s	3.77±2.47 x 10^{-11} cm^2/s	2.91±3.27 x 10^{-10} cm^2/s
1200°C	$\tilde{D}TiTi$	2.20±0.95 x 10^{-10} cm^2/s	1.86±1.44 x 10^{-10} cm^2/s	6.51±4.17 x 10^{-9} cm^2/s
	$\tilde{D}AlAl$	2.76±1.37 x 10^{-10} cm^2/s	2.08±1.64 x 10^{-10} cm^2/s	4.51±4.29 x 10^{-9} cm^2/s
Arrhenius Function Values				
$\tilde{D}o(Ti)$ =		5.39 x 10^{-7} cm^2/s	1.71 x 10-5 cm^2/s	2.39 x 10^2 cm^2/s
Q(Ti)=		92.4 KJ/mol	140 KJ/mol	295 KJ/mol
$\tilde{D}o(Al)$ =		9.33 x 10^{-3} cm^2/s	5.92 cm^2/s	1.37 x 10^{10} cm^2/s
Q(Al)=		214 KJ/mol	298 KJ/mol	525 KJ/mol

Table 7. Interdiffusion results for Ti/Al_2O_3 diffusion couples. These results are from samples: 50(B), 100(A), 100(B) and 148 hours @ 1100°C; 25, 50, 75 and 100 hours @ 1144°C; 25 and 50 hours @ 1200°C.

5.2 α_2-Ti_3Al/Al_2O_3 DIFFUSION COUPLES

Diffusion couples of α_2-Ti_3Al/Al_2O_3 were prepared and heat treated at 1100°C for times up to 195 hours. Only 1100°C was studied due to the difficulty in preparing these samples and the desire to concentrate on phase equilibria at this temperature. Unlike the γ-TiAl phase, it is believed that the solubility of oxygen in α_2-Ti_3Al is significant. The results of van Loo [92van] and Zhang [92Zha] show a maximum solubility in the range 10 -to- 15 at.% O at 1100°C. The original purpose of these sample was to help further

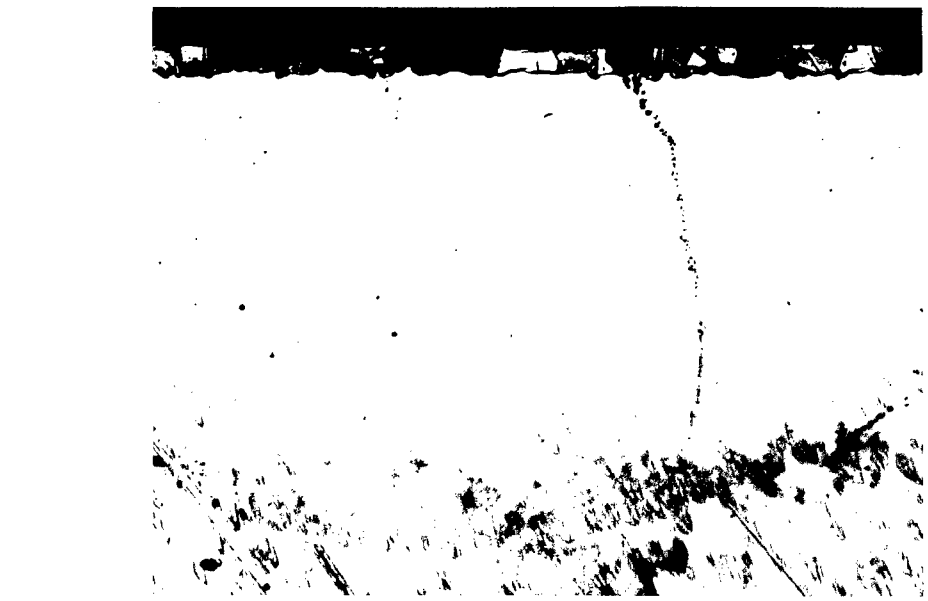

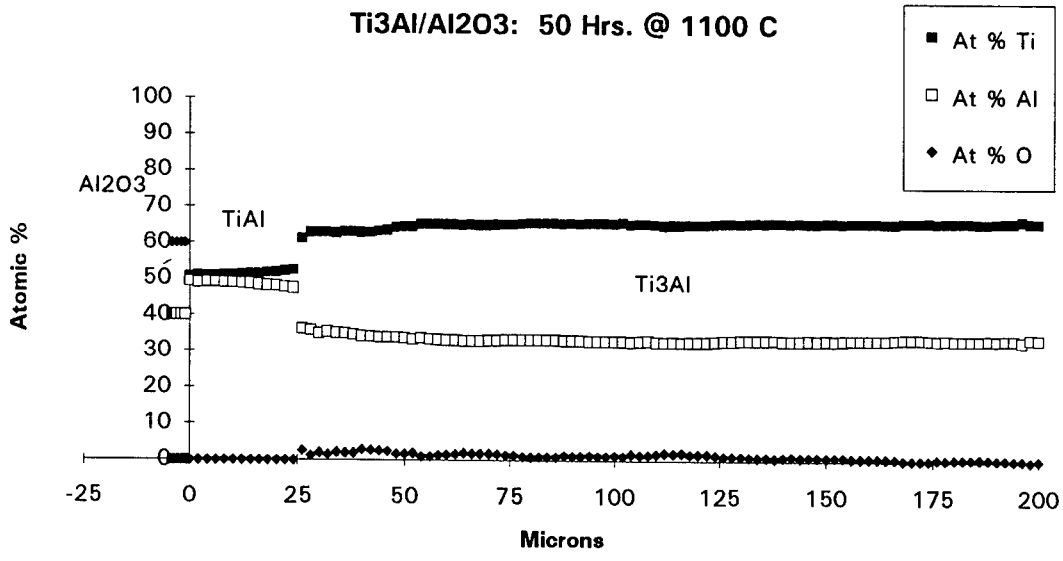

Figure 26. α_2-Ti_3Al/Al_2O_3 diffusion couple at 1100°C for 50 hours. **Top:** Optical micrograph (100X) showing the phases (top to bottom) Al_2O_3, γ-TiAl and α_2-Ti_3Al. **Bottom:** EPMA results of analysis at University of Wisconsin-Madison.

establish the solubility of oxygen in α_2-Ti_3Al. Instead, the kinetics of the reaction between α_2-Ti_3Al (Ti-35 at.% Al) and Al_2O_3 resulted in the formation of γ-TiAl(O) at the interface as shown by the metallograghy and EPMA results of Fig. 26. The EPMA results for all α_2-Ti_3Al/Al_2O_3 couples are given in Appendix A.

5.2.1 Thermodynamic Results

Although the results of these couples do not serve the intended goal of evaluating the maximum solubility of oxygen in α_2-Ti_3Al, the results do show that α_2-Ti_3Al and Al_2O_3 are reactive. Figure 26 shows that the resulting reaction in these couples is the diffusion path α_2-$Ti_3Al(O)|\gamma$-$TiAl(O)|Al_2O_3$. Because the interfaces in this diffusion path are planar, the EPMA results can be used to estimate two-phase equilibrium. These results are given in Tab. 8, and are used to estimate Ti-Al-O phase equilibrium in the conclusions.

Interface	$\gamma \mid Al_2O_3$	$\gamma \mid \alpha_2$	$\alpha_2 \mid \gamma$
C_{Ti}	49.7 ± 1.6	53.9 ± 2.2	61.1 ± 1.4
C_{Al}	50.1 ± 1.5	45.5 ± 3.3	35.8 ± 1.1
C_O	0.2 ± 2.5	0.6 ± 2.6	3.1 ± 2.4

Table 8. EPMA interface compositions from α_2-Ti_3Al/Al_2O_3 diffusion couple results at 1100°C (read: phase | neighboring phase). Compositions in atomic %.

5.2.2 Kinetic Results

The kinetics of the reaction between α_2-Ti_3Al and Al_2O_3 at 1100°C was analyzed for the parabolic growth of γ-TiAl(O) and the values $\tilde{J}i$ and $\tilde{D}ii$ for each couple. The layer thickness results, the $\tilde{J}i$ vs. X and the $\tilde{D}ii$ vs. X plots are given in Appendices B, C and D, respectively. The parabolic growth of the γ-TiAl(O) phase is shown in Fig.

27. Because the kinetics of the reaction indicate diffusion control, the interdiffusion coefficients for Ti and Al in γ-TiAl(O) have been determined assuming interaction between species is negligible. These results are $\tilde{D}_{TiTi} = 5.49 \pm 3.76 \times 10^{-13}$ cm^2/sec and $\tilde{D}_{AlAl} = 5.33 \pm 3.60 \times 10^{-13}$ cm^2/sec, and are based on the results of the 50 and 195 hour samples. The error values reported for $\tilde{D}_{TiTi}$ and $\tilde{D}_{AlAl}$ are the results of averaging $\tilde{D}_{ii}$ in each phase and thus reflect the composition dependency of $\tilde{D}_{ii}$.

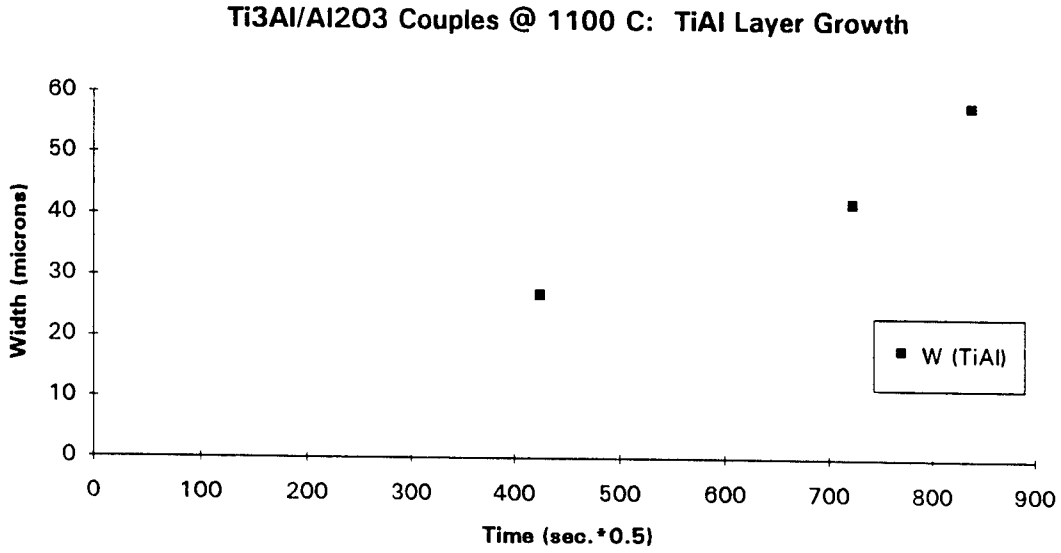

Figure 27. Growth of γ-TiAl(O) in α_2-Ti_3Al/Al_2O_3 couples at 1100°C. K= 6.53 μm/s$^{1/2}$, intercept= -0.65 μm, corr. coef.= 0.990.

5.3 γ-TiAl/Al_2O_3 DIFFUSION COUPLES

Diffusion couples of γ-TiAl/Al_2O_3 were prepared and heat treated at 1100°C for times up to 250 hours. Only 1100°C was studied due to the difficulty in preparing these samples and the desire to concentrate on phase equilibria at this temperature. No thermodynamic or kinetic data could be determined from these samples due to a lack of reaction between γ-TiAl and Al_2O_3. What can be said of these couples is that it is very

likely that two-phase equilibrium exists between these two phases. Figure 28 shows the metallographic and EPMA results for the 100 hour sample. EPMA results for all samples are given in Appendix A. From the EPMA results of Fig. 28 it is apparent that there may be some solubility of Al_2O_3 in γ-TiAl, but these results are not significant because of the error associated with EPMA. Figure 28 indicates that the composition of γ-TiAl at the γ-TiAl | Al_2O_3 interface is Ti-47 at.% Al-6 at.% O, and is a change from the original Ti-50 at.% Al alloy composition. The oxygen analysis of this sample is quite high, compared to the 0 -to- 4 at.% O indicated by the other samples, and is probably in error. As a results, the Ti and Al compositions are low because of the assumption $C_{Ti} + C_{Al} + C_O = 1$. Better EPMA results were obtained for the other samples.

5.4 α_2-$Ti_3Al(O)$ PHASE EQUILIBRIA SAMPLES

Metallography and EPMA results of Ti/Al_2O_3 diffusion couples treated at 1200 and 1250°C indicated the presence of the phase α_2-$Ti_3Al(O)$ as a region in the diffusion path of these couples. These results are consistent with the presence of this phase in Ti/Al_2O_3 couples in the temperature range 900 -to- 1144°C, but is contradictory to the binary Ti-Al phase diagram which indicates that the maximum stable temperature of this phase to be ~1164°C. As a phase in Ti/Al_2O_3 diffusion couples, α_2-$Ti_3Al(O)$ indicates the presence of 3 -to- 8 at.% O. To study if oxygen has a stabilizing effect on this phase, samples of compositions described in section 4.3.2.1 were prepared. Samples of each material, binary, 3 at.% O and 8 at.% O, were heated to 1200°C and 1250°C, within the α -Ti region of the Ti-Al binary diagram, and then quenched in water. This was done in an effort to retain the high temperature structure for analysis by XRD at room temperature. Figures 29 and 30 show the X-ray results for each sample quenched from 1200 and 1250° C, respectively.

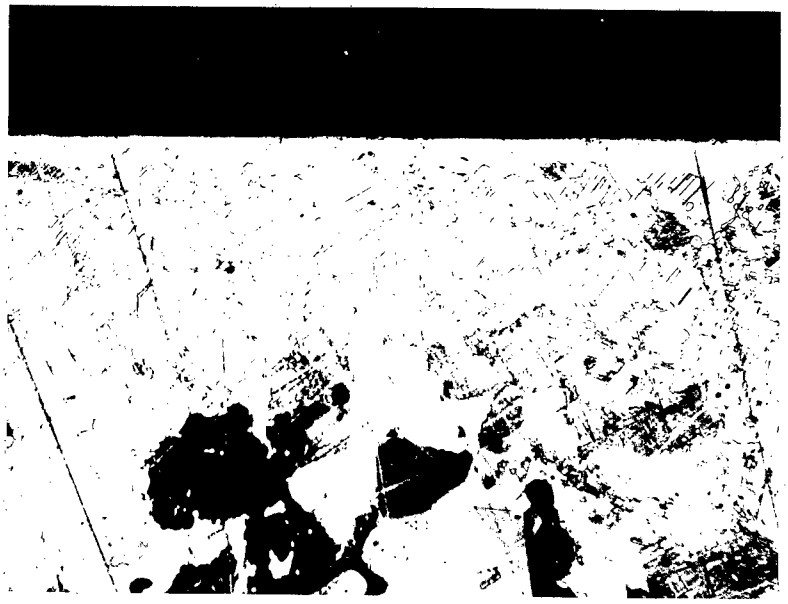

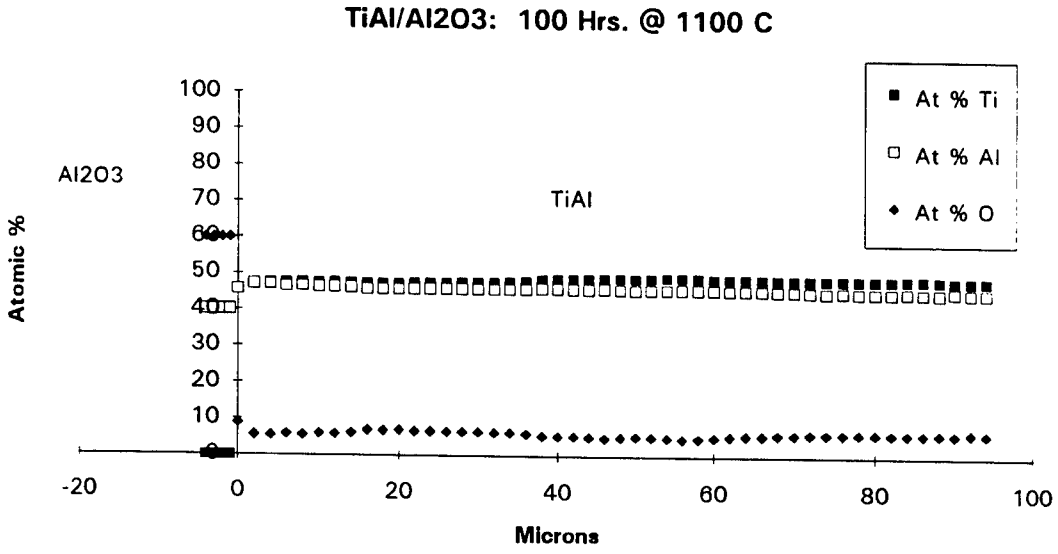

Figure 28. γ-TiAl/Al_2O_3 diffusion couple at 1100°C for 100 hours. **Top:** Optical micrograph (100X) showing the phases (top to bottom) Al_2O_3 and γ-TiAl. **Bottom:** EPMA results of analysis at University of Wisconsin-Madison.

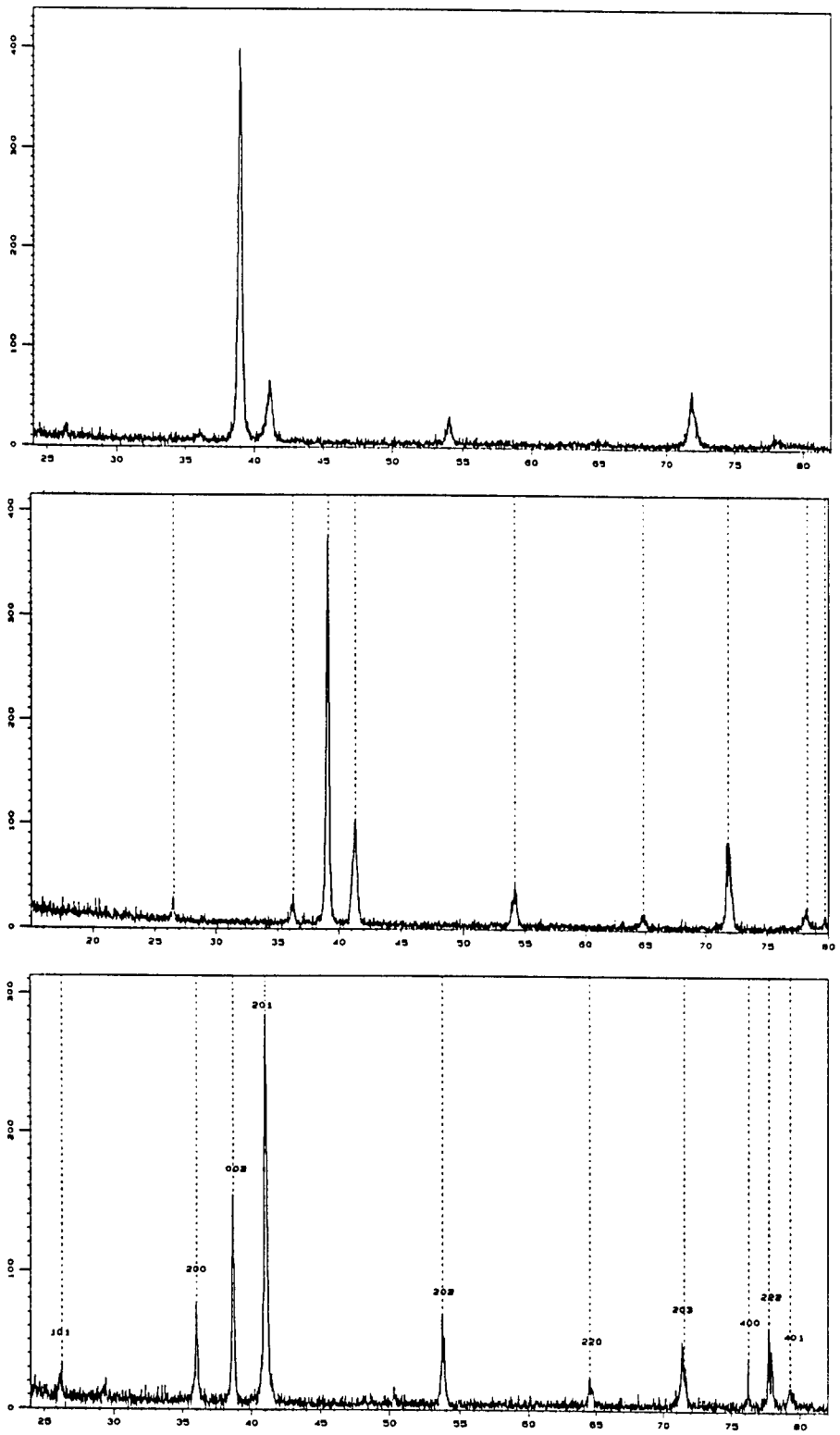

Figure 29. XRD spectrums for samples quenched from 1200°C. **Top:** Ti-34 at.% Al. **Middle:** Ti-34.5 at.% Al-3 at.% O. **Bottom:** Ti-31 at.% Al-8 at.% O.

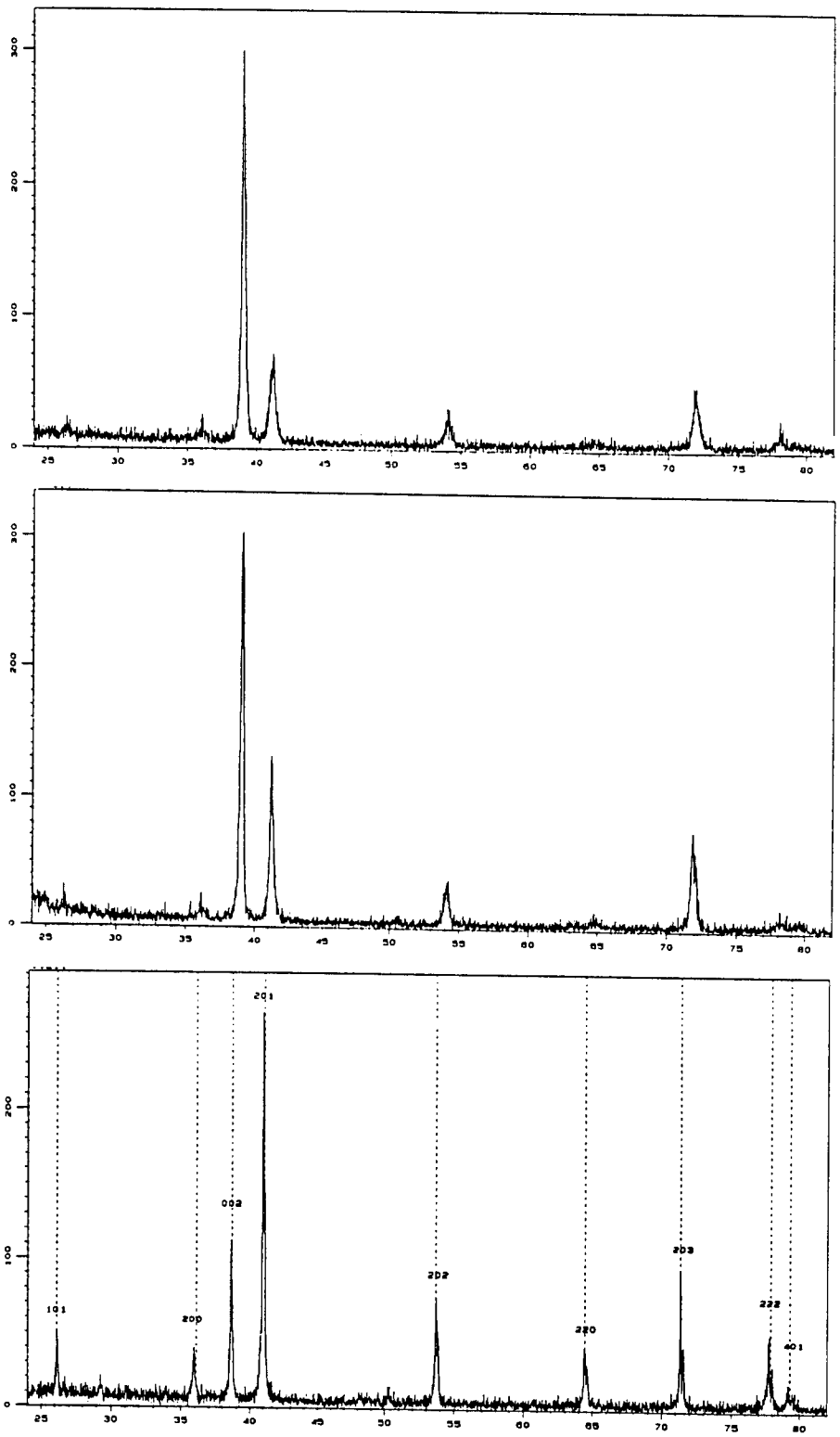

Figure 30. XRD spectrums for samples quenched from 1250°C. **Top:** Ti-34 at.% Al. **Middle:** Ti-34.5 at.% Al-3 at.% O. **Bottom:** Ti-31 at.% Al-8 at.% O.

Figures 29 and 30 show similar results for both temperatures. The major difference observed is that the spectrum for the 8 at.% O sample differs from that of the binary and the 3 at.% O samples, which are similar. The peaks of the 8 at.% O samples have been labeled because these patterns match the DO_{19} (ordered hcp) structure (JCPDS 14-451) of α_2-Ti_3Al reported by Goldak and Parr [61Gol]. The patterns for the binary and 3 at.% O samples show many of the peaks associated with the DO_{19} structure, but differ significantly in relative peak intensity. The α_2-Ti_3Al and α-Ti (JCPDS 5-682) phases can be distinguished by the presence of the $\alpha_2(101)$ peak. The binary an 3 at.% sample patterns indicate this peak but it is poorly defined, especially in the binary samples. This may be do to transformation of the α-Ti structure to the DO_{19} structure upon quenching. This transformation is dependent upon diffusion and may not have been completed due to the rapid quench. However, annealing of the samples quenched from 1200°C for 115 hours at 800°C did not significantly change any of the patterns, except for some refinement of the peaks.

Since the room temperature structure for all three of these samples is likely to be the DO_{19}, these results are not conclusive as to whether or not oxygen has a stabilizing effect on α_2-Ti_3Al. If α_2-Ti_3Al is not stabilized by oxygen the question can be raised pertaining to why the 8 at.% O samples showed the DO_{19} structure while the binary and 3 at.% O samples did not. Yet, these X-ray results, together with the metallographic and EPMA evidence, do suggest that α_2-Ti_3Al is stabilized by the addition of oxygen, and that stabilization lies somewhere between 3 and 8 at.% O in the temperature range 1200 - to- 1250°C. In order to resolve this issue, high temperature XRD is necessary.

5.5 γ-TiAl(O) PHASE EQUILIBRIA SAMPLES

Due to the potential of γ-TiAl as a metal matrix material, investigation into the solubility of oxygen in this phase was necessary. EPMA results for the solubility of oxygen in γ-TiAl contradicted an initial estimate of <1 at.% O solubility. Therefore, a study utilizing Atom-Probe Field Ion Microscopy (APFIM) was performed with the cooperation of Dr. M.K. Miller, Oak Ridge National Laboratories, Oak Ridge, TN. For this study, the intent was to prepare samples super-saturated in oxygen content by arc-melting, and then precipitate out Al_2O_3 during an equilibrium type anneal at 1100°C. Once equilibrium fractions of Al_2O_3 and γ-TiAl(O) existed in the samples, the γ-TiAl(O) matrix was to be analyzed by APFIM. The samples of this study are described in detail in section 4.3.2.2.

Figure 31 shows the microstructure of an annealed γ-TiAl(O) sample containing 2 at.% O. This sample shows Al_2O_3 precipitates (dark gray) dispersed throughout the γ-TiAl matrix. A third phase not identified in this study, probably α_2-Ti_3Al, may also be present in this sample as evident by the small regions which are light gray in appearance. Kawabata et al. [92Kaw] noted the presence of only α_2-Ti_3Al in γ-TiAl samples containing 0.08 and 0.72 at.% O and a Ti:Al ratio of ~1. This identification came as a result of XRD analysis of annealed samples prepared for mechanical testing. In addition, they also report that the solubility limit of oxygen in γ-TiAl decreased with increasing Al content. Therefore, it is likely that the sample of Fig. 31 is of a three-phase composition. This indicates that, at 1100°C, the boundary which separates the two-phase region α_2-Ti_3Al+γ-TiAl and three-phase region α_2-Ti_3Al+γ-TiAl+Al2O3 in ternary space lies somewhere between 0.72 and 2.0 at.% O.

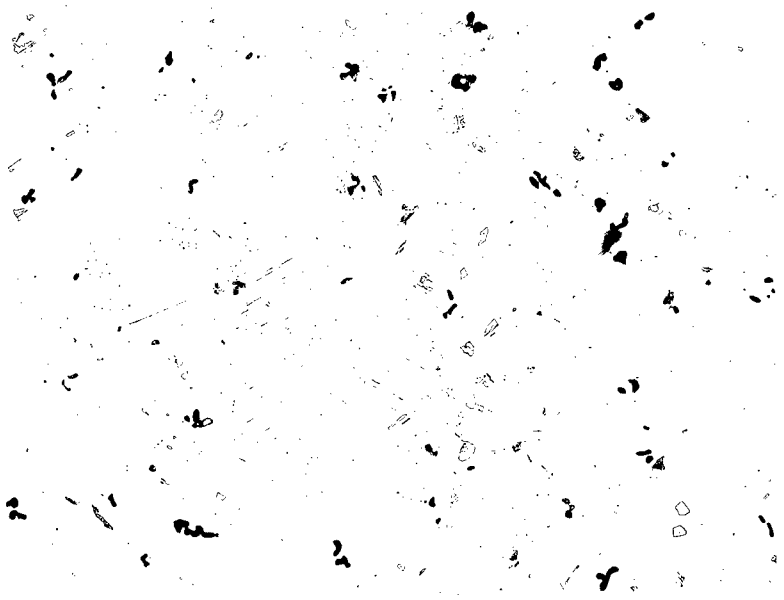

Figure 31. Optical micrograph of the Ti-49 at.% Al-2 at.% O sample annealed at 1100° C. Al_2O_3 precipitates (dark gray) in γ-TiAl matrix. 200X.

In the process of preparing samples for APFIM it was determined that the samples containing 2 at.% O and the 1 at.% O were to high in Al_2O_3 volume fraction to permit electro-polishing for analysis. Two samples containing 0.5 at.% O were analyzed by Dr. Miller. The first sample analyzed was all γ-TiAl, and gave an oxygen content of 608 ± 200 at. ppm. This result is in agreement with that of Huguet and Menand [94Hug] who found the solubility of oxygen in γ-TiAl(O) at 1000°C to be 300 ± 150 at. ppm. Their results came from an extensive study of both single phase γ-TiAl samples ($Ti_{48}Al_{52}$) ranging in oxygen contents from high purity γ-TiAl to 2 at.% O, and two-phase γ-TiAl+α_2-Ti_3Al samples ($Ti_{52}Al_{48}$ and $Ti_{54}Al_{46}$) of normal impurity level (~2500 at.ppm O). The

second sample analyzed by Dr. Miller was found to be two-phase, γ-TiAl+α_2-Ti_3Al. A short analysis of the α_2-Ti_3Al phase gave ~5 at.% O, but is not statistically quotable since it was based on only 300 atoms. Results by Huguet and Menand showed an oxygen content in α_2-Ti_3Al at 1000°C of 15000 ± 900 at. ppm. Combined, these three studies show that α_2-Ti_3Al+γ-TiAl two-phase equilibria is stable to $Ti_{48}Al_{52}$, and that the solubility limit for oxygen in γ-TiAl is between 300 and 600 at. ppm.

6.0 CONCLUSIONS

In this thesis, two basic considerations are discussed in relation to the interfacial stability of the ideal composite systems Ti/Al_2O_3, α_2-Ti_3Al/Al_2O_3 and γ-$TiAl/Al_2O_3$. The first of these considerations is the importance of thermodynamic phase equilibria in both choosing composite materials and in explaining the interfacial stability observed at composite interfaces. As a result of this study, and the work of previous studies [85Wri, 87Mur, 92Kat, 73Tre, 90DeK, 92Li, 92Zha, 92Kaw, 94Hug], Ti-Al-O phase equilibria can be estimated at 900, 1000, 1144, 1200 and 1250°C and better estimated at 1100°C. Figures 32-37 show the phase relations of the Ti-Al-O system at these temperatures for oxygen concentrations <60 at.%. These ternary isothermal sections are in general agreement with those presented by Li et al. [92Li] and Zhang et al. [92Zha], except in the γ-TiAl region. This study has demonstrated that at 1100°C the solubility limit of oxygen in γ-TiAl is <0.5 at.%. This level is believed to be valid over the entire temperature range studied for the atomic ratio Ti:Al=1. In addition, evidence was presented which indicates that oxygen has a stabilizing effect on the phase α_2-Ti_3Al (DO_{19}) to temperatures in excess of the binary congruent temperature. This is demonstrated in Fig.'s 36 and 37 by an isolated α_2-Ti_3Al region in ternary space.

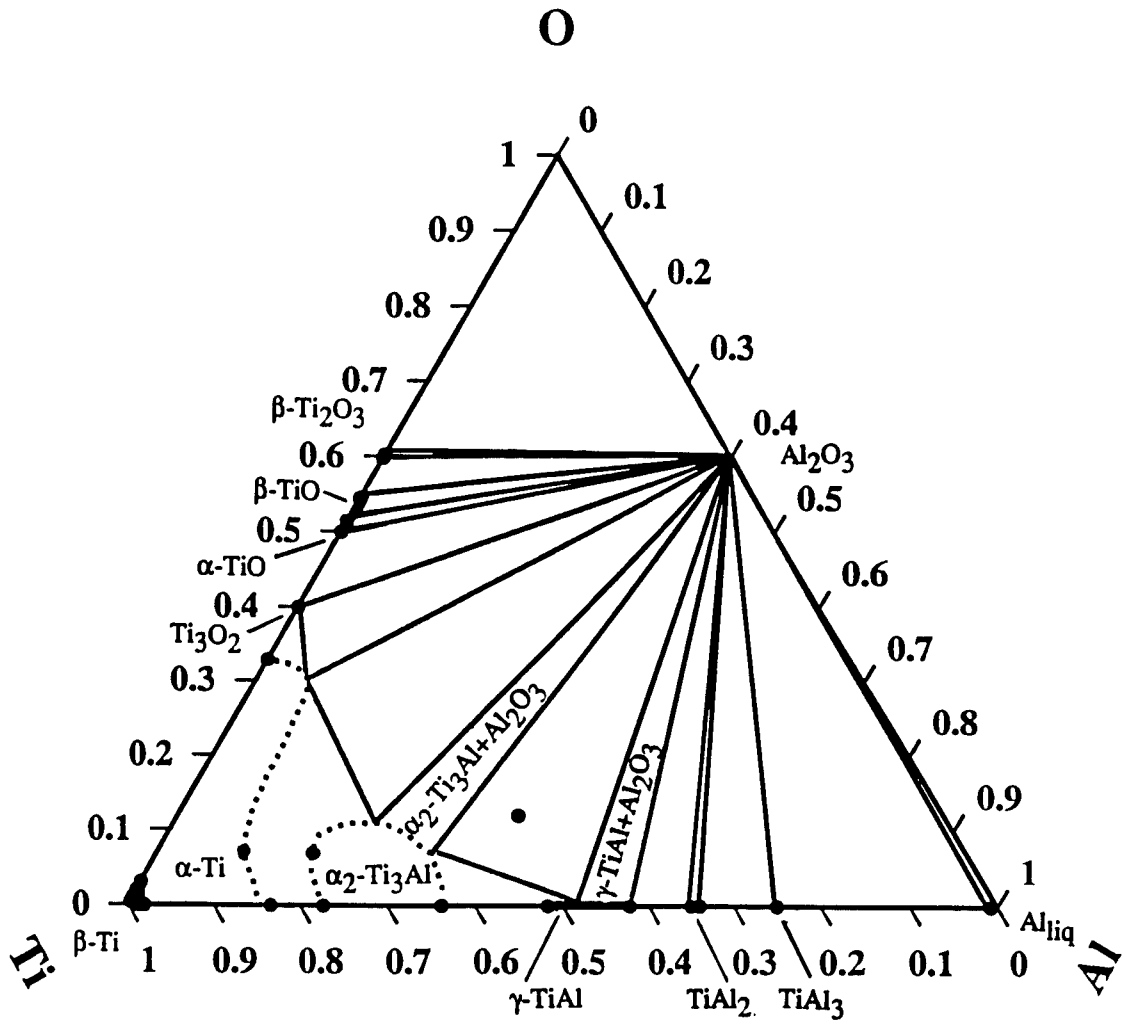

Figure 32. Ti-Al-O phase equilibrium at 900°C. Atomic fractions.

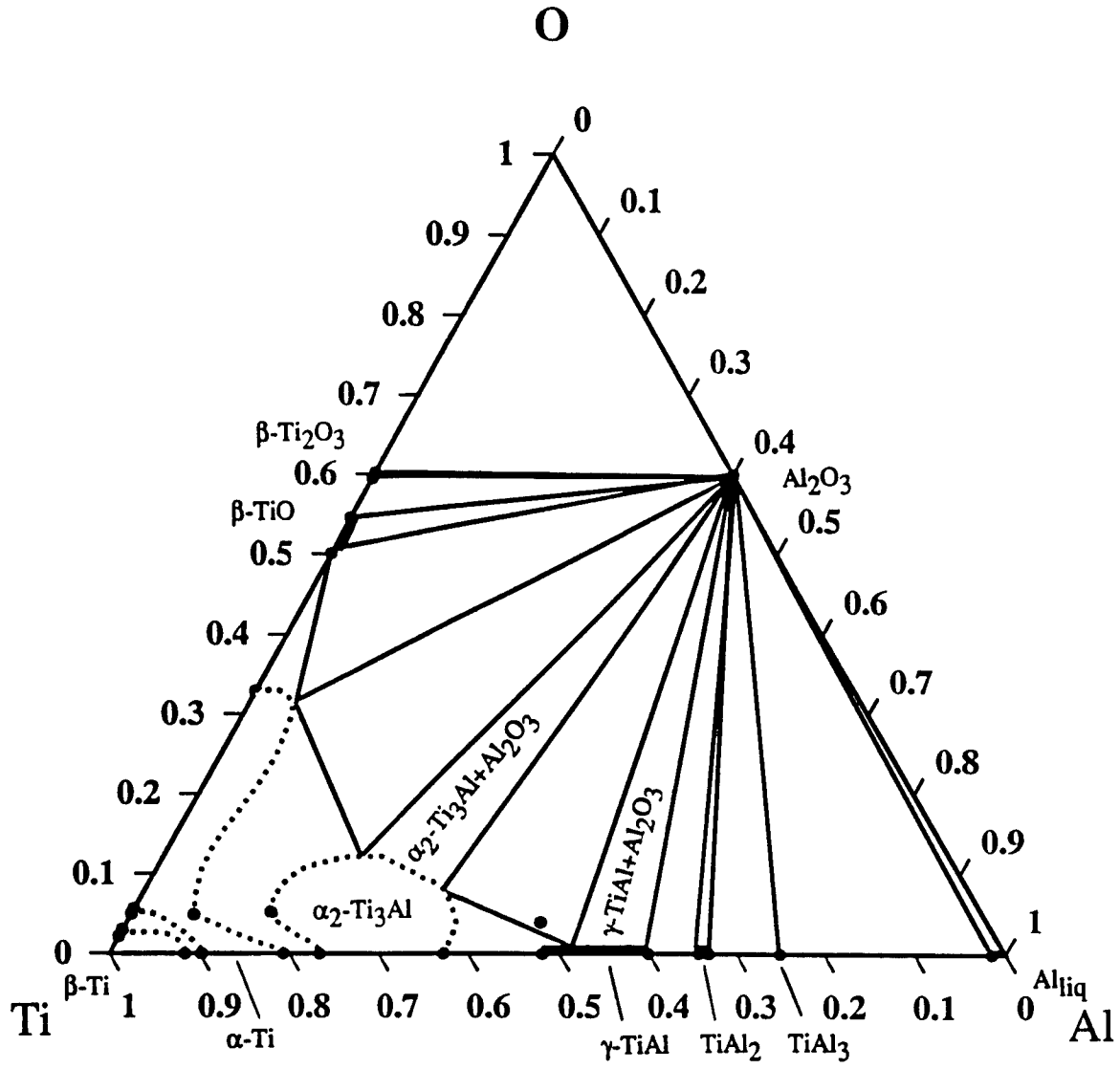

Figure 33. Ti-Al-O phase equilibrium at 1000°C. Atomic fractions.

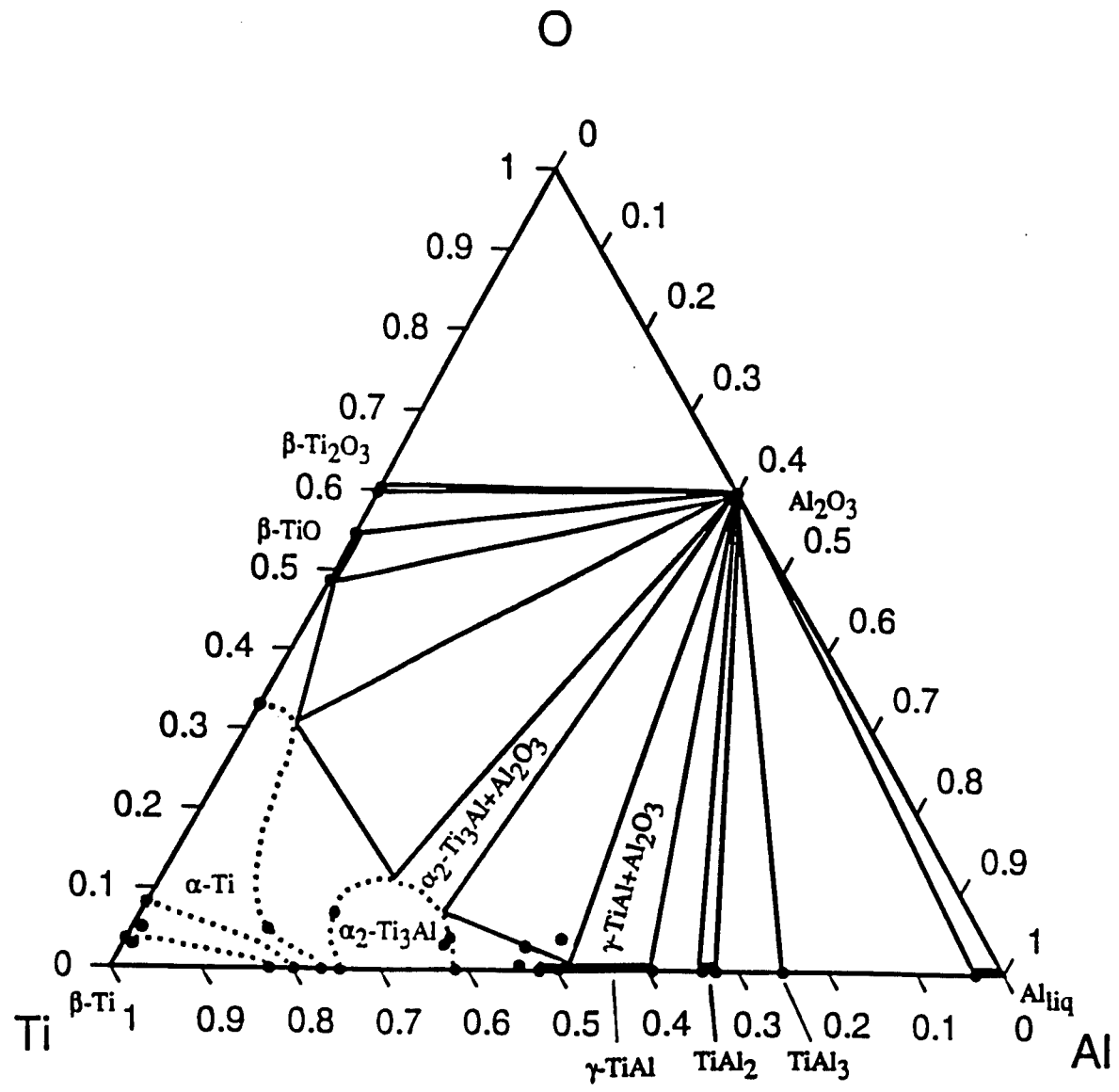

Figure 34. Ti-Al-O phase equilibrium at 1100°C. Atomic fractions.

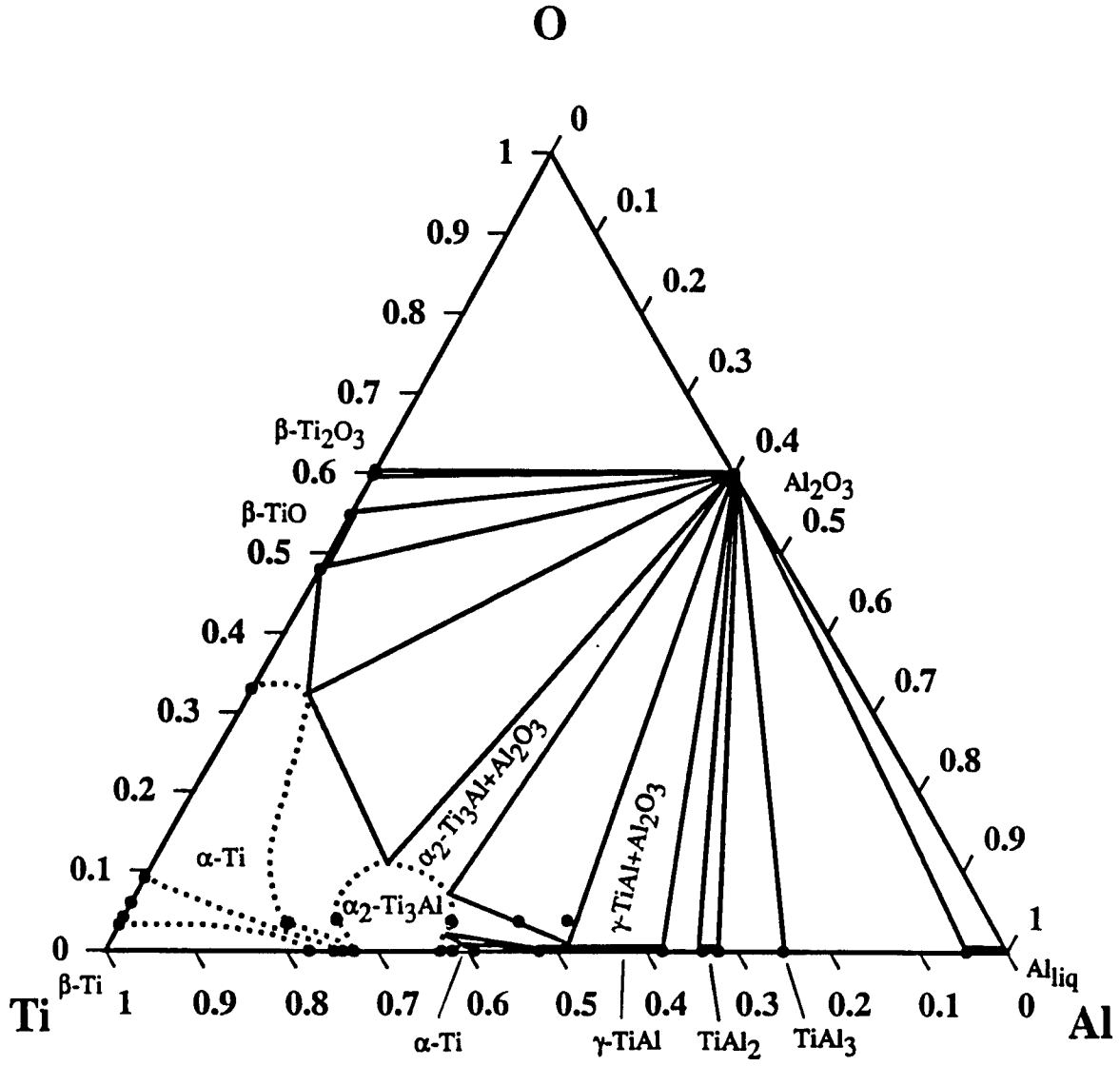

Figure 35. Ti-Al-O phase equilibrium at 1144°C. Atomic fractions.

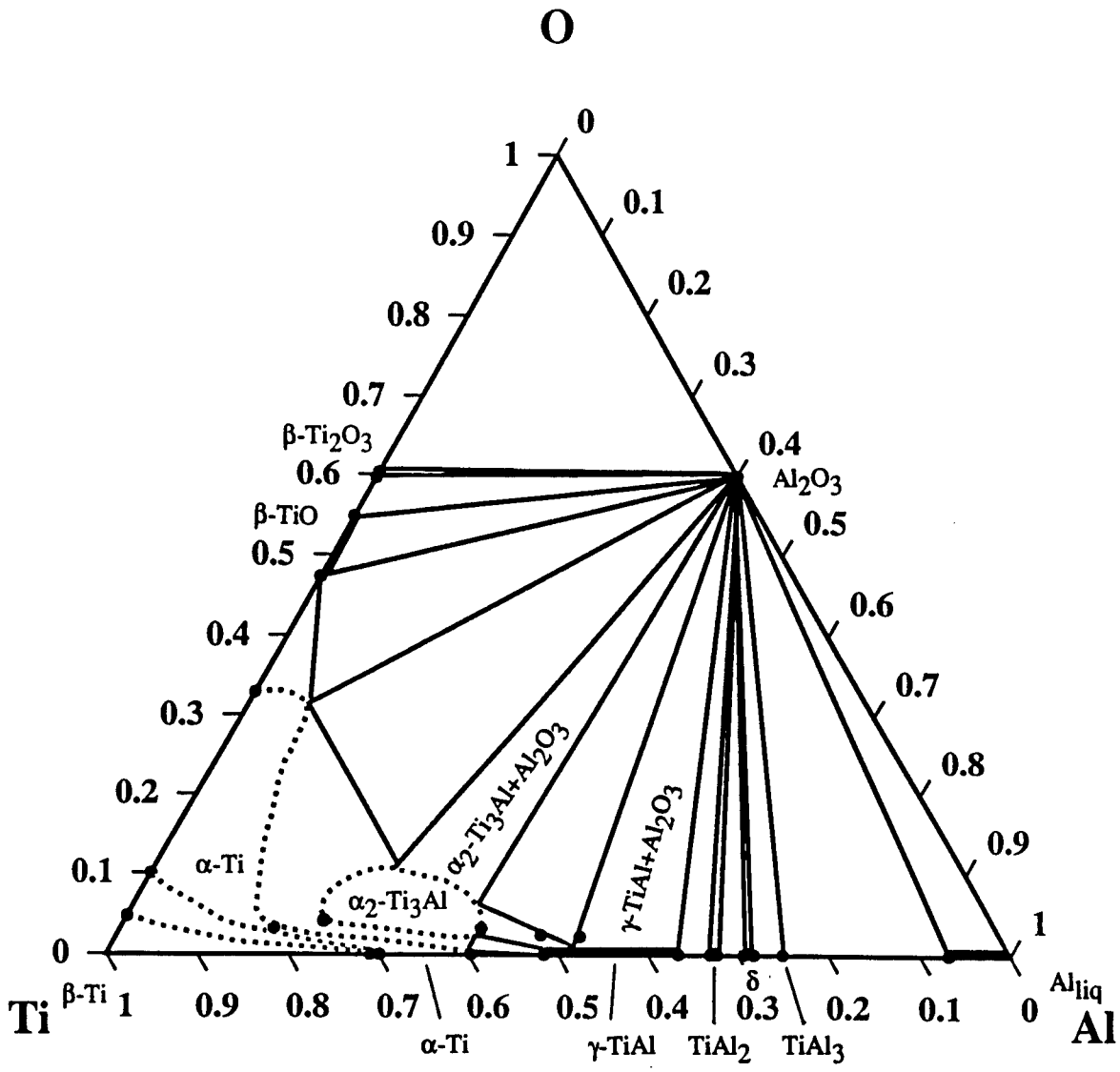

Figure 36. Ti-Al-O phase equilibrium at 1200°C. Atomic fractions.

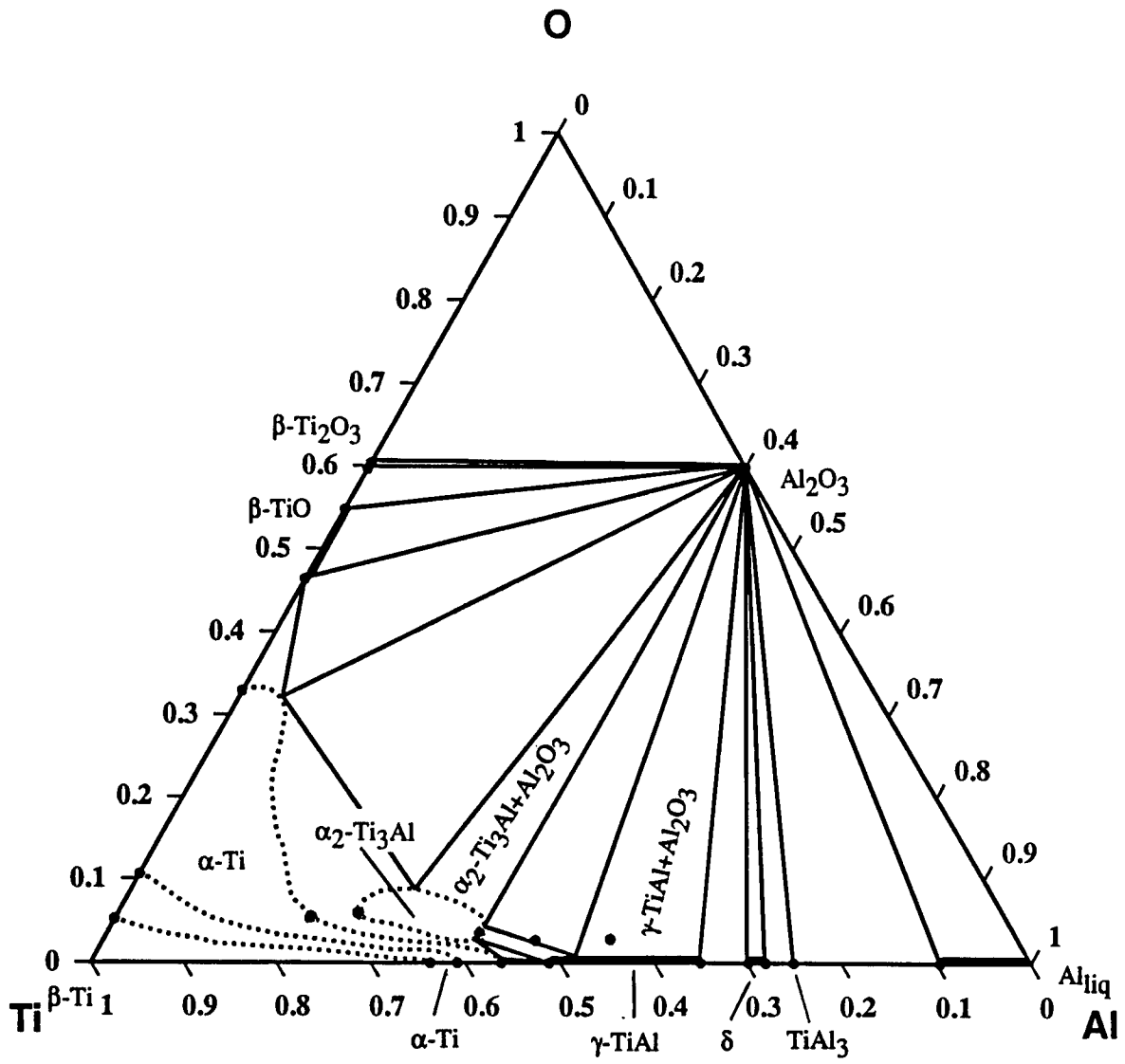

Figure 37. Ti-Al-O phase equilibrium at 1250°C. Atomic fractions.

The second consideration addressed was the kinetics of interfacial instability. With the presentation of Fig.'s 32-37, it is clear that all Ti, α_2-Ti_3Al and γ-TiAl binary matrices are not in equilibrium with Al_2O_3. Each of the systems studied were found to react at the metal|oxide interface at a rate consistent with diffusion controlled kinetics. For Ti/Al_2O_3 diffusion couples, Class III interfaces were observed over the entire 900 -to- 1250°C temperature range, characterized by the diffusion path β-Ti|α-Ti|α_2-Ti_3Al|γ-TiAl|Al_2O_3. The presence of a non-planar interface between α_2-Ti_3Al and γ-TiAl at 900 and 1000°C could not be shown to be the result of bulk-diffusion kinetic as first hypothesized. Instead, it is concluded that grain-boundary diffusion is the mechanism dominant in this region of the diffusion path. In this same region of the diffusion path, Al was found to be the more mobile than Ti over the temperature range 1100 -to- 1250°C. Given this result, the EPMA evidence and the assumption that product phase growth occurs due to reactions at interfaces; α-Ti, α_2-Ti_3Al and γ-TiAl are believed to form at the α-Ti|β-Ti, α_2-Ti_3Al|α-Ti and γ-TiAl|α_2-Ti_3Al interfaces, respectively. In addition, given the considerations presented by Lin et al. [89Lin], the sequence in which these phases form is: 1) α-Ti, 2) γ-TiAl and 3) α_2-Ti_3Al. The growth of each of these phases follows parabolic kinetics, as shown in Fig.'s 18-23. Figure 38 shows how well the parabolic constants determined estimate the total reaction with respect to time at 900 and 1000°C. These temperatures are of importance because this is the range used in the consolidation of composites of alpha and beta Ti matrices. Because oxygen levels less than ~3 at.% could not be measured with certainty by EPMA, the penetration of oxygen into β-Ti is not reported in this thesis or accounted for in Fig. 38. Interdiffusion coefficients were calculated for the diffusion of titanium and aluminum in α-Ti, α_2-Ti_3Al and γ-TiAl. These results are presented in Tab's 6 and 7, and are comparable to binary values reported in the literature.

These coefficient values were determined so that they would be available for future reference.

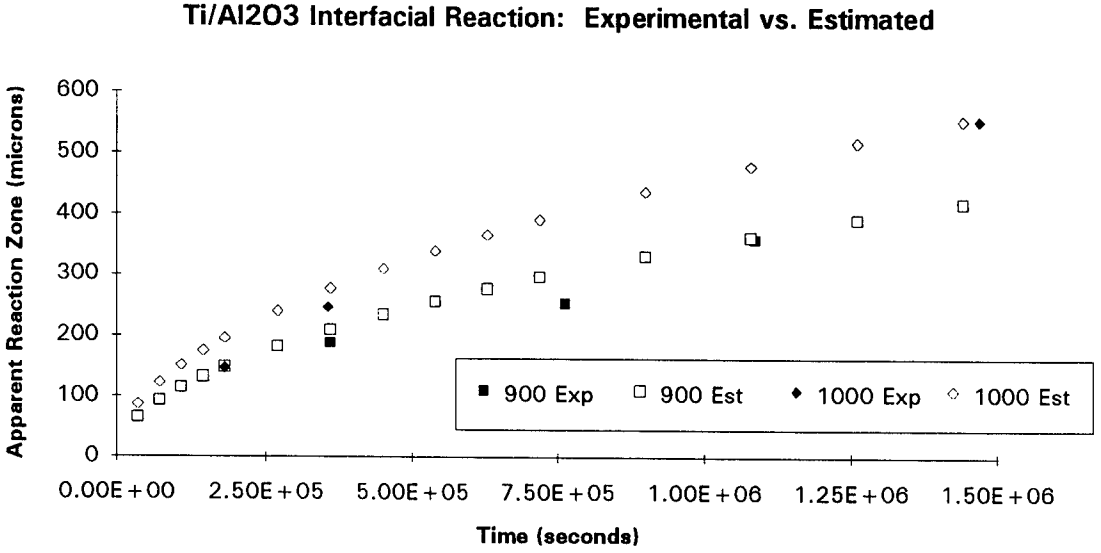

Figure 38. Reaction layer width vs. time in Ti/Al_2O_3 couples at 900 and 1000°C. Experimental results and estimated growth from parabolic kinetic results.

α_2-$Ti_3Al|Al_2O_3$ diffusion couples were studied only at 1100°C. This composite system exhibited Class III interfaces, characterized by the diffusion path α_2-$Ti_3Al|\gamma$-$TiAl|Al_2O_3$. The reaction producing γ-TiAl in these couples is believed to occur at the γ-$TiAl|\alpha_2$-Ti_3Al interface, with the parabolic growth rate shown in Fig. 27. The interdiffusion coeficients for Ti and Al in γ-TiAl were determined to be $\tilde{D}_{TiTi} = 5.49 \pm 3.76 \times 10^{-13}$ cm^2/sec. and $\tilde{D}_{AlAl} = 5.33 \pm 3.60 \times 10^{-13}$ cm^2/sec. The γ-TiAl|Al2O3 diffusion couples annealed at 1100°C exhibited Class II interfaces, characterized by limited solubility of Al and O in γ-TiAl as shown in Fig. 28. No kinetic results were obtained for this system due to lack of reliable composition gradient data.

In retrospect, the major contribution as a result of this study include the estimation of Ti-Al-O phase equilibria, the determination of parabolic constants for interfacial reactions, and the reporting of the diffusion coefficient results. Each of which deserves further study. However, before further work is performed in these areas, the issue of oxygen determination must be resolved. At the time of this research, EPMA was by far the most time efficient technique available to analyze diffusion couples. Unfortunately, whether the oxygen analysis was done by difference or quantitatively determined, an error of $\pm$ 2.5 at.% could be expected. In the establishment of Ti-Al-O phase equilibria, an error of $\pm$ 2.5 at.% for oxygen was not unreasonable, except in the case of the γ-TiAl phase. On the other hand, in calculating interdiffusion data, this same error was found to be very significant. As a result, no results for the interdiffusion of oxygen could be reported. A study which accounts for the effect of surface oxide during oxygen determination by EPMA is needed. In the area of Ti-Al-O phase equilibria, work in the following areas is recommended: 1) preparation of phase equilibria samples to better establish the ternary boundaries of the phases β-Ti, α-Ti, α2-Ti_3Al and γ-TiAl, and the three-phase regions α-Ti+α2-Ti_3Al+Al_2O_3 and α2-Ti_3Al+γ-TiAl+Al_2O_3. 2) preparation of α2-Ti_3Al(O) samples for a high-temperature XRD study to confirm if oxygen has a stabilizing effect on this phase to 1250°C. The parabolic growth results obtained also need to be confirmed. Because all diffusion couples were bonded prior to being annealed, the bonding stage may have an effect other than producing an initial reaction layer, which was accounted for. In the area of determining diffusion coefficients, work in the following areas is recommended: 1) solve the problem of oxygen determination by EPMA. 2) confirm the accuracy of the results reported, since no other studies of Ti-Al-O interdiffusion were found in the literature. 3) apply the reported coefficients in the calculation of layer growth in Ti/Al_2O_3 diffusion couples. The reported parabolic growth results should be useful for

comparison. 4) prepare single-phase diffusion couples, with interface markers, for the determination of intrinsic coefficients. Intrinsic coefficients are needed, in the author's opinion, in order to interpret interdiffusion results from multiphase ternary couples.

APPENDIX A: ELECTRON-PROBE MICROANALYSIS RESULTS

This appendix contains the EPMA results of all the diffusion couple samples analyzed in this study. The samples, in order of presentation, are those of the types: 1) Ti/Al_2O_3, 2) α_2-Ti_3Al/Al_2O_3 and 3) γ-$TiAl/Al_2O_3$. These results are in the form of composition vs. position plots, with the composition units in atomic percent and the position units in microns measured from the metal|ceramic interface. The results appear in order of increasing temperature and time, respectively. Comments accompanying each plot indicate the site at which the analysis was performed, and additional notes if warranted. Details of the analysis can be found in section 4.2.2.

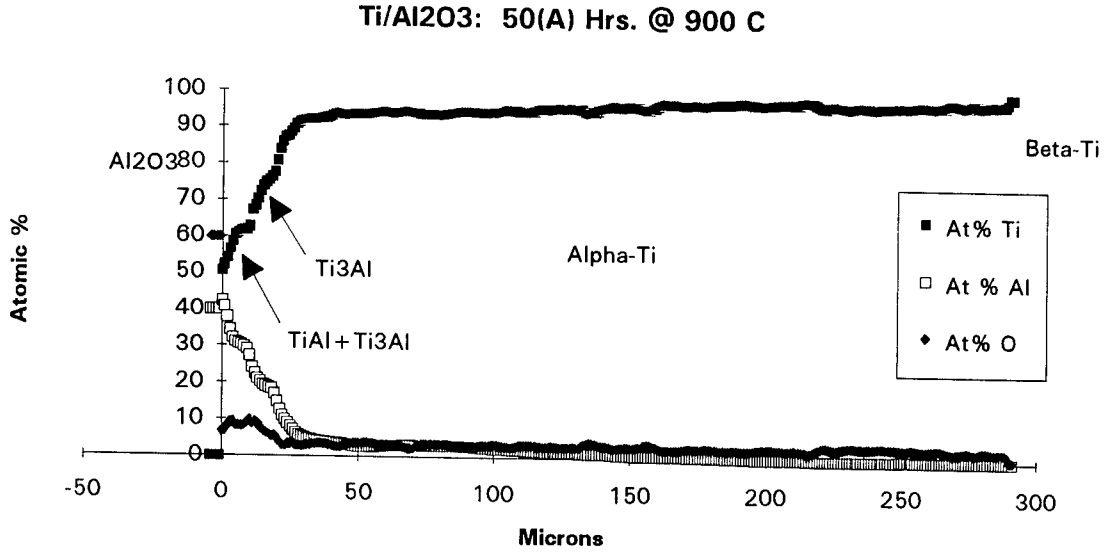

EPMA performed at the University of Wisconsin-Madison. Typical results.

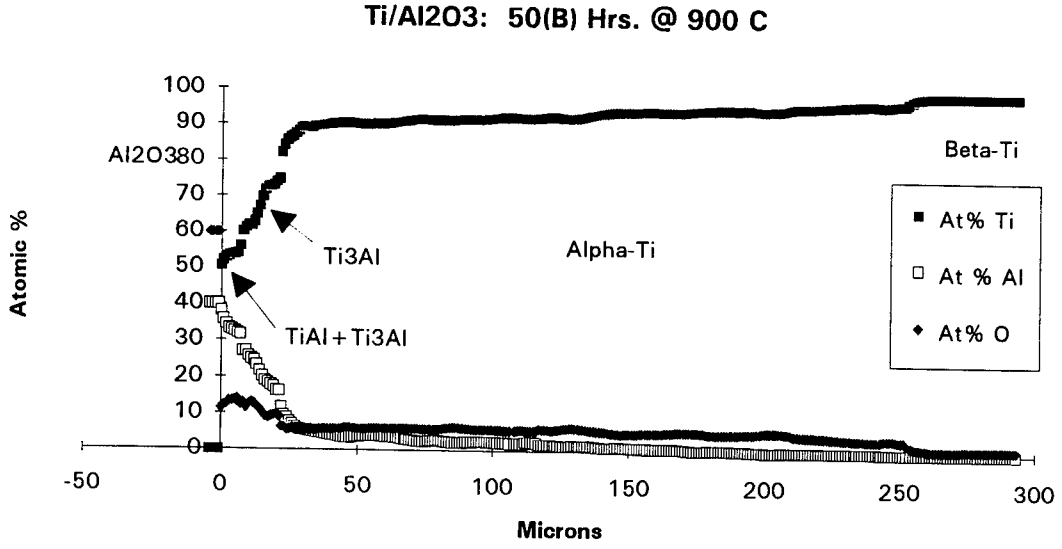

EPMA performed at Sandia National Laboratories. Typical results.

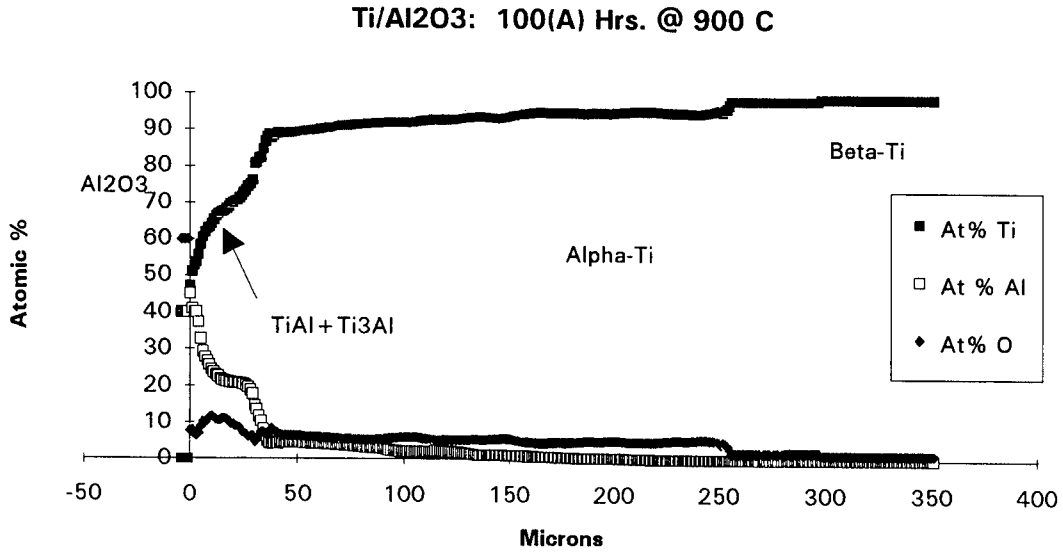

EPMA performed at the University of Wisconsin-Madison. Typical results.

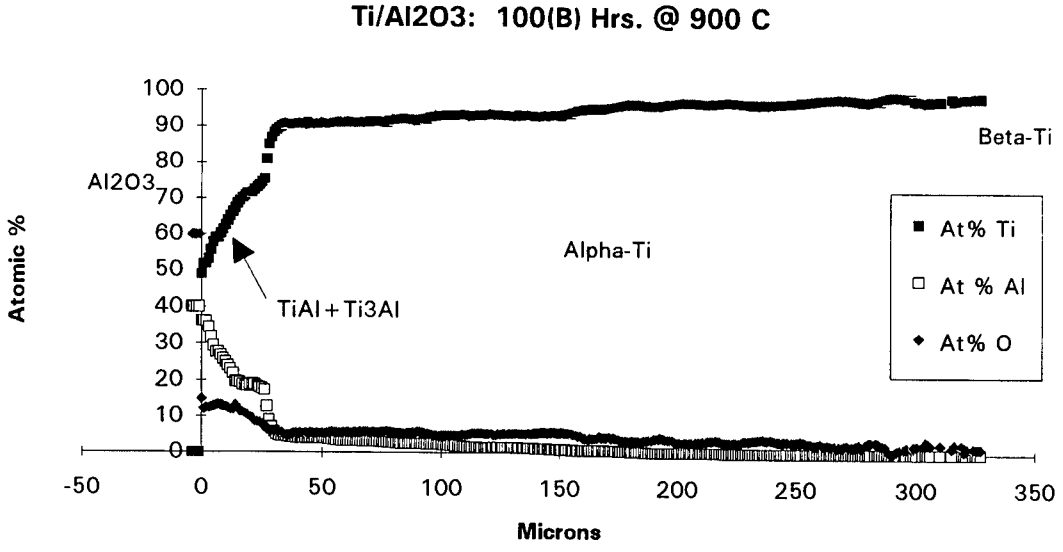

EPMA performed at Sandia National Laboratories. Typical results.

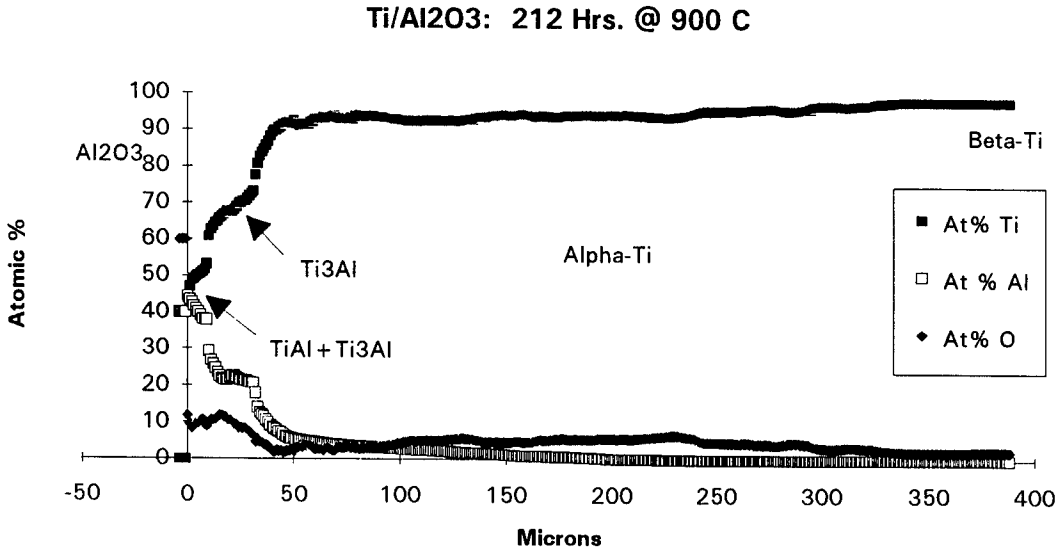

EPMA performed at Sandia National Laboratories. Typical results.

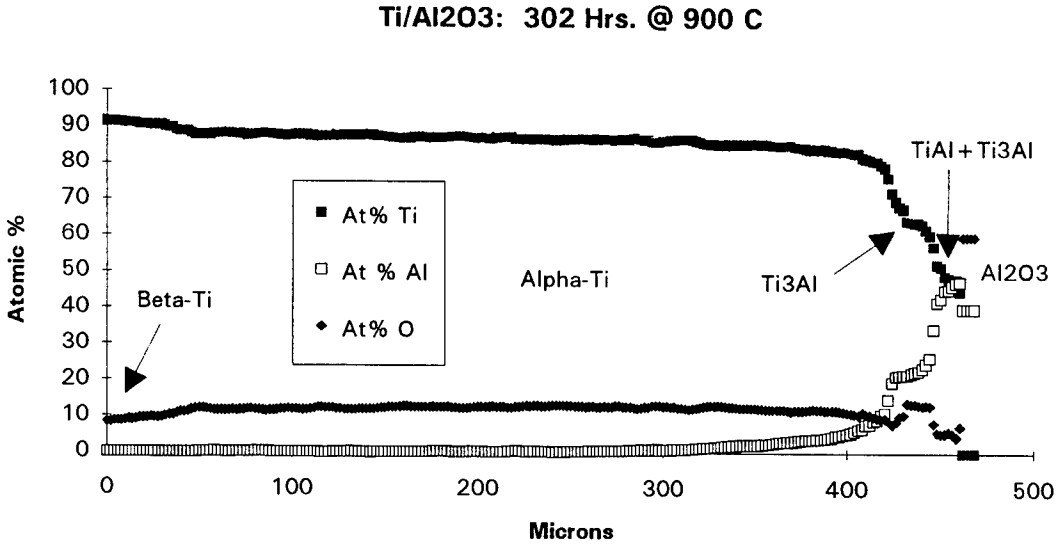

EPMA performed at the University of Wisconsin-Madison. Slightly high oxygen results.

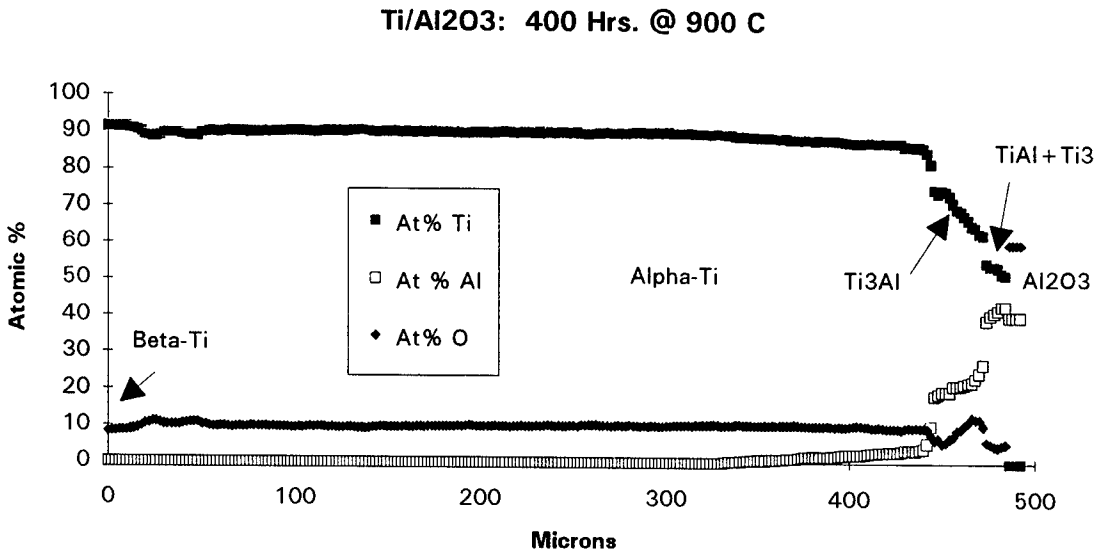

EPMA performed at the University of Wisconsin-Madison. Slightly high oxygen results.

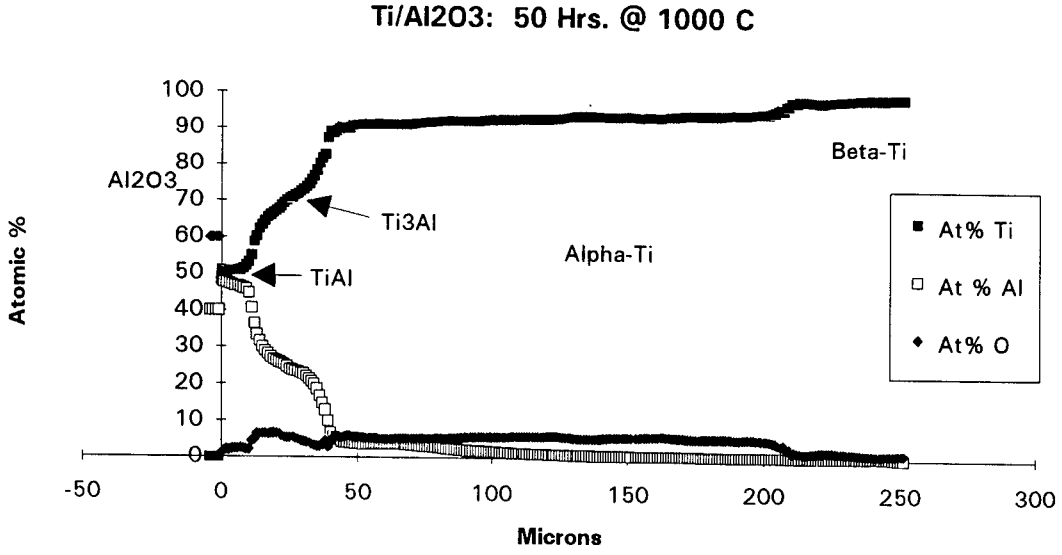

EPMA performed at Sandia National Laboratories. Typical results.

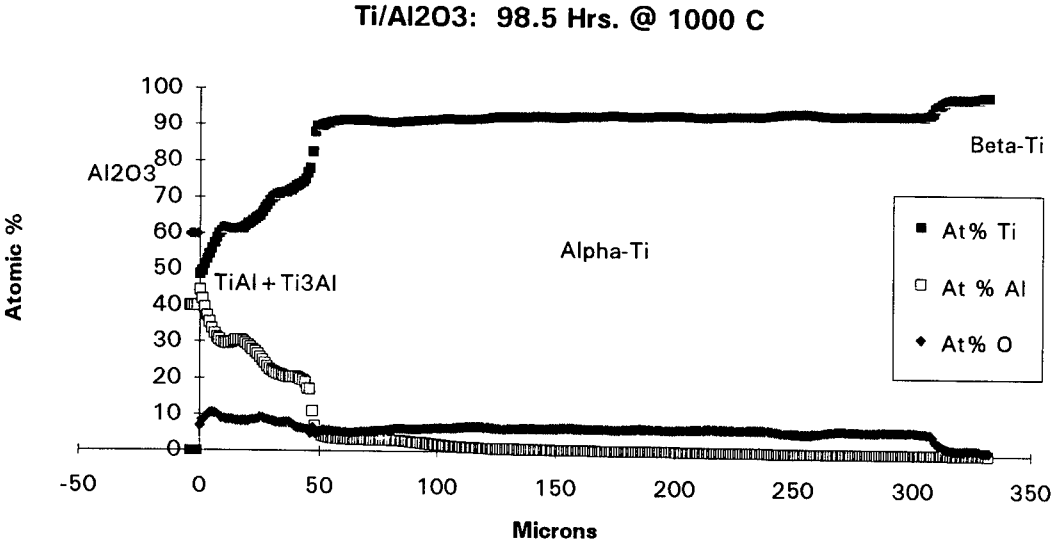

EPMA performed at Sandia National Laboratories. Typical results.

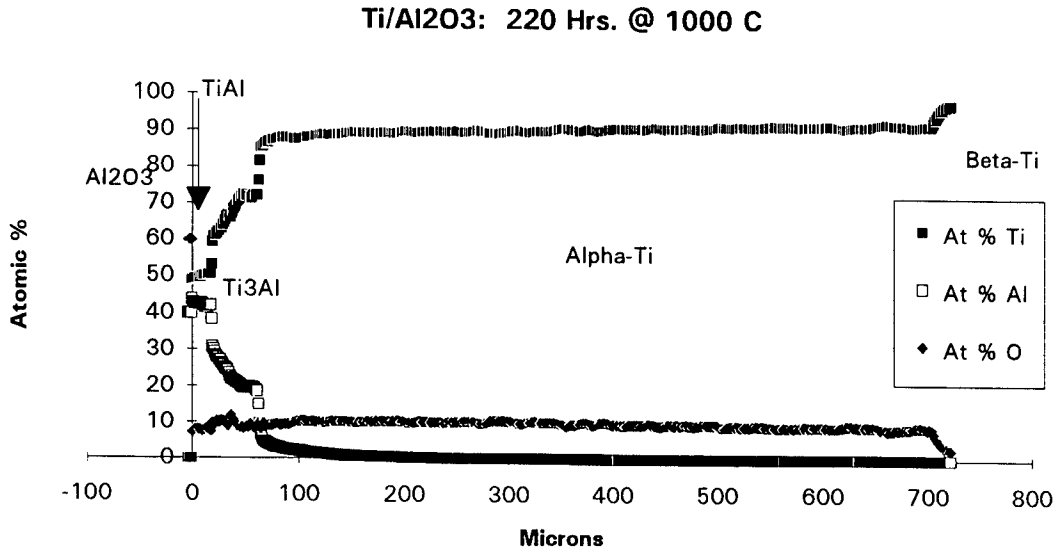

EPMA performed at Sandia National Laboratories. Typical results.

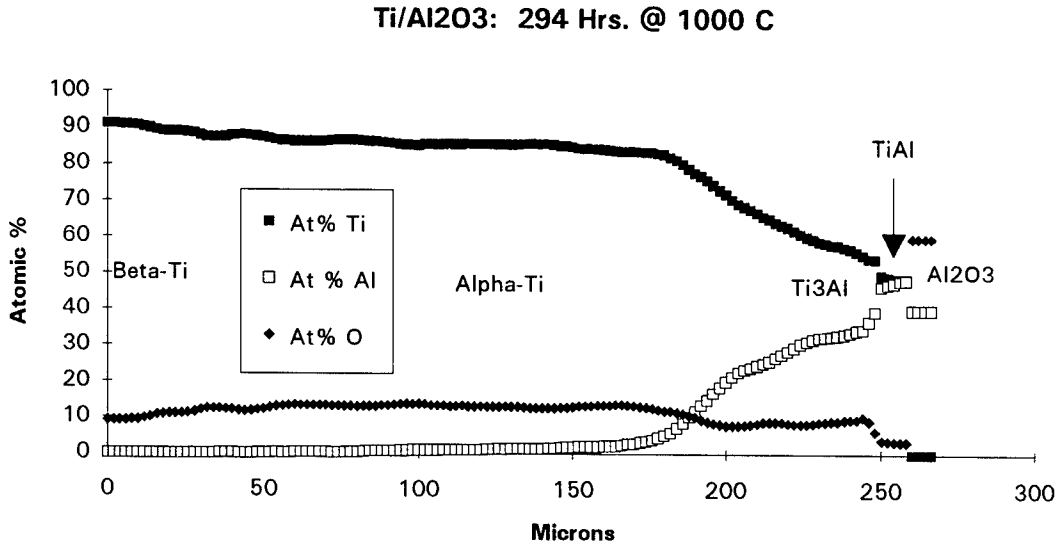

EPMA performed at the University of Wisconsin-Madison. Typical results.

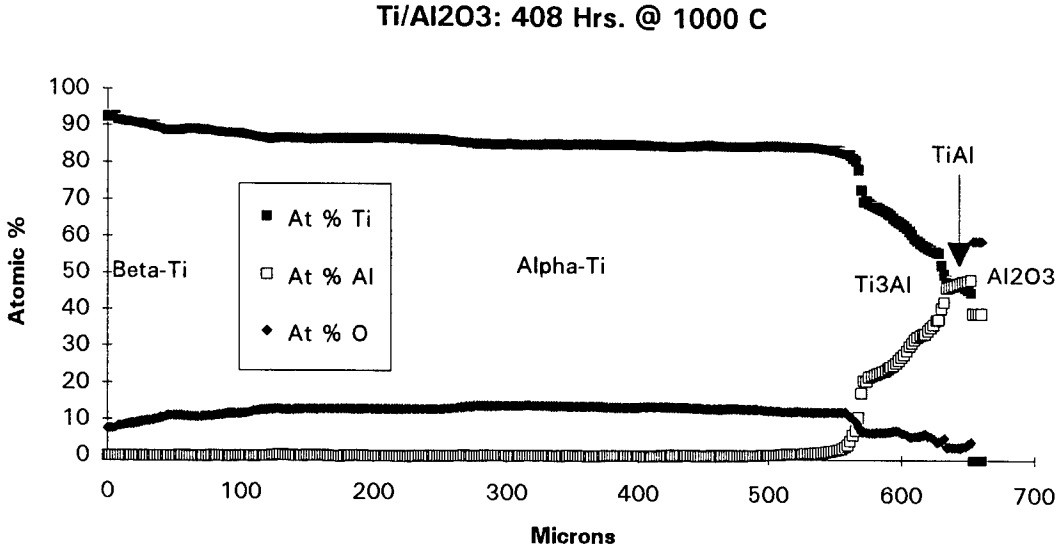

EPMA performed at Sandia National Laboratories. Typical results.

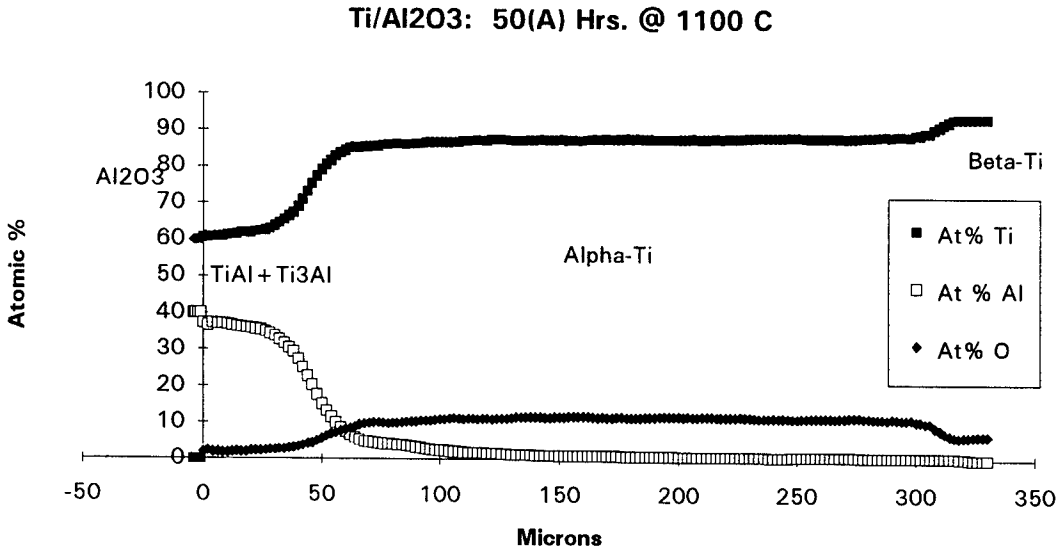

EPMA performed at University of Wisconsin-Madison. Typical results.

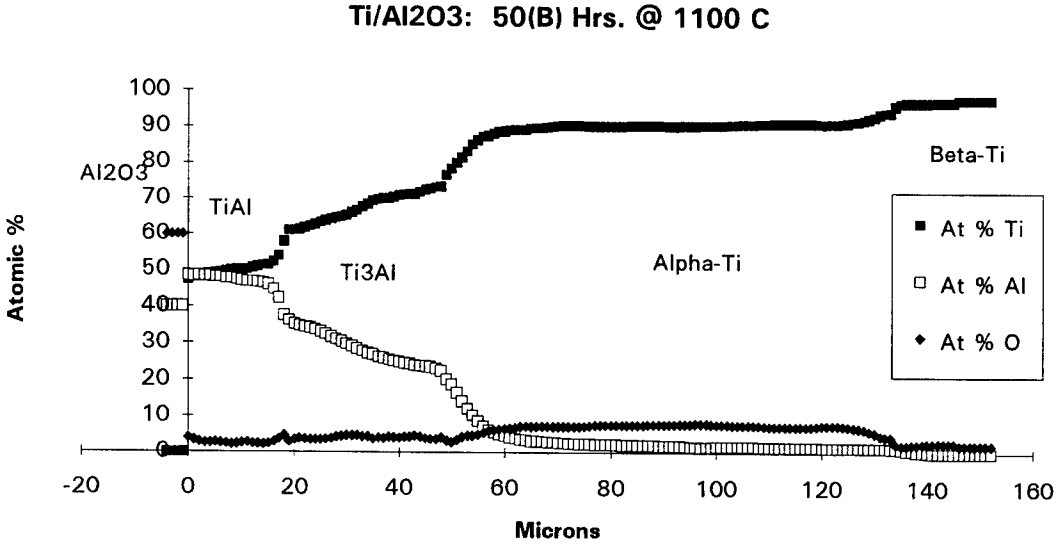

EPMA performed at Sandia National Laboratories. Typical results.

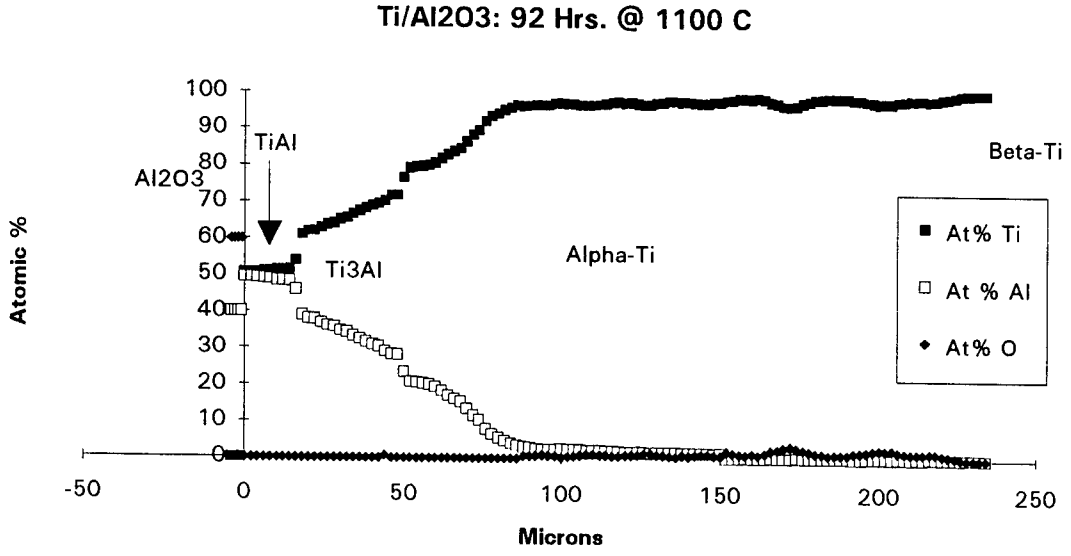

EPMA performed at the University of Wisconsin-Madison. Low oxygen results.

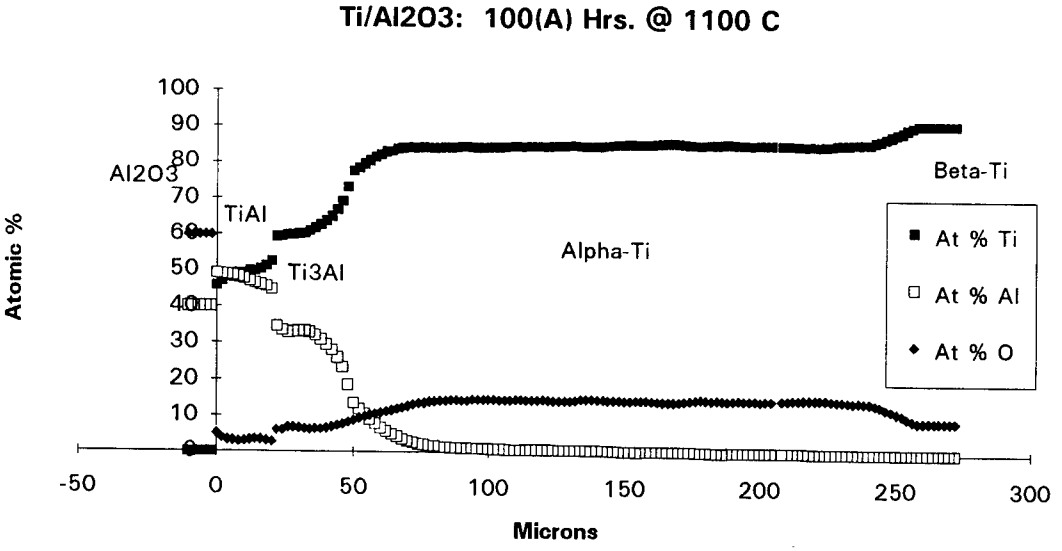

EPMA performed at the University of Wisconsin-Madison. Typical results.

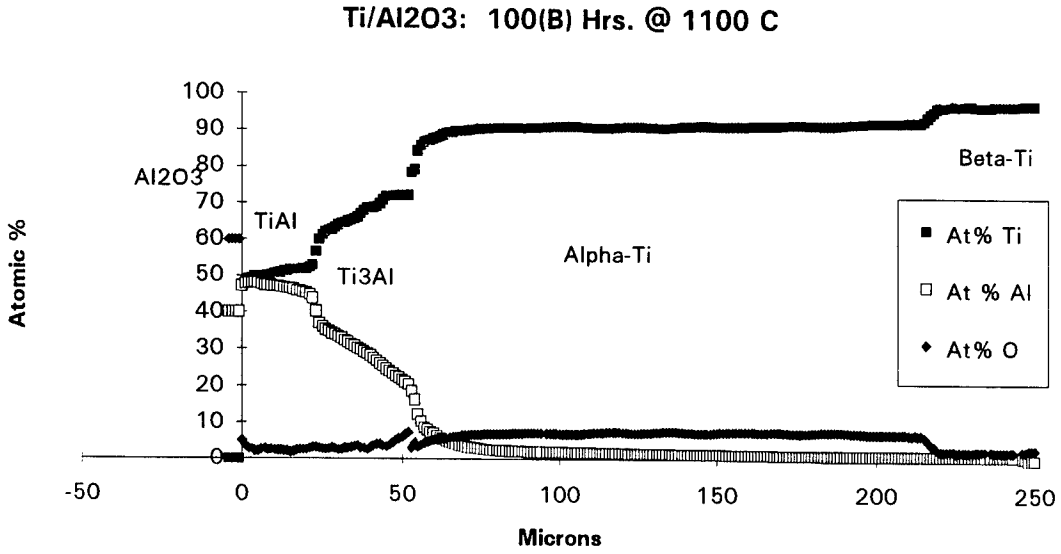

EPMA performed at Sandia National Laboratories. Typical results.

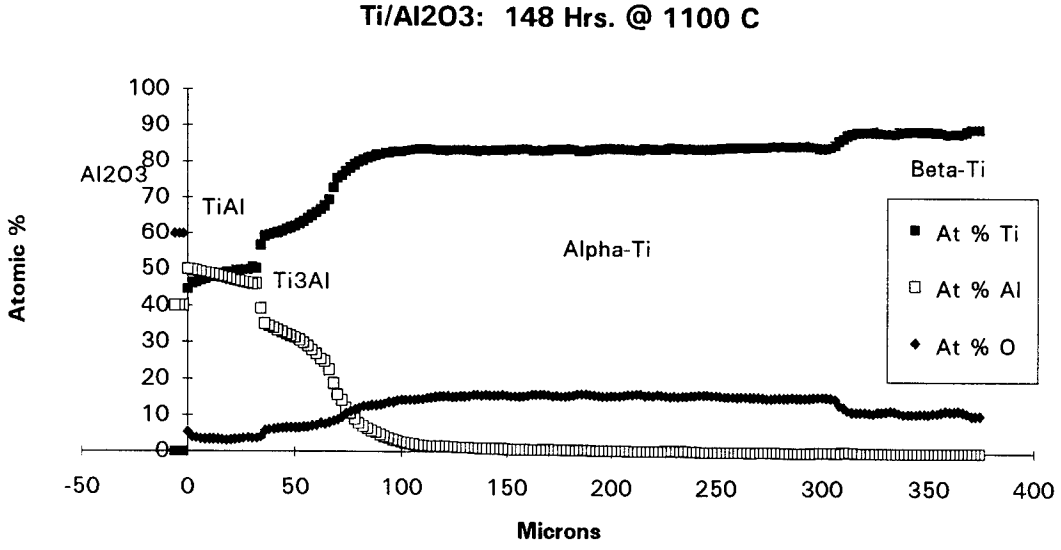

EPMA performed at the University of Wisconsin-Madison. Slightly high oxygen results.

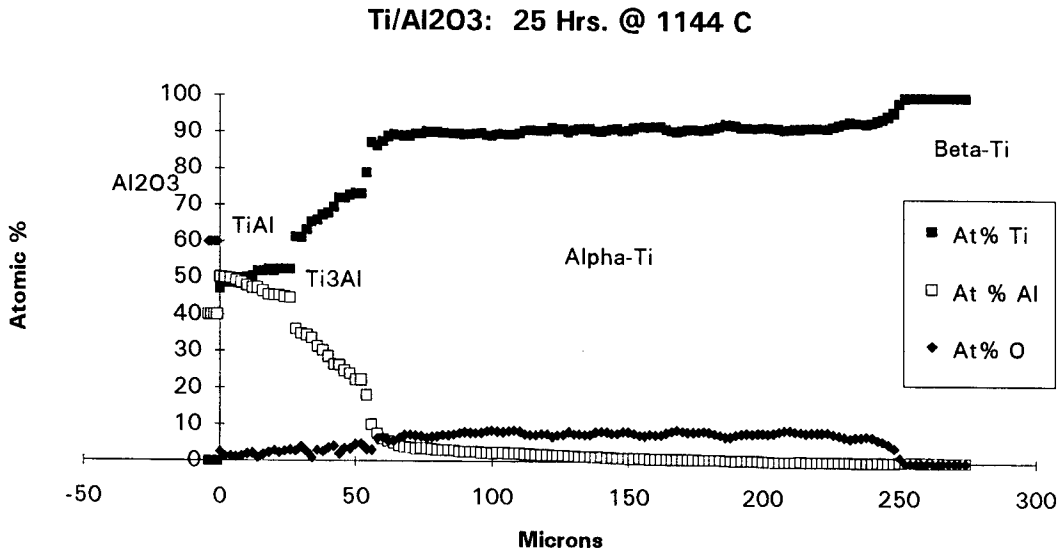

EPMA performed at Sandia National Laboratories. Typical results.

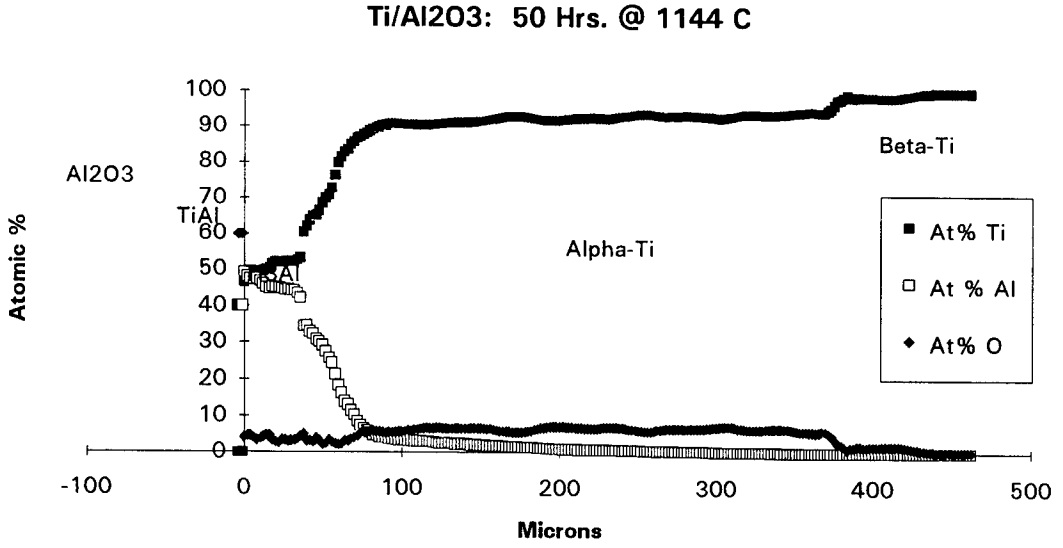

EPMA performed at Sandia National Laboratories. Typical results.

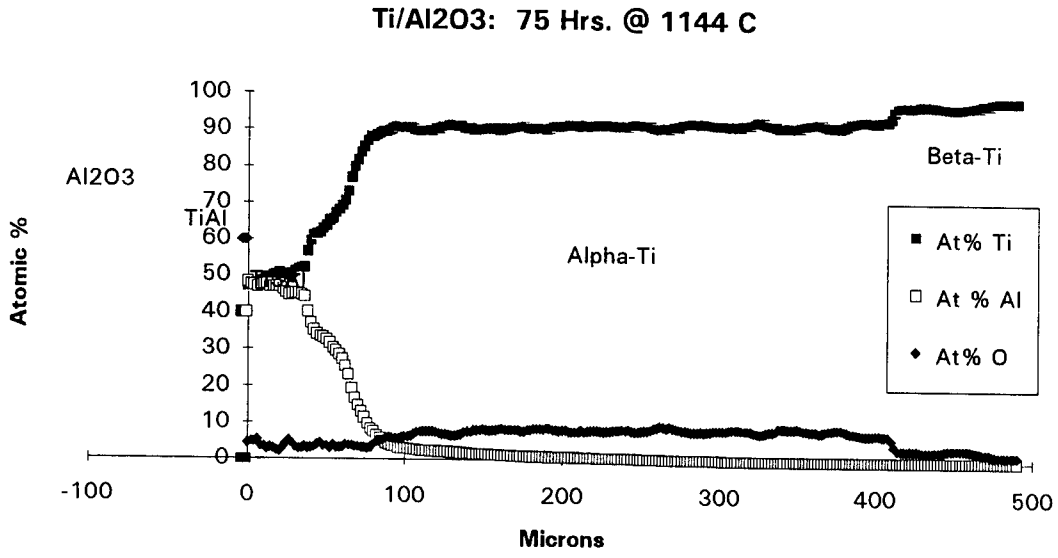

EPMA performed at Sandia National Laboratories. Typical results.

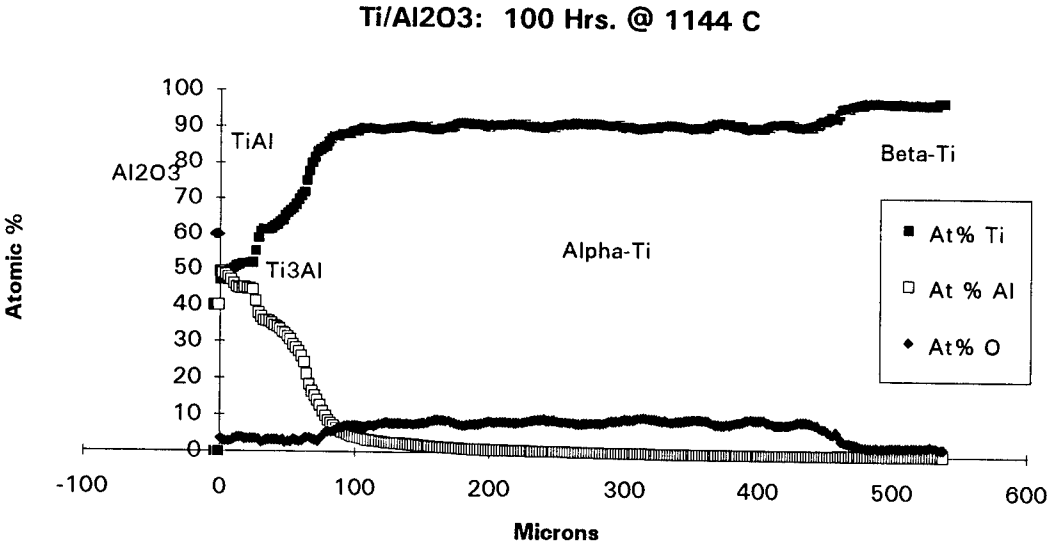

EPMA performed at Sandia National Laboratories. Typical results.

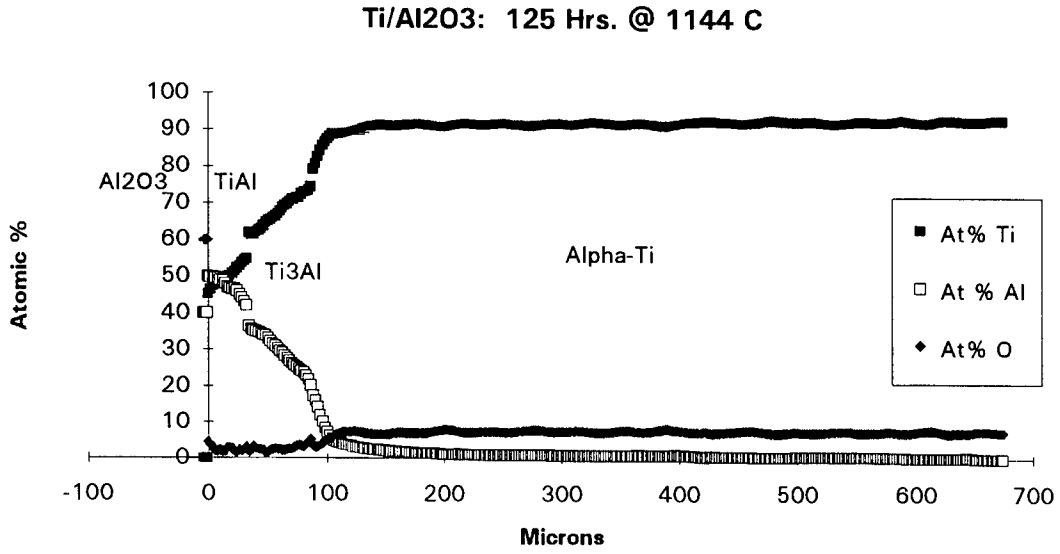

EPMA performed at Sandia National Laboratories. Due to the lack of an α-Ti|β-Ti transition, this sample may be oxygen saturated.

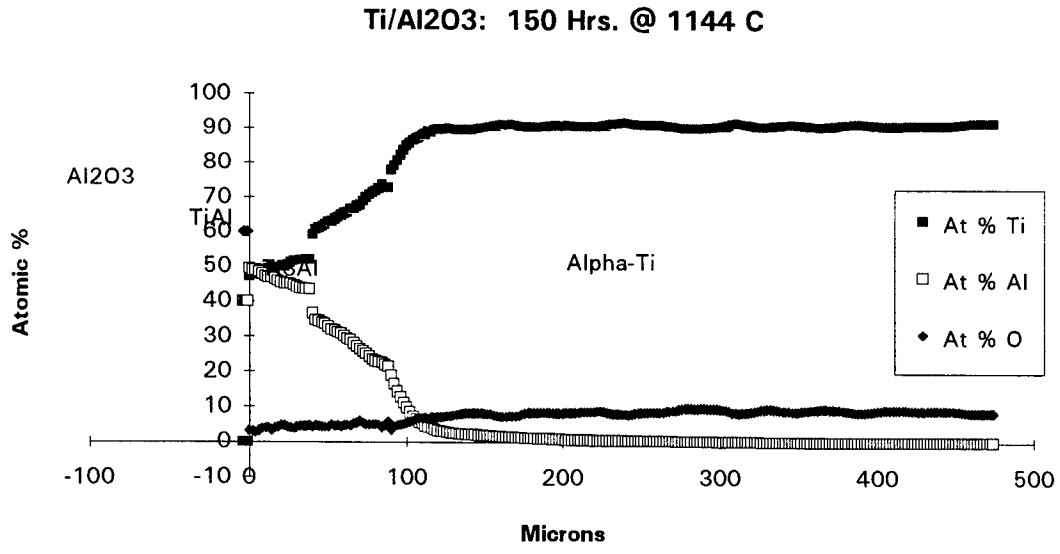

EPMA performed at Sandia National Laboratories. Due to the lack of an α-Ti|β-Ti transition, this sample may be oxygen saturated.

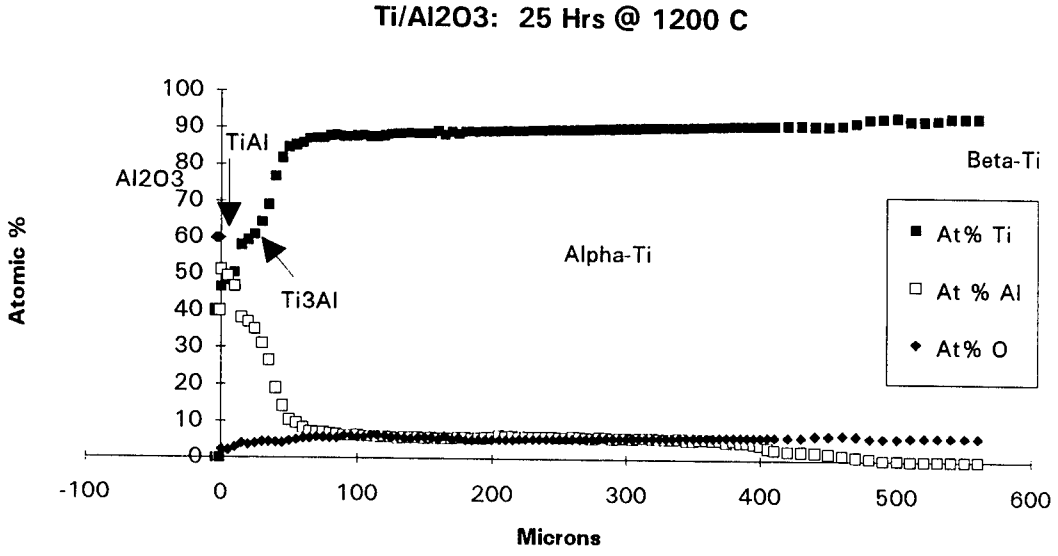

EPMA performed at the University of Wisconsin-Madison. α-Ti|β-Ti transition poorly defined. Although oxygen levels are not excessive, it does not return to boundary level expected in β-Ti.

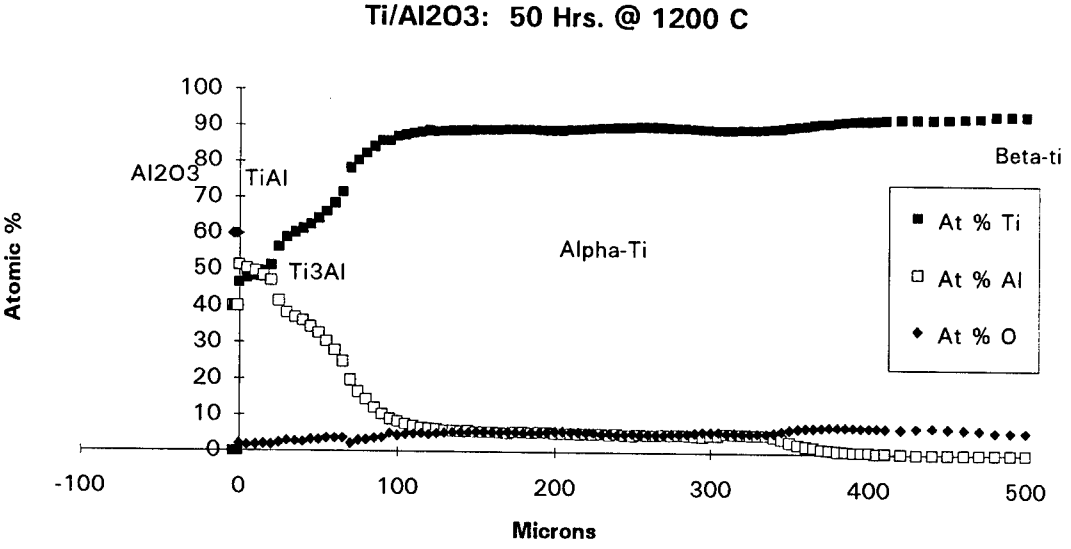

EPMA performed at the University of Wisconsin-Madison. α-Ti|β-Ti transition poorly defined. Although oxygen levels are not excessive, it does not return to boundary level expected in β-Ti.

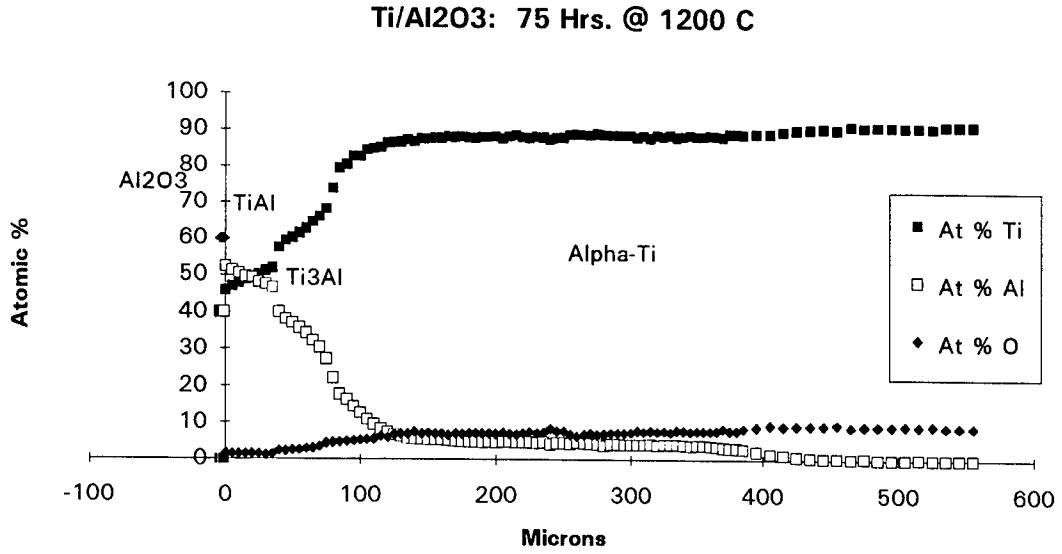

EPMA performed at the University of Wisconsin-Madison. α-Ti|β-Ti transition poorly defined. Although oxygen levels are not excessive, it does not return to boundary level expected in β-Ti.

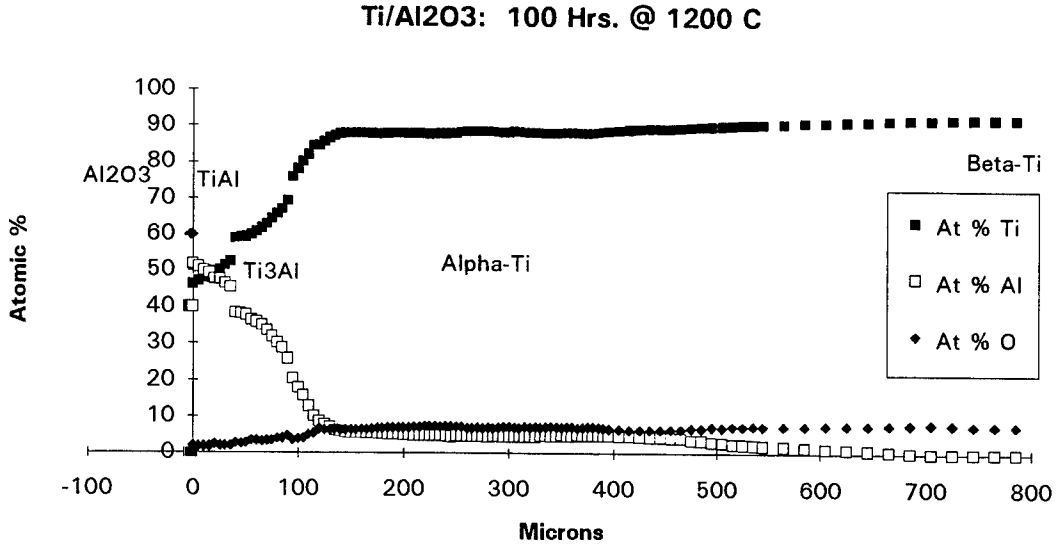

EPMA performed at the University of Wisconsin-Madison. α-Ti|β-Ti transition poorly defined. Although oxygen levels are not excessive, it does not return to boundary level expected in β-Ti.

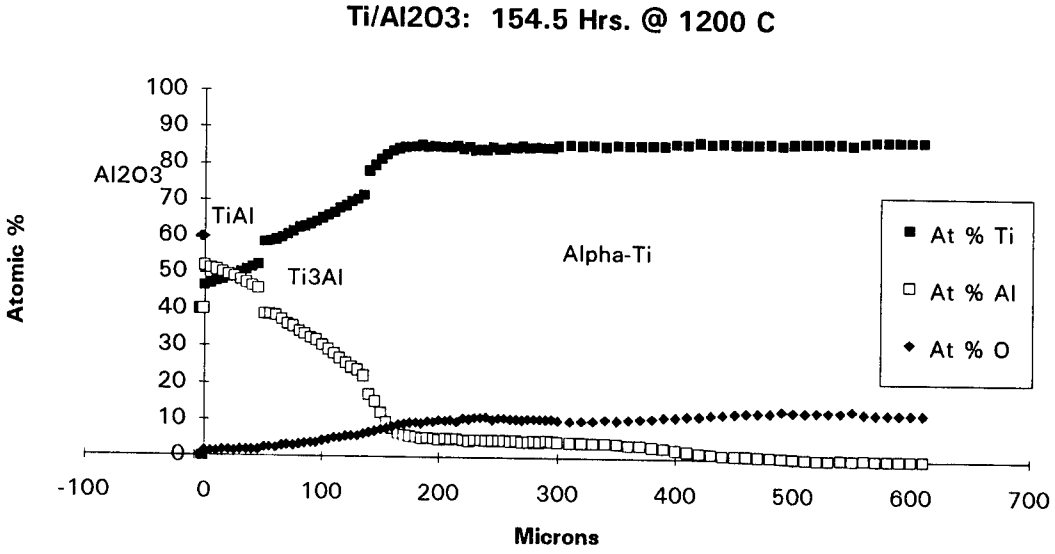

EPMA performed at the University of Wisconsin-Madison. α-Ti|β-Ti transition not apparent. Sample may be saturated in oxygen.

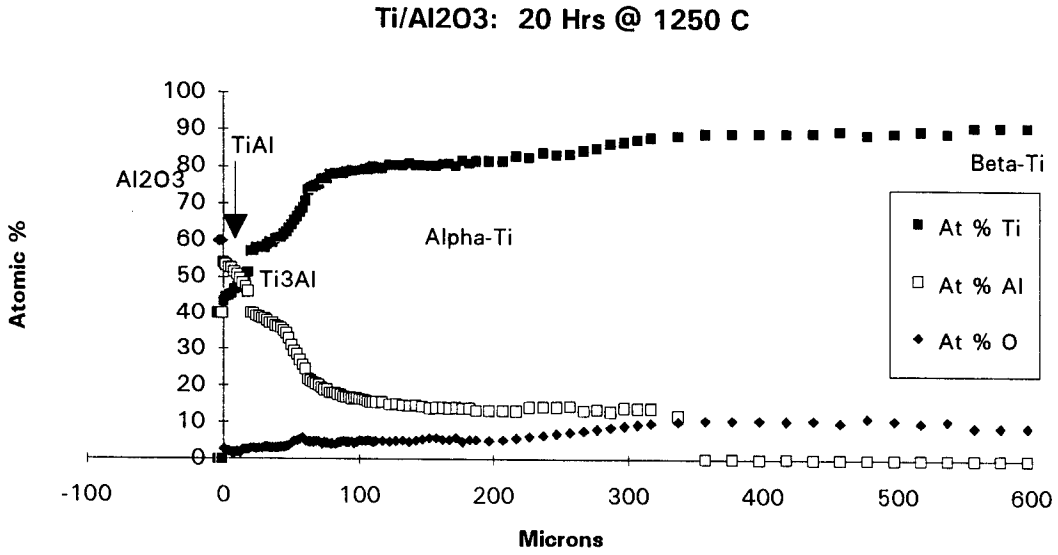

EPMA performed at the University of Wisconsin-Madison. α-Ti|β-Ti transition poorly defined. Although oxygen levels are not excessive, it does not return to boundary level expected in β-Ti.

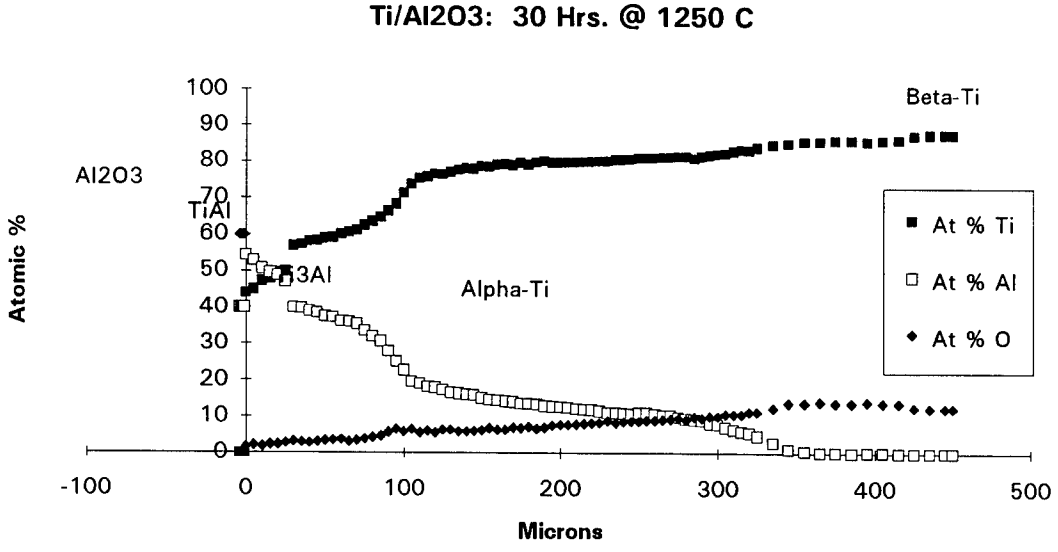

EPMA performed at the University of Wisconsin-Madison. α-Ti|β-Ti transition poorly defined. Although oxygen levels are not excessive, it does not return to boundary level expected in β-Ti.

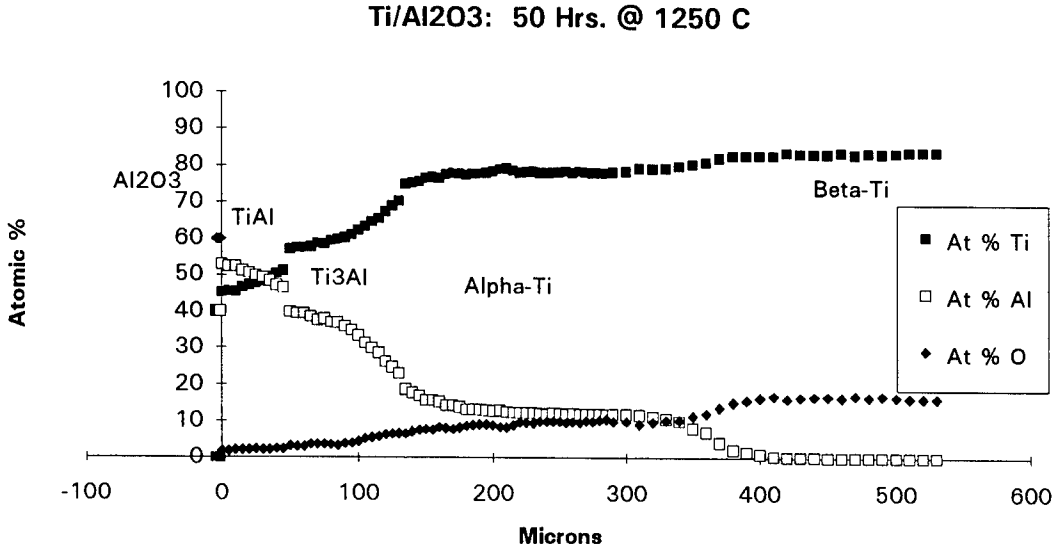

EPMA performed at the University of Wisconsin-Madison. α-Ti|β-Ti transition poorly defined. Sample may be saturated in oxygen.

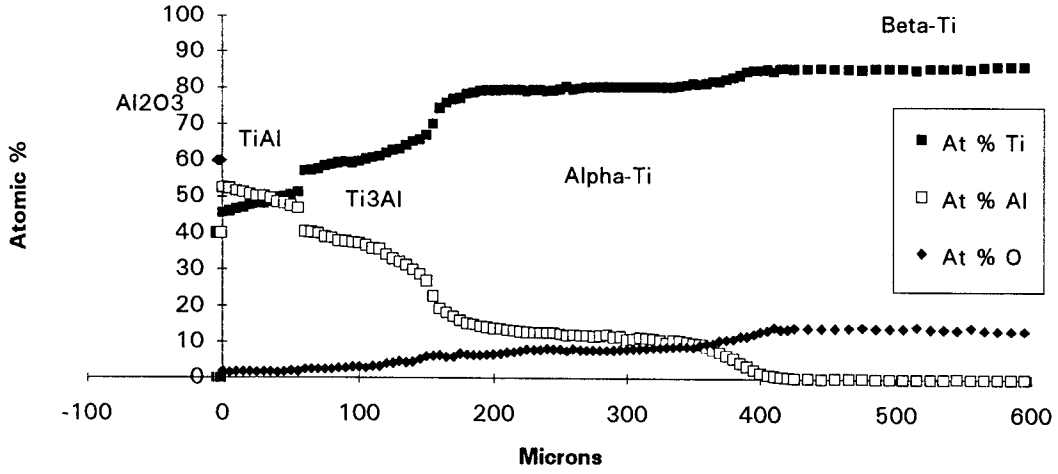

EPMA performed at the University of Wisconsin-Madison. α-Ti|β-Ti transition poorly defined. Sample may be oxygen saturated.

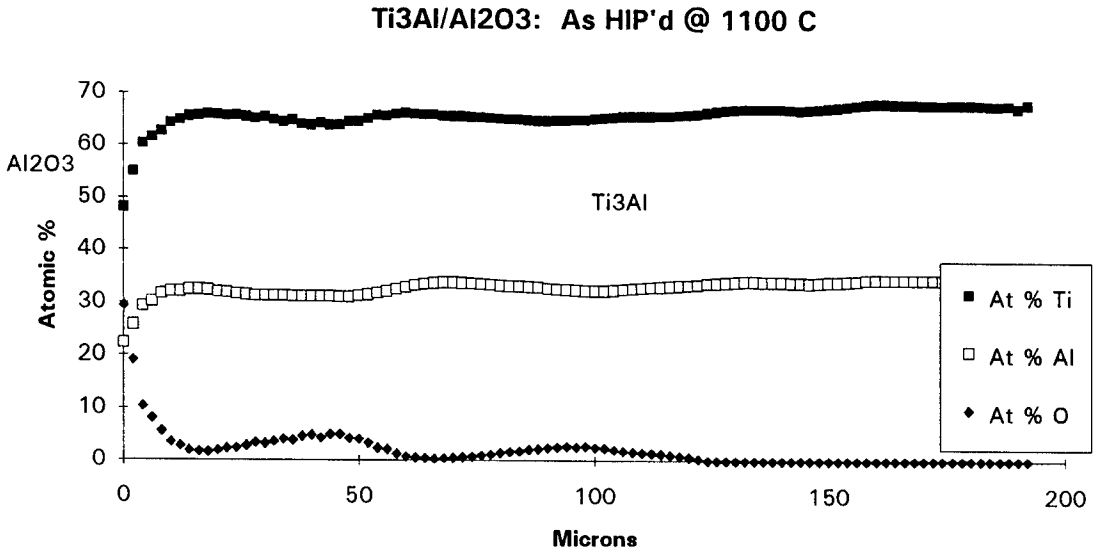

EPMA performed at the University of Wisconsin-Madison. Probe not stable throughout the analysis.

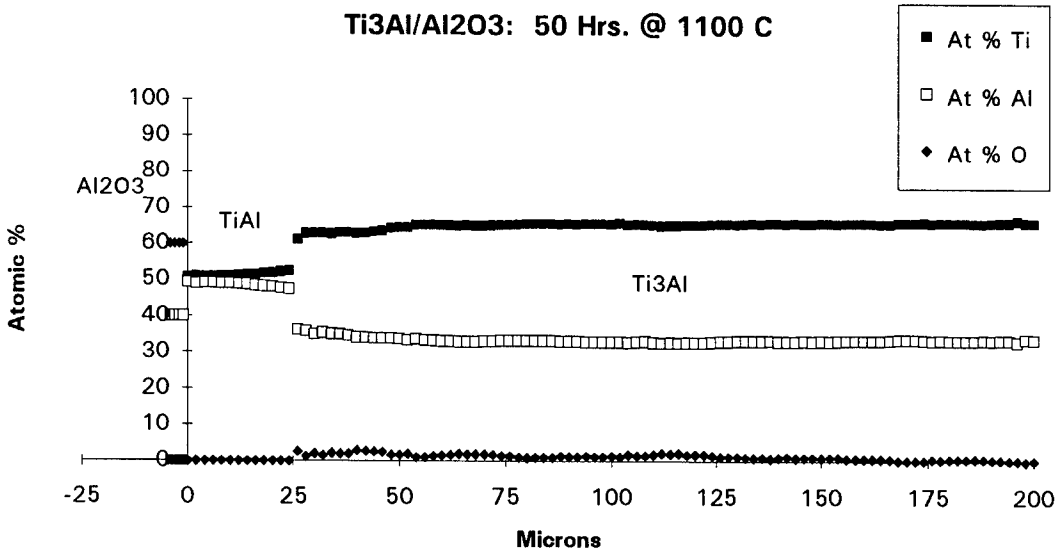

EPMA performed at the University of Wisconsin-Madison. Typical results.

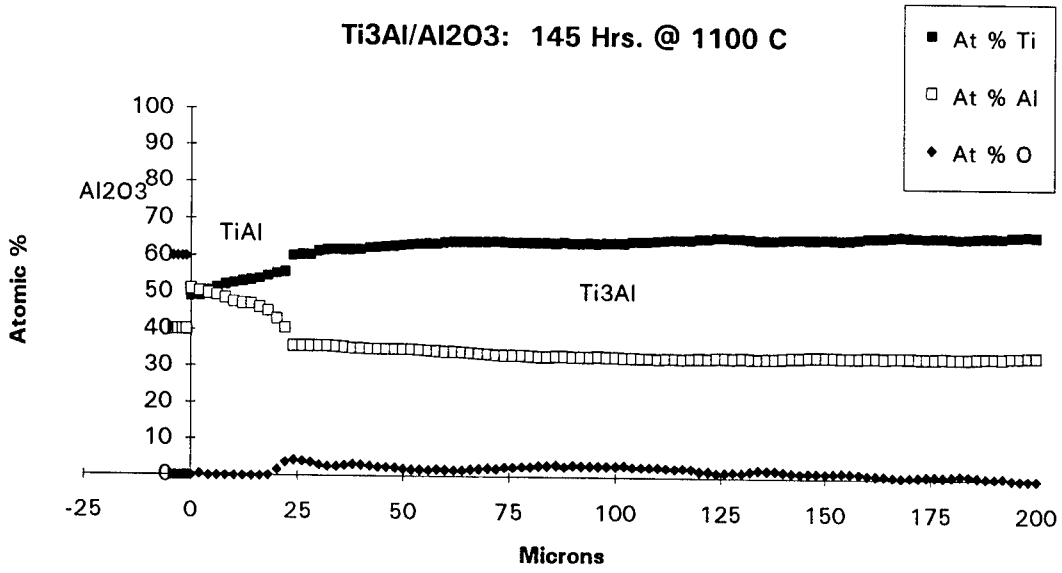

EPMA performed at the University of Wisconsin-Madison. Typical results.

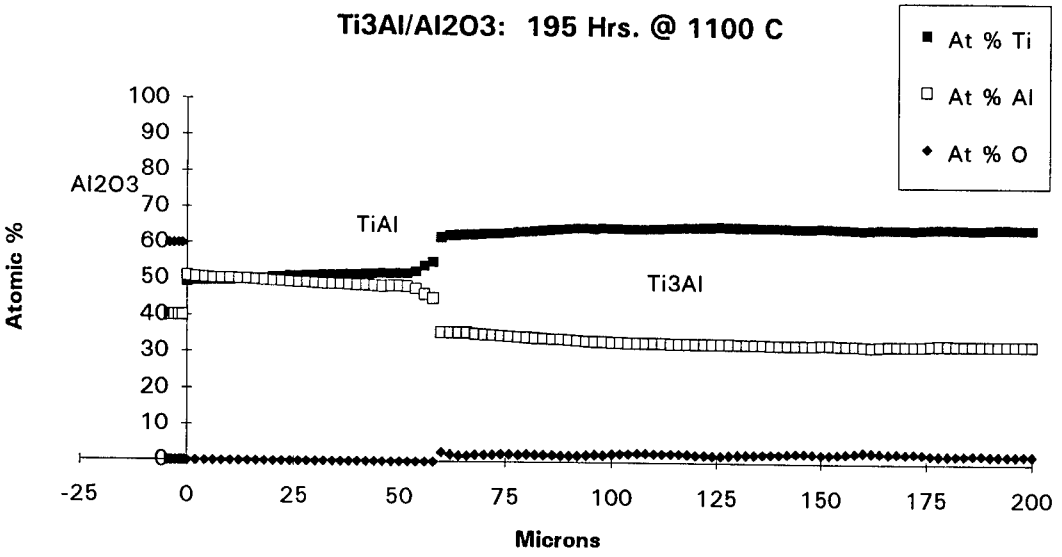

EPMA performed at the University of Wisconsin-Madison. Typical results.

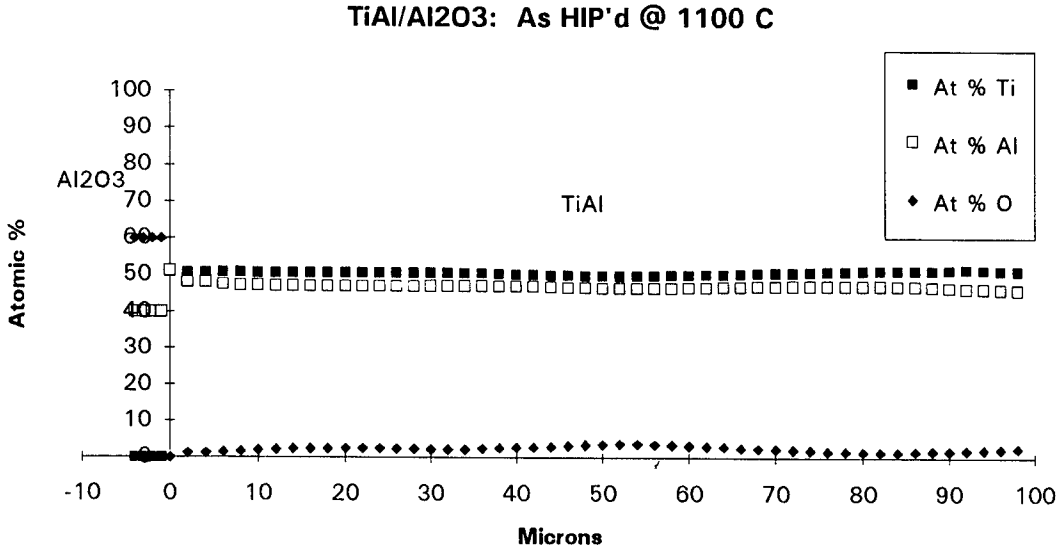

EPMA performed at the University of Wisconsin-Madison. Slightly high oxygen results.

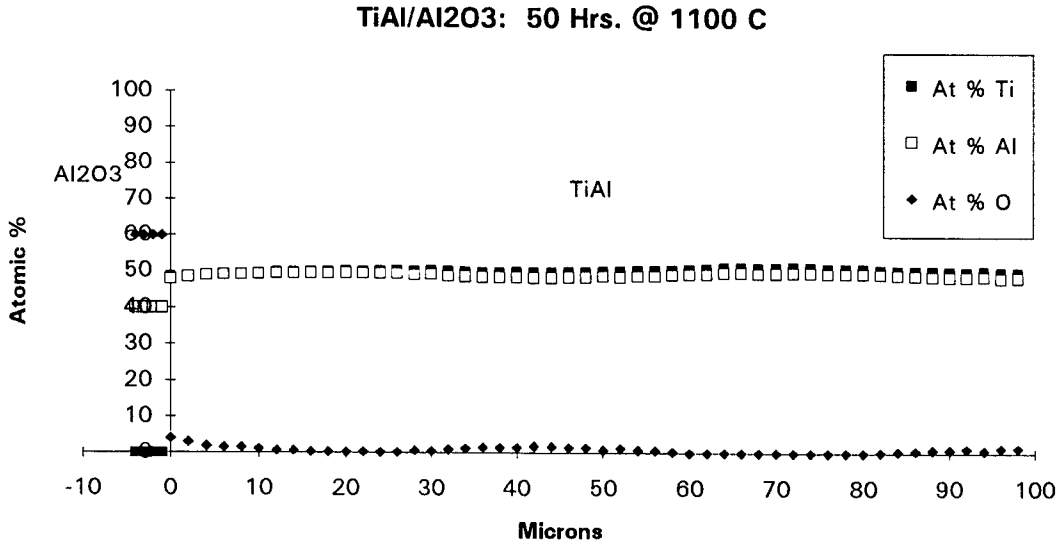

EPMA performed at the University of Wisconsin-Madison. Typical results.

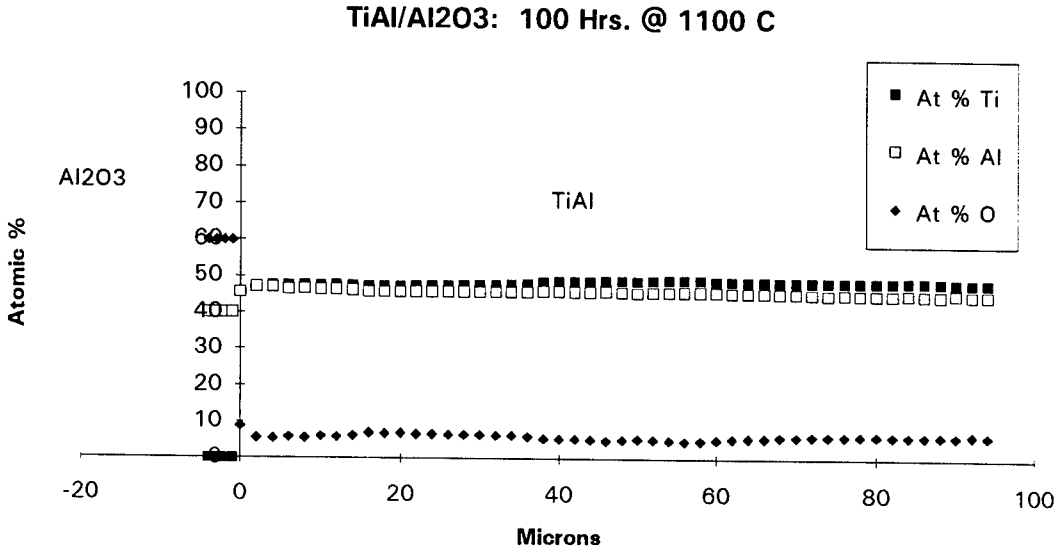

EPMA performed at the University of Wisconsin-Madison. High oxygen results.

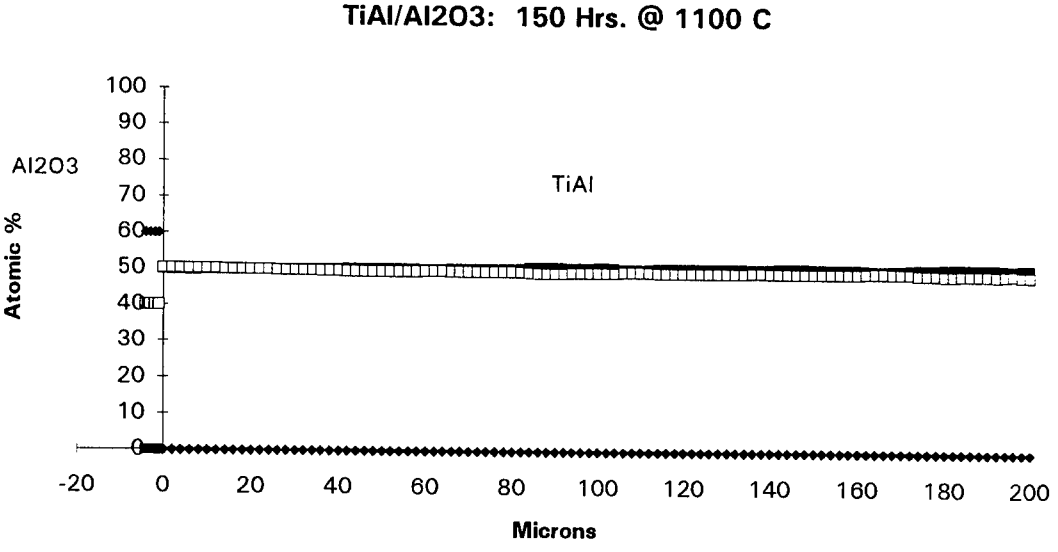

EPMA performed at the University of Wisconsin-Madison. Low oxygen results.

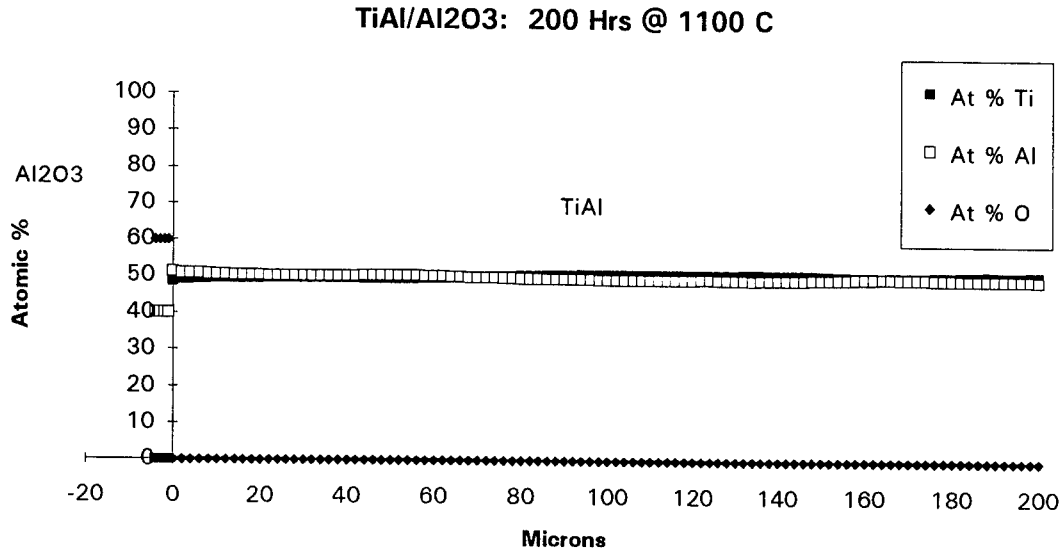

EPMA performed at the University of Wisconsin-Madison. Low oxygen results.

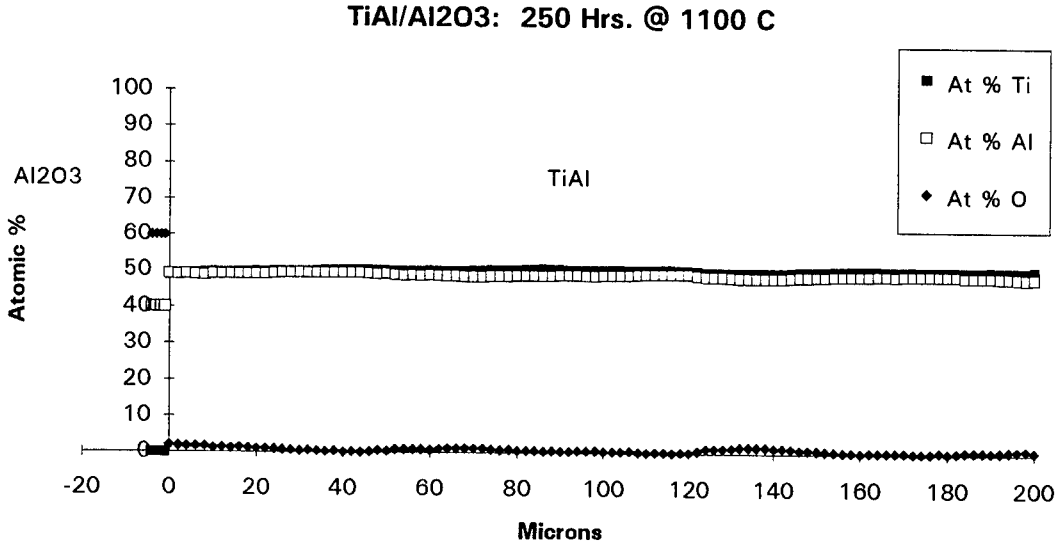

EPMA performed at the University of Wisconsin-Madison. Typical results.

APPENDIX B: LAYER GROWTH MEASUREMENTS

This appendix contains the layer width measurements for the phase(s) formed at the interface of the diffusion couples prepared for this study. The samples, in order of presentation, are those of the types: 1) Ti/Al_2O_3 and 2) α_2-Ti_3Al/Al_2O_3. The results are in table form, with the tables in order of increasing temperature. The results presented are based upon eleven measurements on each sample, not at random. Measurements were made using a scaled rule on micrographs of the samples. These results are plotted in the results sections 5.1.2 and 5.2.2.

900°C: Layer Thickness Results (W, microns)

Time (Hrs.)	γ-TiAl	±σ	α_2-Ti_3Al	±σ	α-Ti	±σ
100	2	2	13	3	173	11
212	7	3	14	4	233	13
302	9	3	15	4	335	14
400	9	3	19	4	393	15

1000°C: Layer Thickness Results (W, microns)

Time (Hrs.)	γ-TiAl	±σ	α_2-Ti_3Al	±σ	α-Ti	±σ
50	6	3	19	5	123	10
98.5	9	4	25	6	213	13
220	12	5	32	7	n.a.	n.a.
408	17	5	54	8	483	18

1100°C: Layer Thickness Results (W, microns)

Time (Hrs.)	γ-TiAl	±σ	α_2-Ti_3Al	±σ	α-Ti	±σ
50	16	8	18	8	42	6
100	21	9	22	10	155	13
148	32	7	26	5	219	16
151.5	24	6	28	9	227	18
293	39	11	43	10	374	9
312	40	9	42	11	n.a.	n.a.

1144°C: Layer Thickness Results (W, microns)

Time (Hrs.)	γ-TiAl	±σ	α_2-Ti_3Al	±σ	α-Ti	±σ
25	19	4	12	4	154	8
50	26	4	17	6	280	10
75	31	5	21	8	313	13
100	38	5	27	8	322	18

1200°C: Layer Thickness Results (W, microns)

Time (Hrs.)	γ-TiAl	±σ	α_2-Ti_3Al	±σ	α-Ti	±σ
25	19	5	17	5	114	13
50	25	5	30	8	171	10
75	35	6	38	9	n.a.	n.a.

1250°C: Layer Thickness Results (W, microns)

Time (Hrs.)	γ-TiAl	±σ	α_2-Ti_3Al	±σ	α-Ti	±σ
20	20	3	43	3	154	24
30	30	3	62	4	n.a.	n.a.
50	44	2	80	3	n.a.	n.a.
70	60	3	95	2	n.a.	n.a.

APPENDIX C: INTERDIFFUSION FLUX CALCULATION RESULTS

This appendix contains the interdiffusion flux results for chosen diffusion couples. The samples, in order of presentation, are those of the types: 1) Ti/Al_2O_3, and 2) α_2-Ti_3Al/Al_2O_3. These results are in the form of interdiffusion flux vs. position plots, with the flux units in atomic fraction*centimeters/second and the position units in microns measured from the metal|ceramic interface. The results appear in order of increasing temperature and time, respectively. Comments accompany these results where instructive. These results were calculated from the EPMA results of App. A using the Boltzmann-Matano methodology presented in section 3.3.

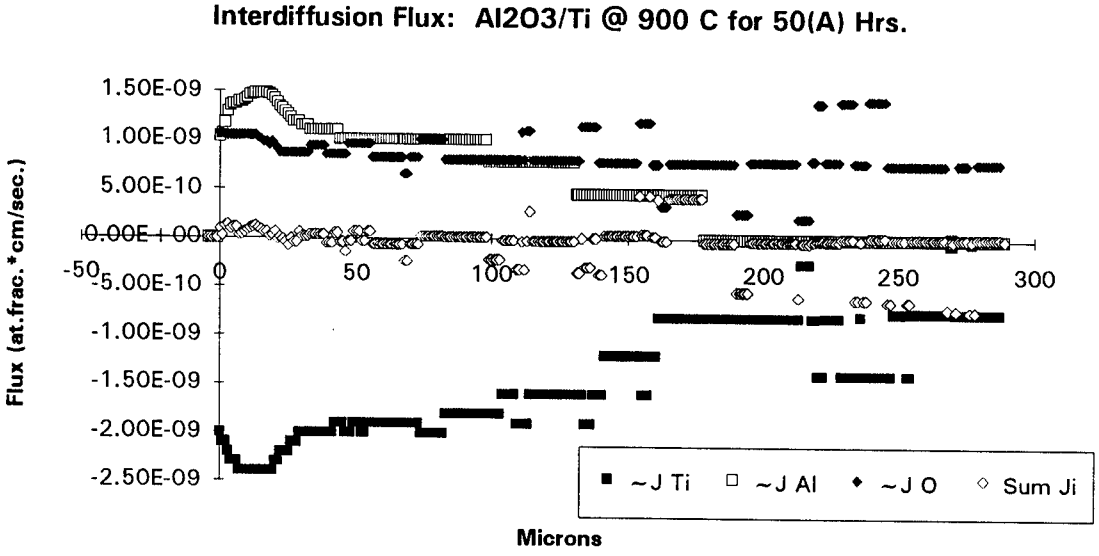

Scatter due to scatter in EPMA results (applies throughout these results).

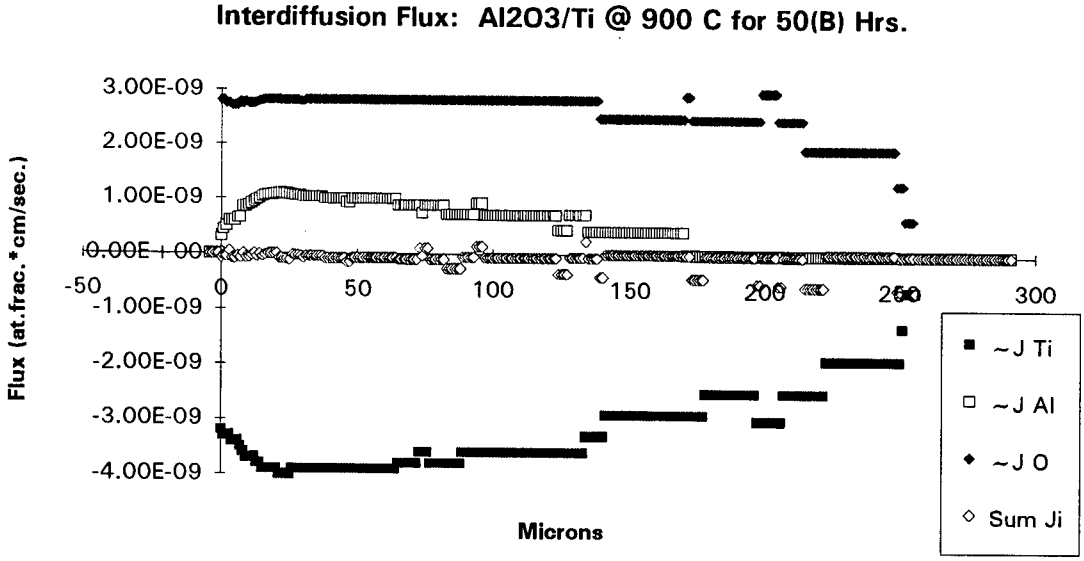

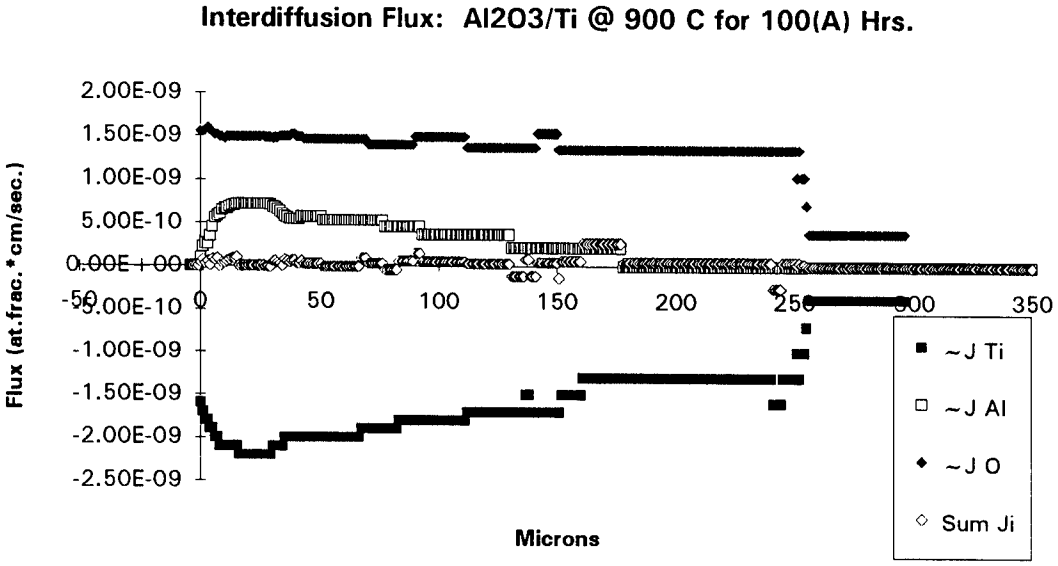

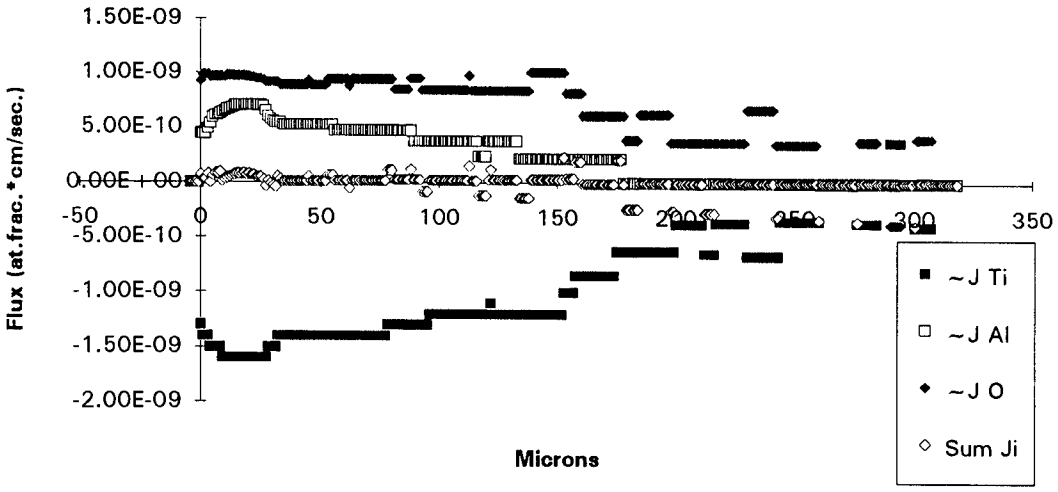

Scatter due to scatter in EPMA results.

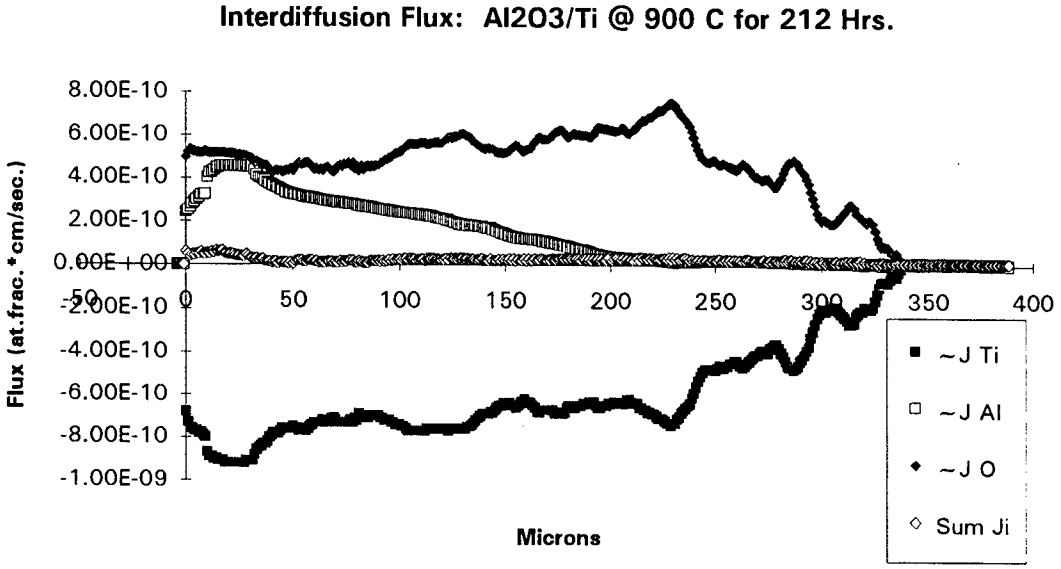

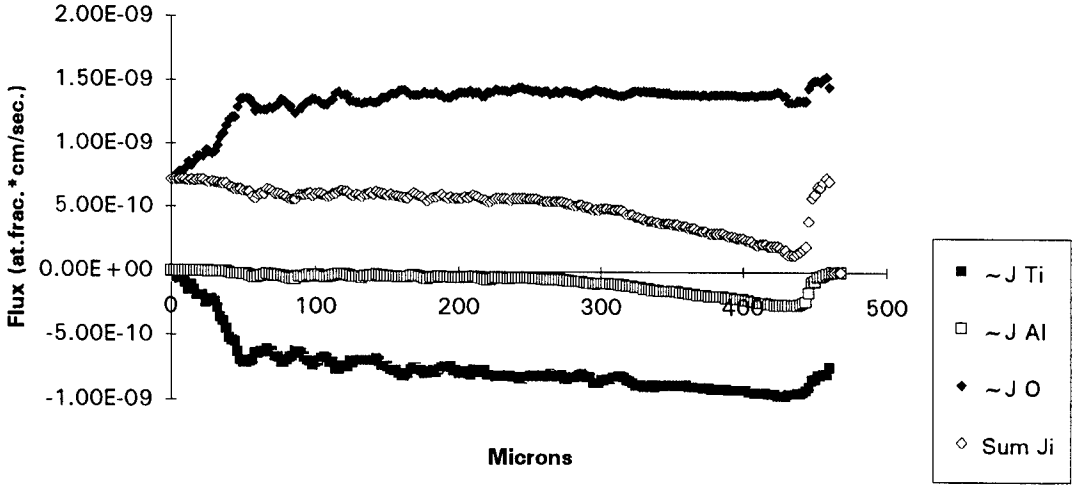

Sum J_i and J_O in error due to oxygen not returning to boundary level in β-Ti.

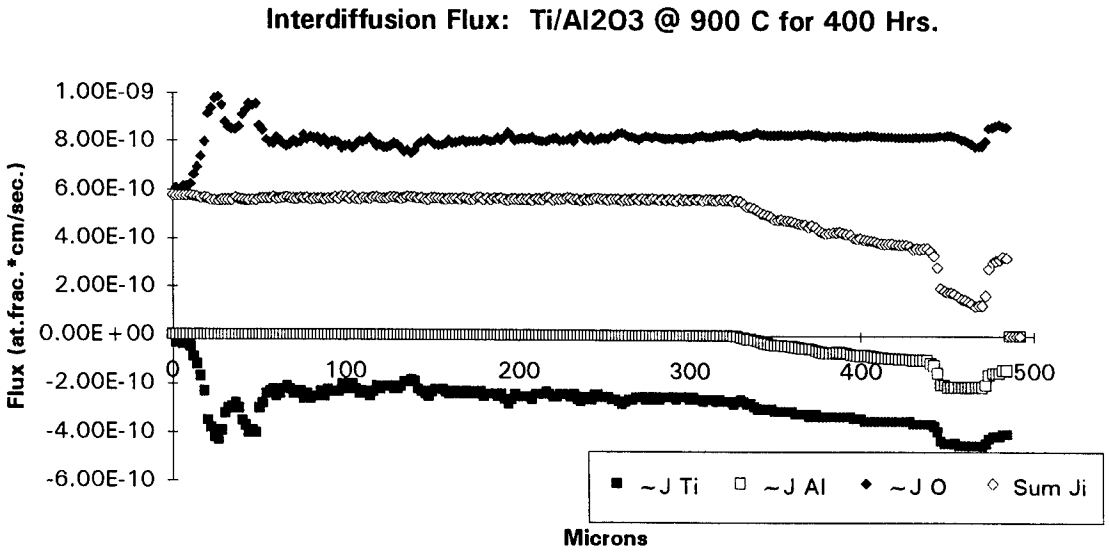

Sum J_i and J_O in error due to oxygen not returning to boundary level in β-Ti.

Interdiffusion Flux: Al2O3/Ti @ 1000 for 50 Hrs.

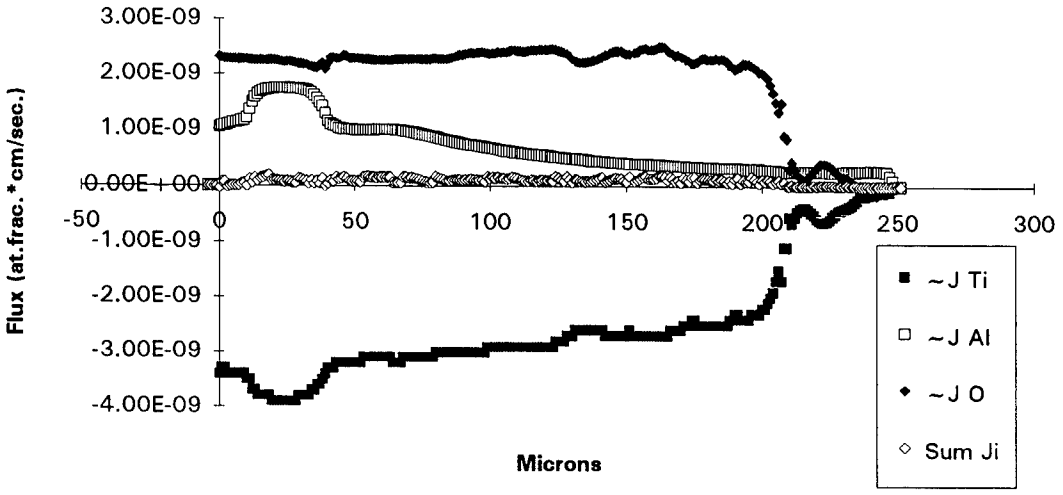

Interdiffusion Flux: Al2O3/Ti @ 1000 for 98.5 Hrs.

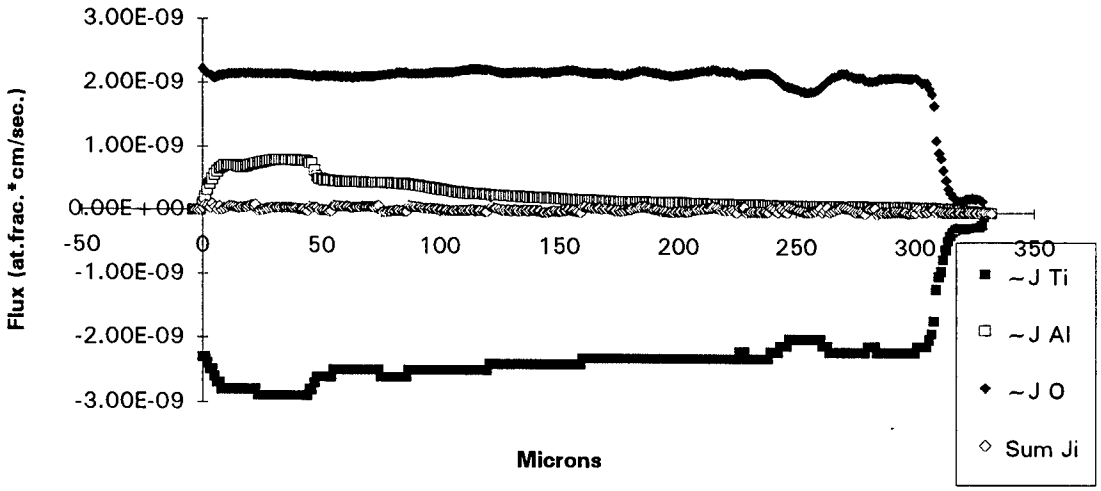

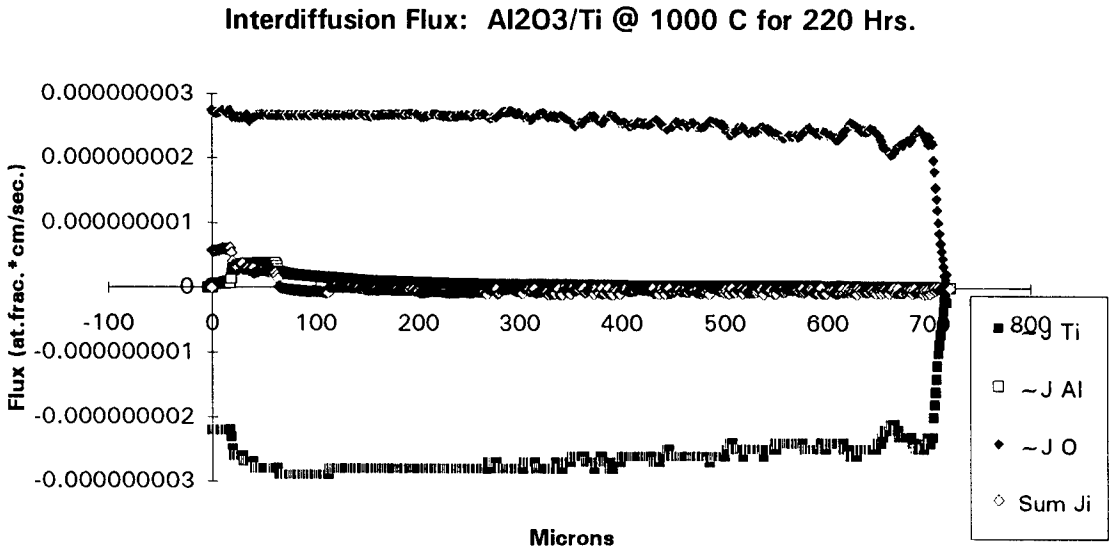

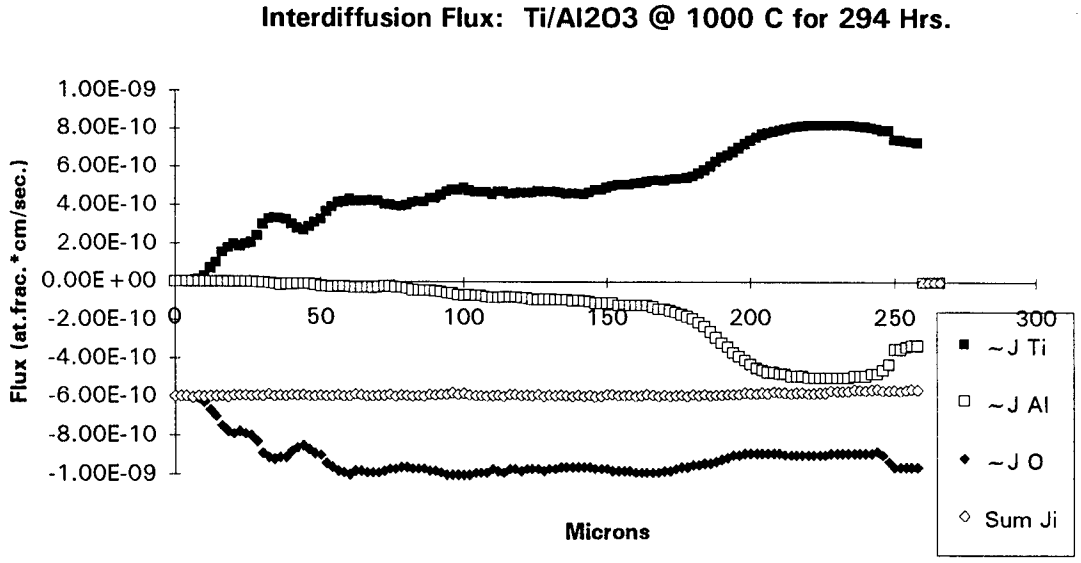

Sum J_i and J_O in error due to oxygen not returning to boundary level in β-Ti.

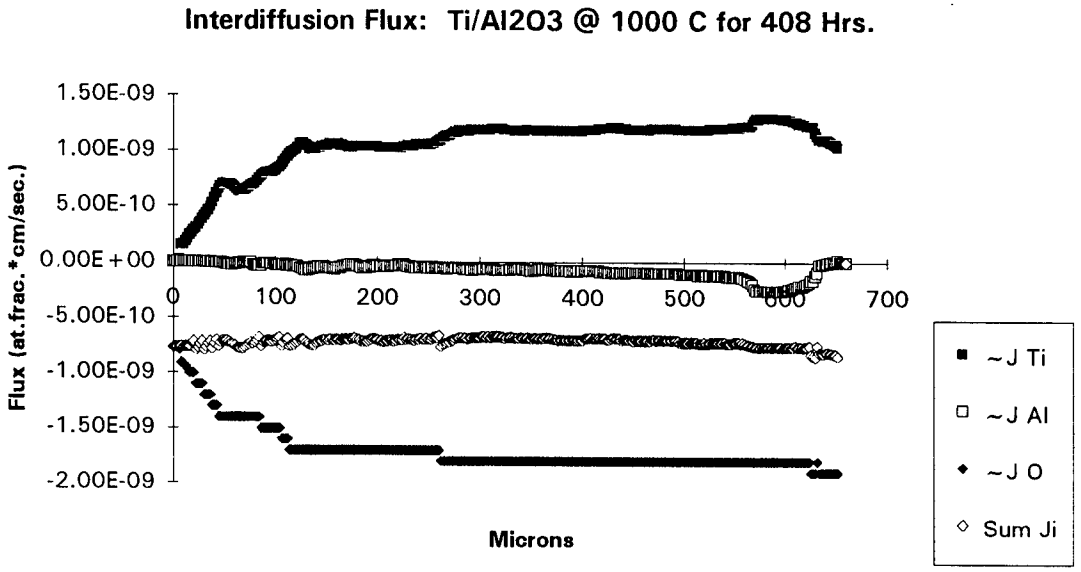

Sum J_i and J_O in error due to oxygen not returning to boundary level in β-Ti.

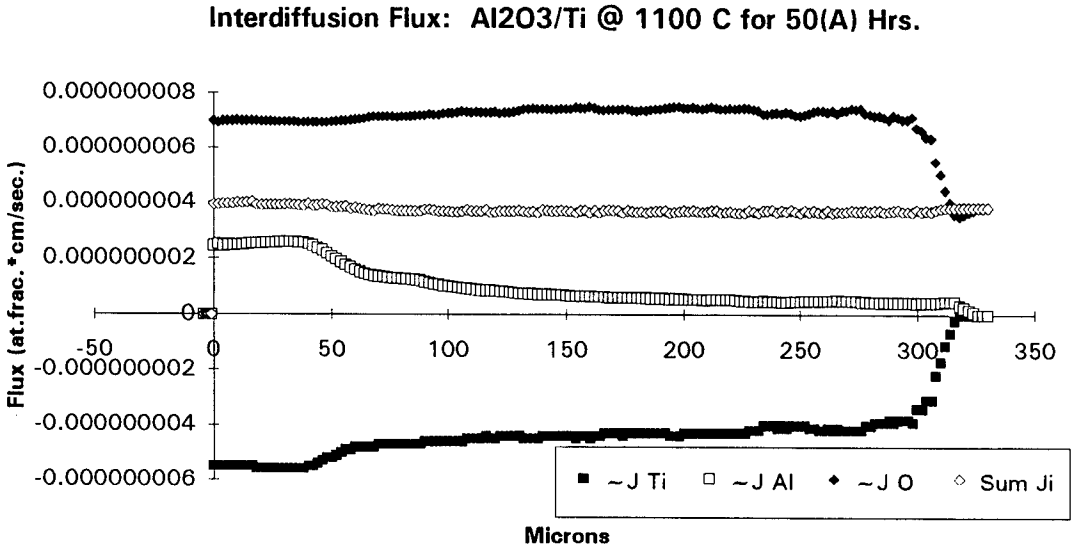

Sum J_i and J_O in error due to oxygen not returning to boundary level in β-Ti.

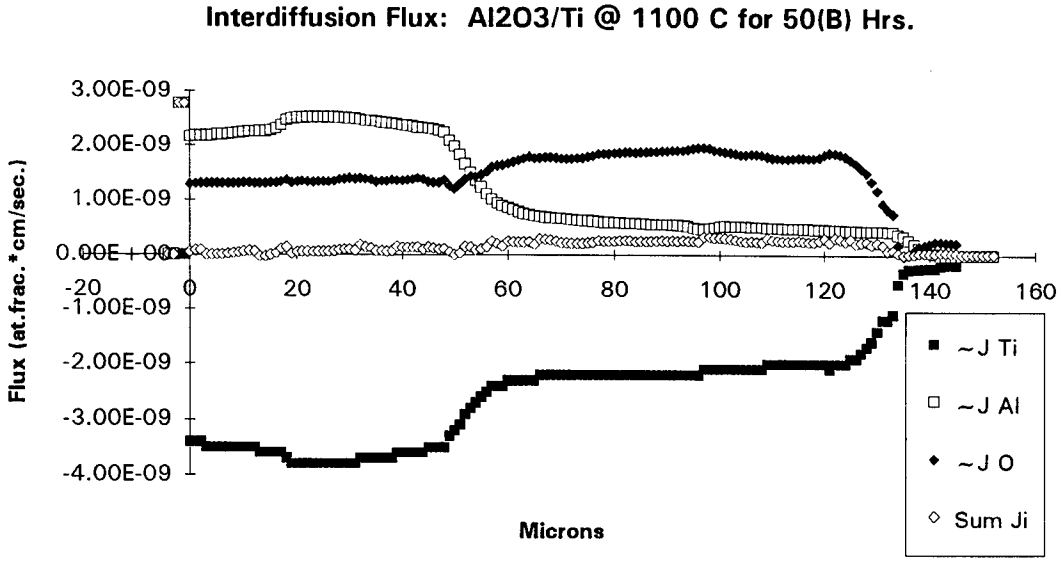

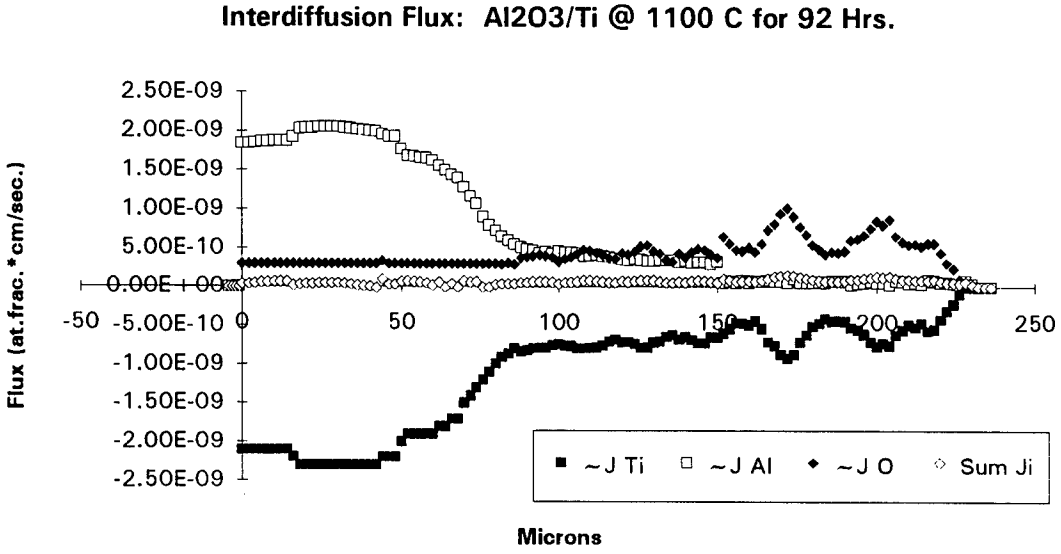

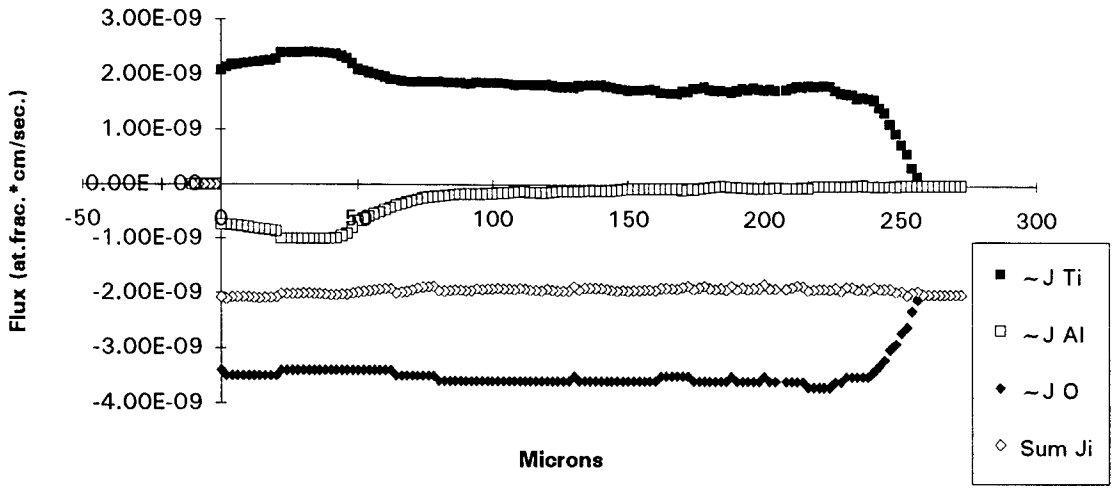

Sum J_i and J_O in error due to oxygen not returning to boundary level in β-Ti.

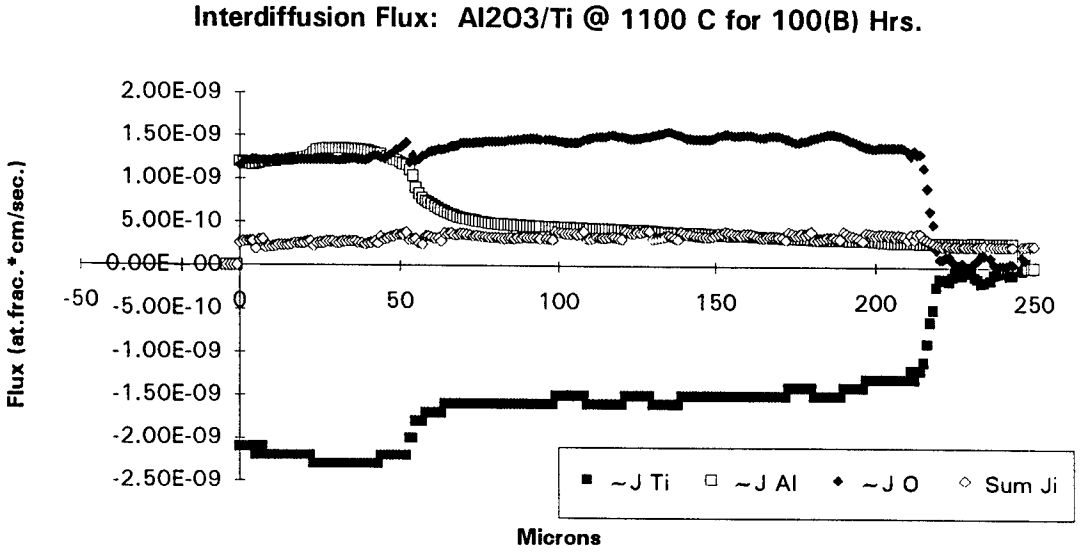

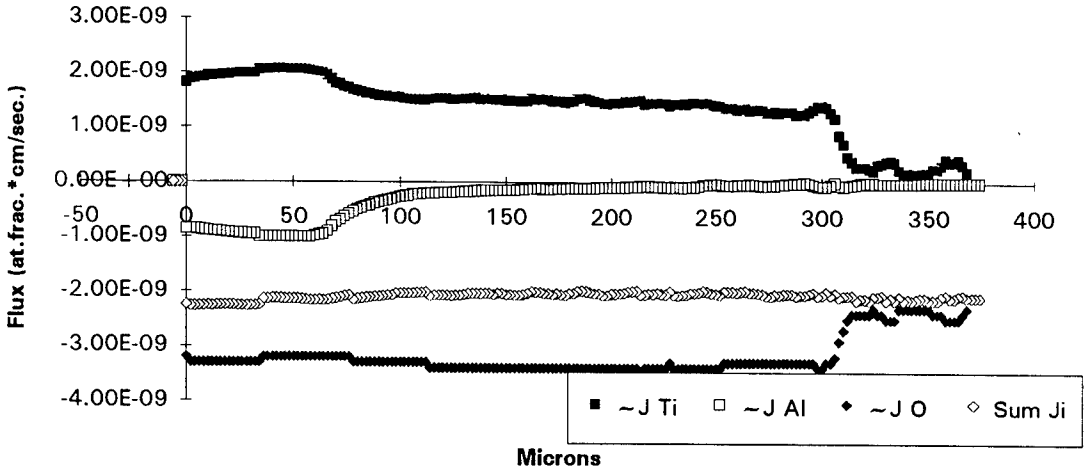

Sum J_i and J_O in error due to oxygen not returning to boundary level in β-Ti.

Interdiffusion Flux: Al2O3/Ti @ 1144 C for 25 Hrs.

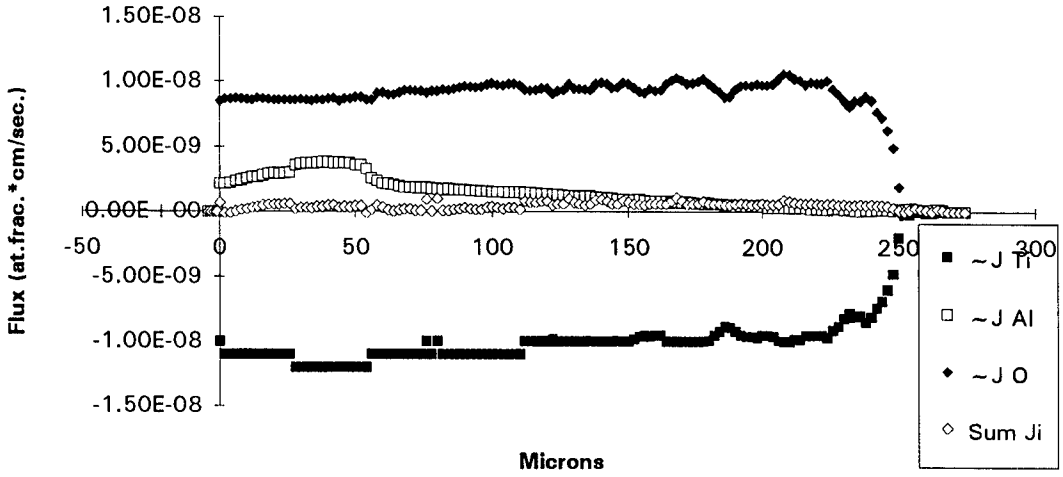

Interdiffusion Flux: Al2O3 @ 1144 C for 50 Hrs.

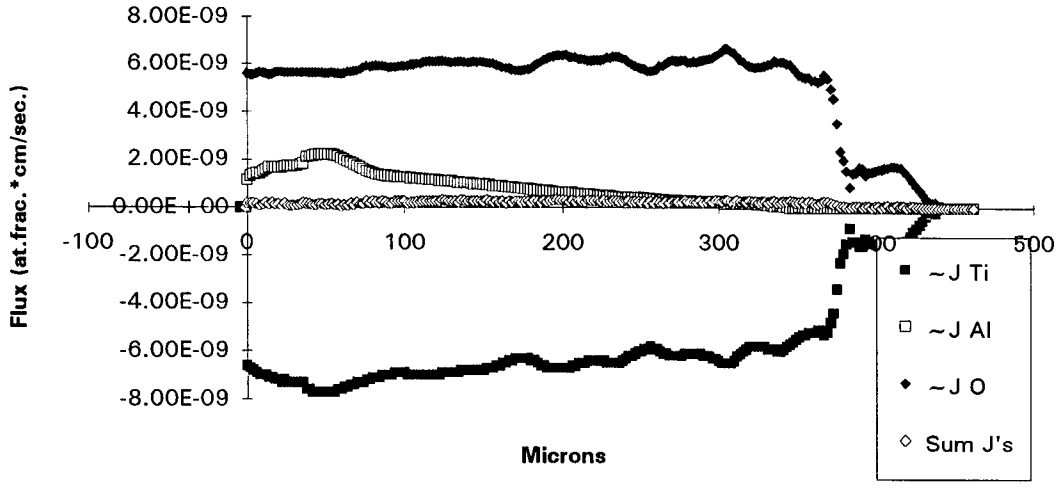

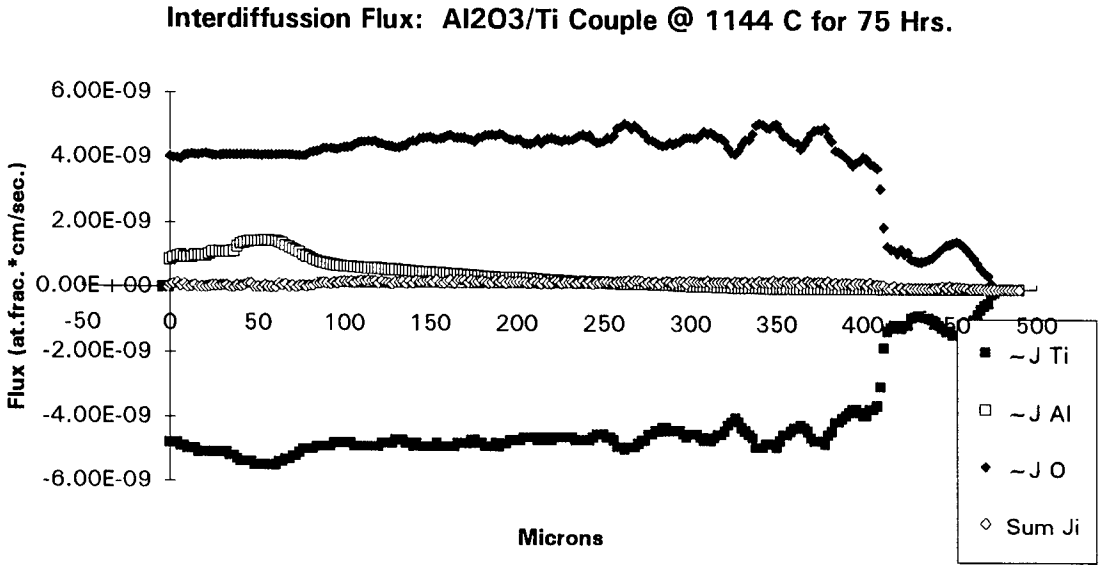
Interdiffussion Flux: Al2O3/Ti Couple @ 1144 C for 75 Hrs.
6.00E-09
4.00E-09
2.00E-09
0.00E+00
-2.00E-09
-4.00E-09
-6.00E-09
-50
0
50
100
150
200
250
300
350
400
450
500
Flux (at.frac.*cm/sec.)
Microns
~J Ti
~J Al
~J O
Sum Ji

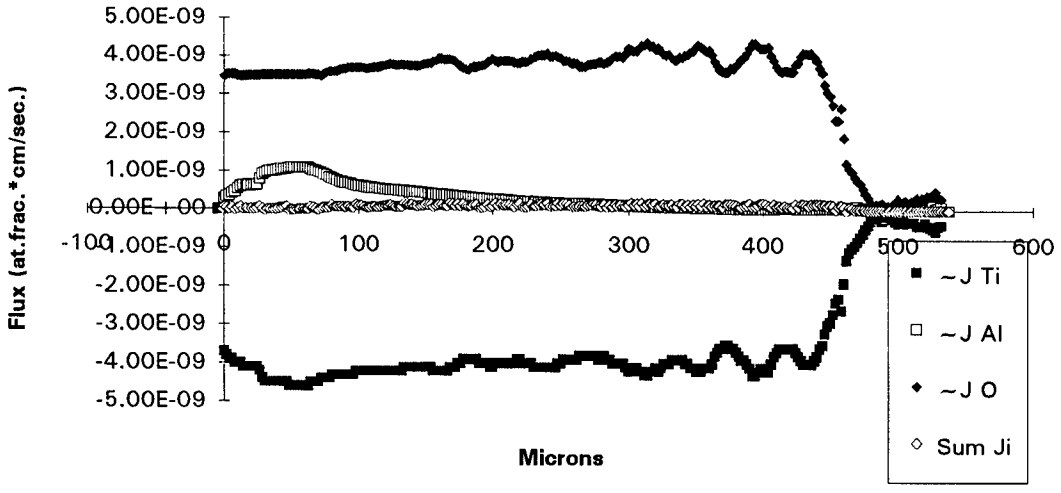
Interdiffusion Flux: Al2O3/Ti @ 1144 C for 100 Hrs.
5.00E-09
4.00E-09
3.00E-09
2.00E-09
1.00E-09
0.00E+00
-1.00E-09
-2.00E-09
-3.00E-09
-4.00E-09
-5.00E-09
-100
0
100
200
300
400
500
600
Flux (at.frac.*cm/sec.)
Microns
~J Ti
~J Al
~J O
Sum Ji

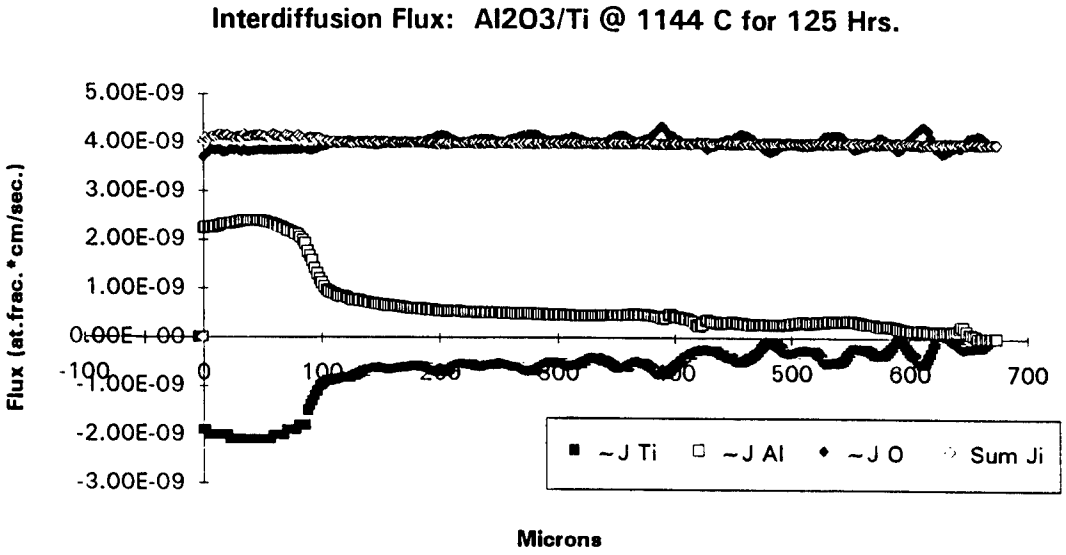

Sum J_i and J_O in error due to oxygen not returning to boundary level in β-Ti.

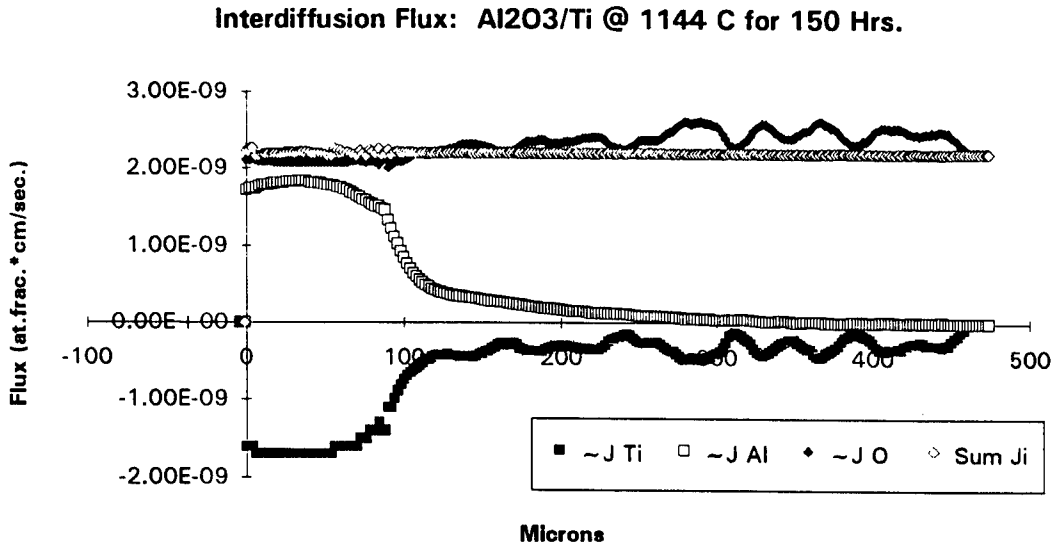

Sum J_i and J_O in error due to oxygen not returning to boundary level in β-Ti.

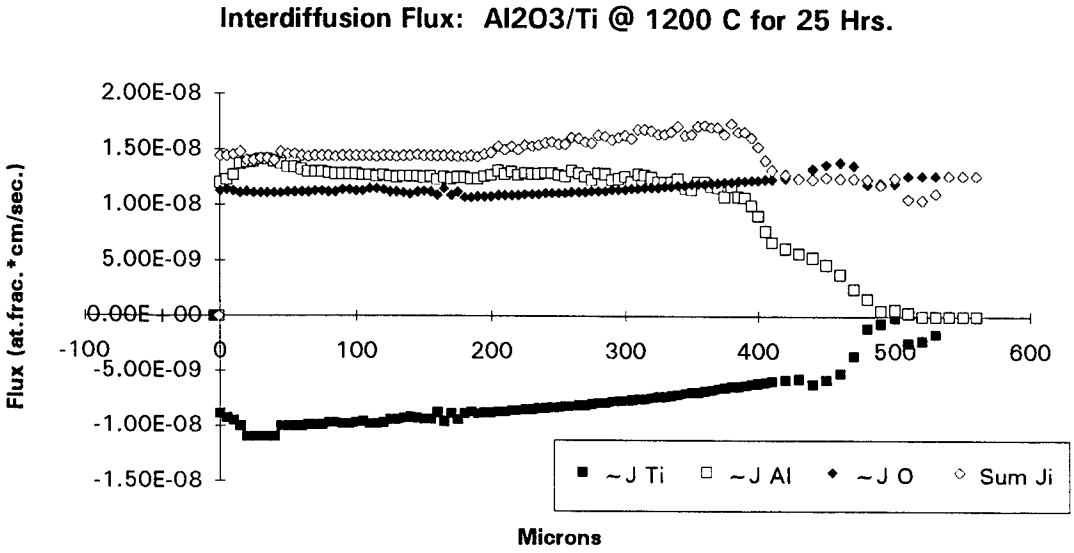

Sum J_i and J_O in error due to oxygen not returning to boundary level in β-Ti.

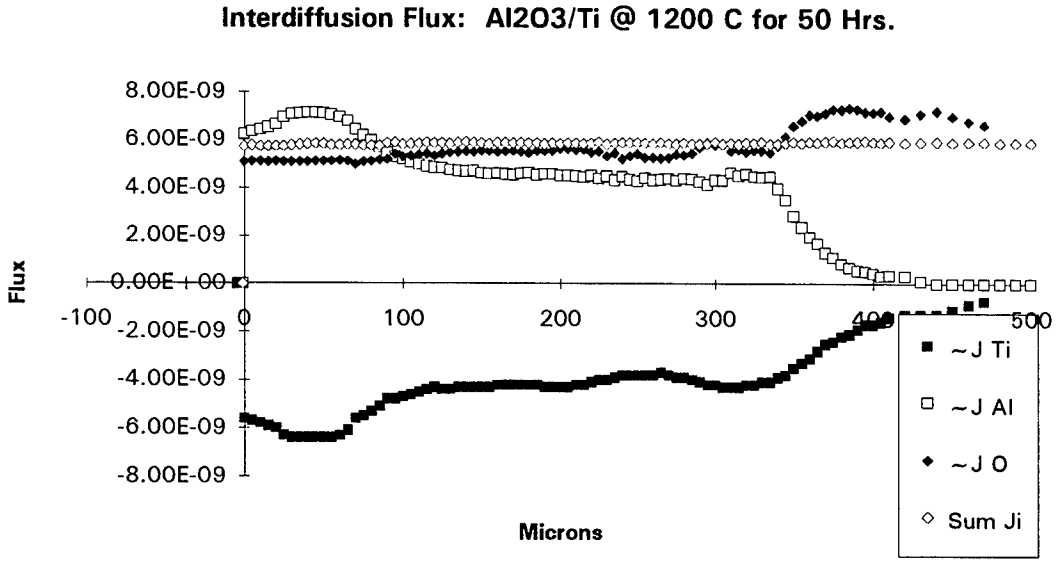

Sum J_i and J_O in error due to oxygen not returning to boundary level in β-Ti.

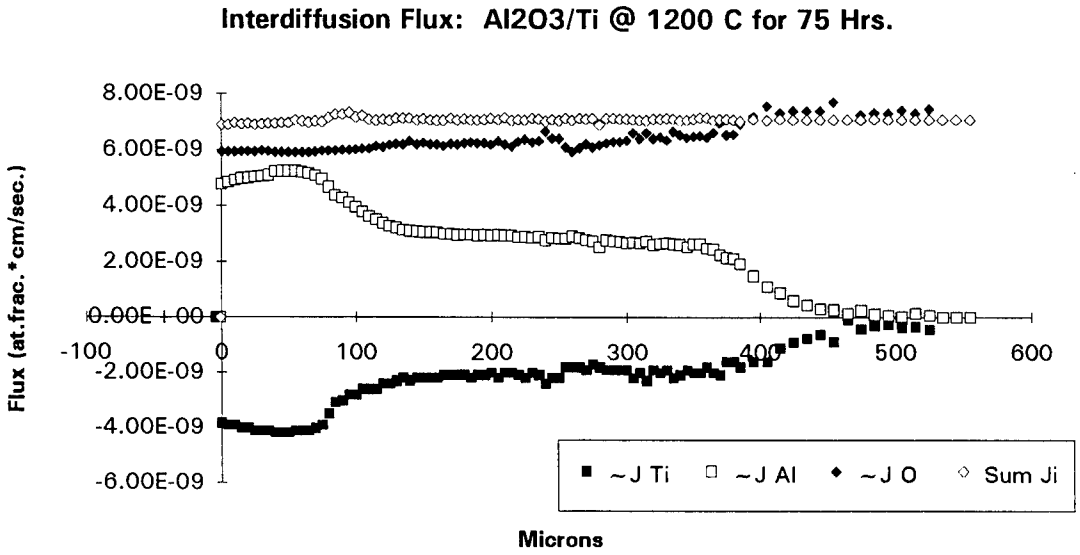

Sum J_i and J_O in error due to oxygen not returning to boundary level in β-Ti.

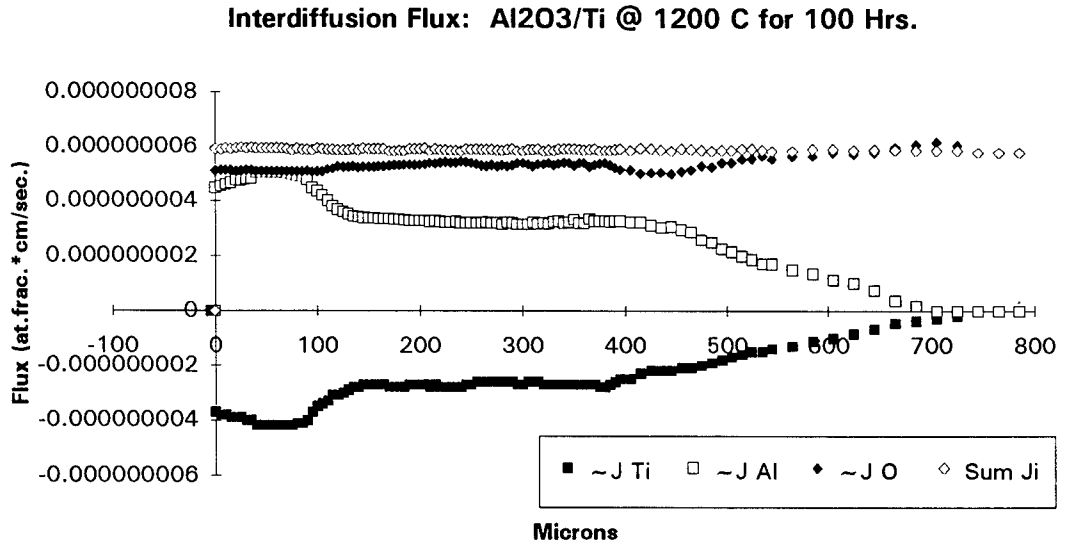

Sum J_i and J_O in error due to oxygen not returning to boundary level in β-Ti.

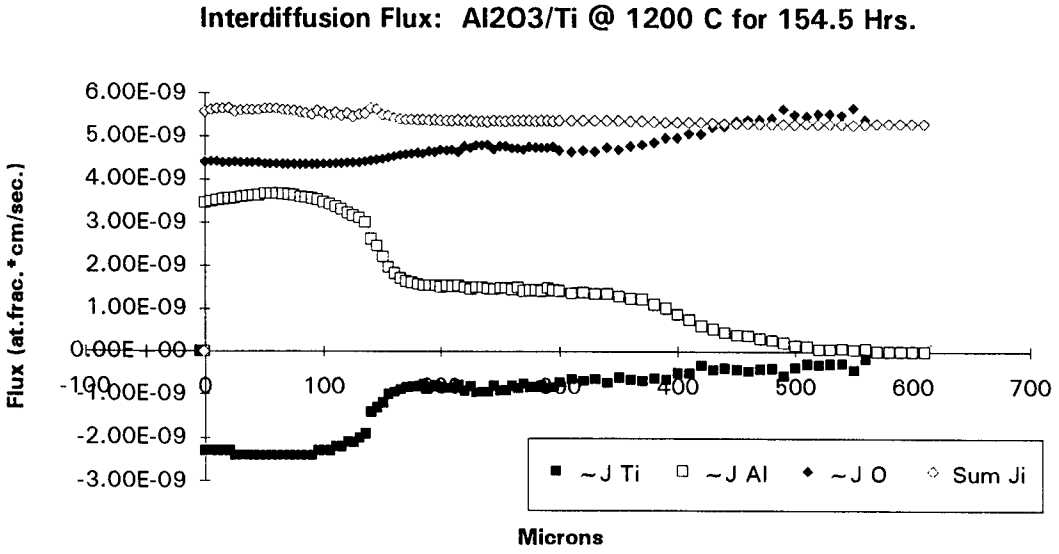

Sum J_i and J_O in error due to oxygen not returning to boundary level in β-Ti.

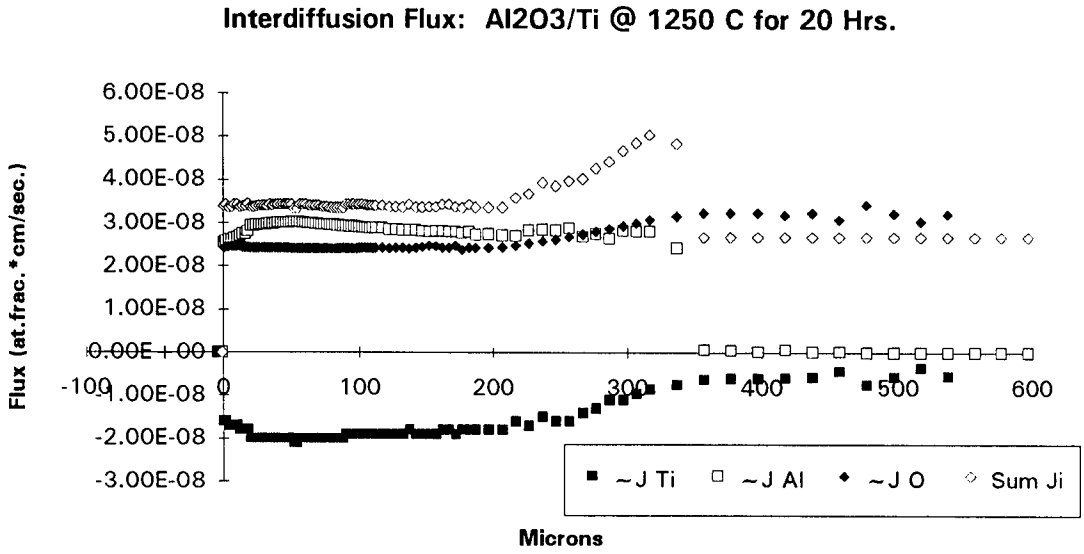

Sum J_i and J_O in error due to oxygen not returning to boundary level in β-Ti.

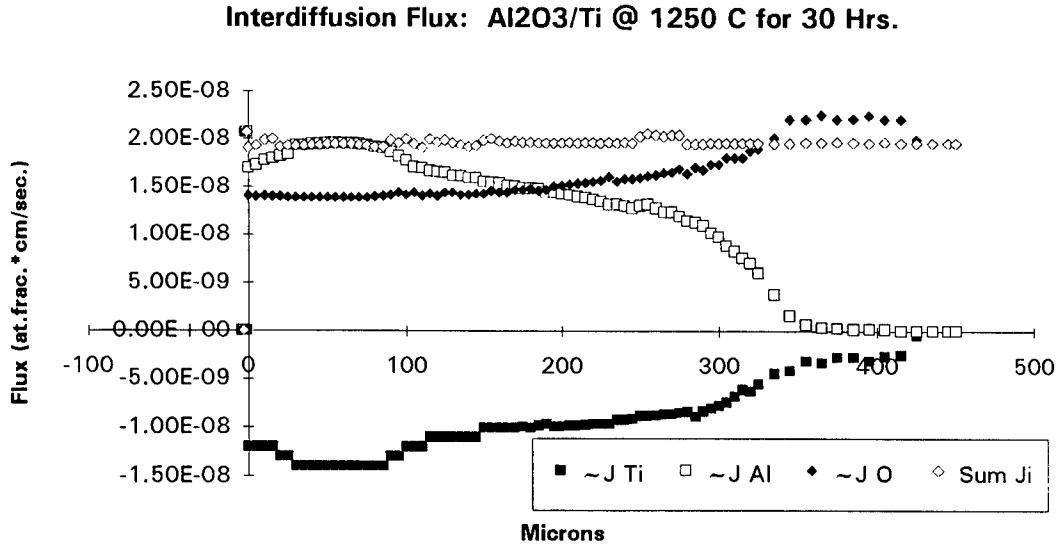

Sum J_i and J_O in error due to oxygen not returning to boundary level in β-Ti.

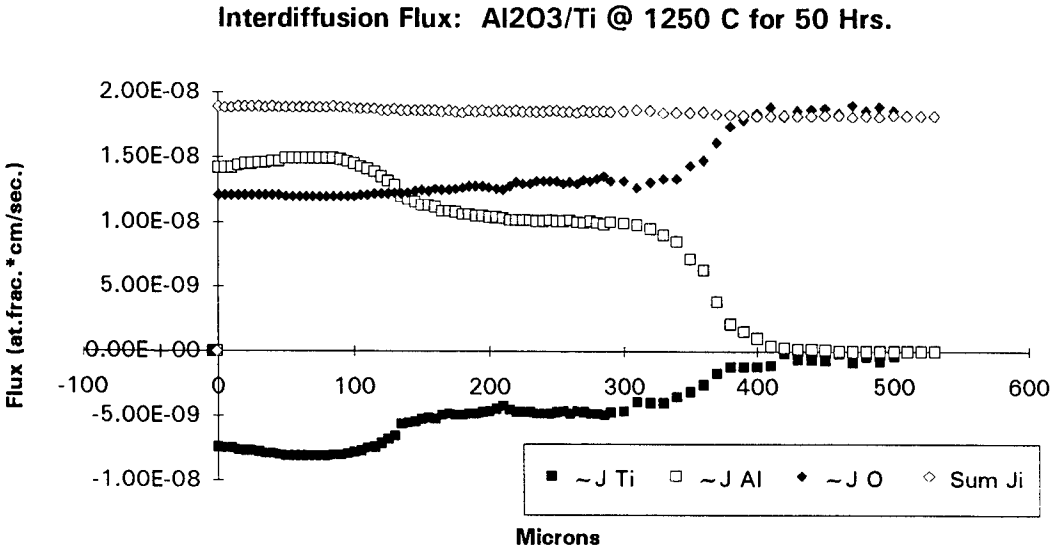

Sum J_i and J_O in error due to oxygen not returning to boundary level in β-Ti.

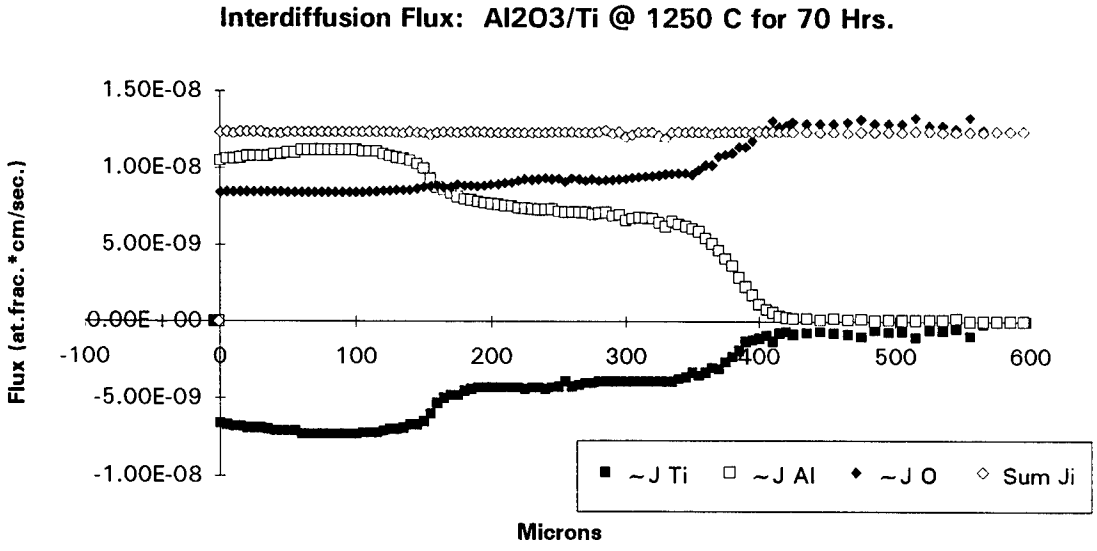

Sum J_i and J_O in error due to oxygen not returning to boundary level in β-Ti.

Interdiffusion Flux: Ti3Al/Al2O3 @ 1100 C for 50 Hrs.

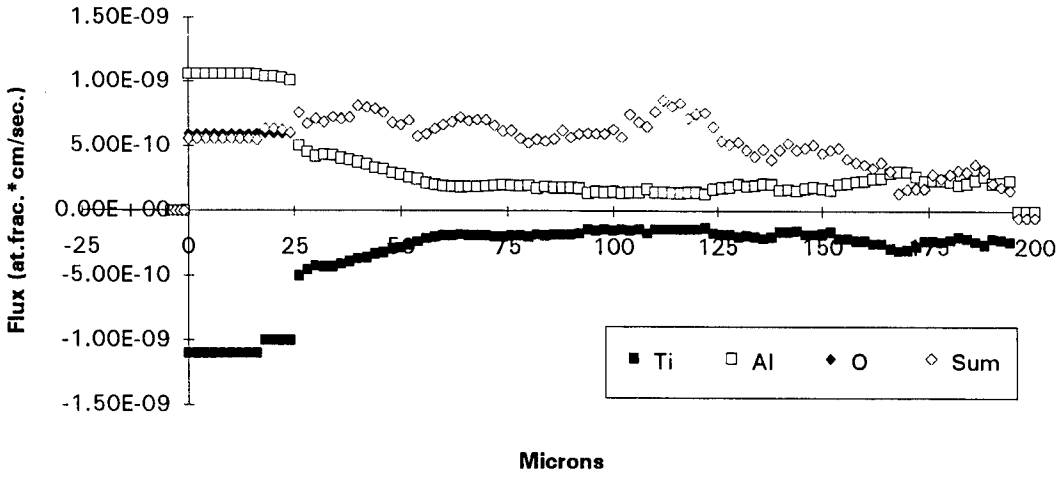

Interdiffusion Flux: Ti3Al/Al2O3 @ 1100 C for 145 Hrs.

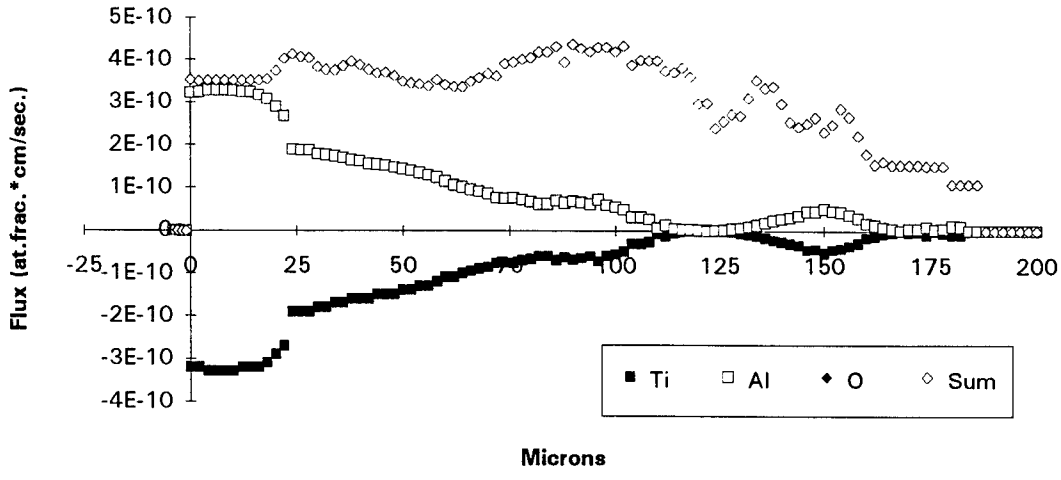

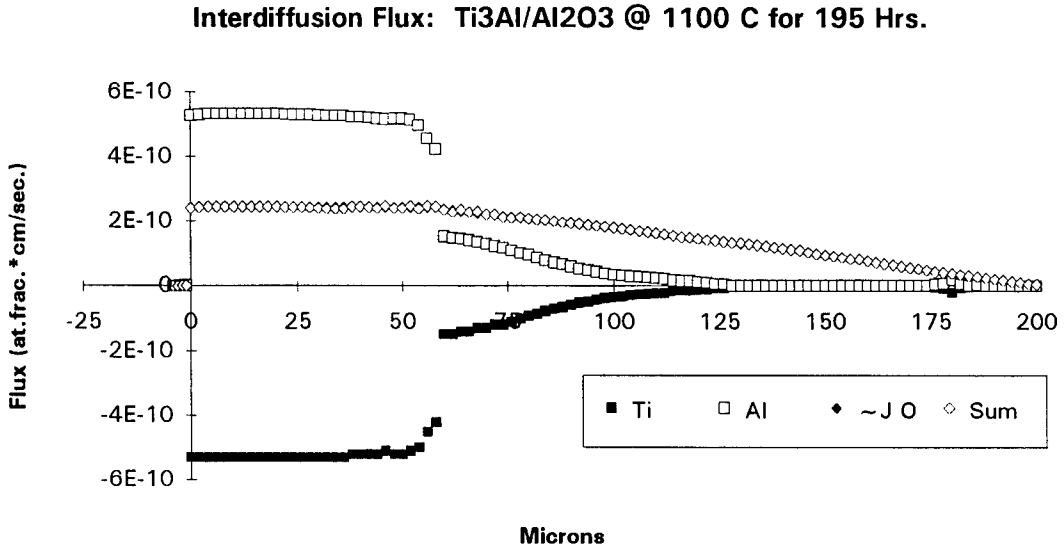
Interdiffusion Flux: Ti3Al/Al2O3 @ 1100 C for 195 Hrs.
Flux (at.frac.*cm/sec.)
6E-10
4E-10
2E-10
0
-2E-10
-4E-10
-6E-10
-25
0
25
50
100
125
150
175
200
Ti
Al
~J O
Sum
Microns

APPENDIX D: INTERDIFFUSION COEFFICIENT CALCULATION RESULTS

This appendix contains the interdiffusion coefficient results for chosen diffusion couples. The samples, in order of presentation, are those of the types: 1) Ti/Al_2O_3, and 2) α_2-Ti_3Al/Al_2O_3. These results are in the form of interdiffusion coefficient vs. position plots, with the coefficient units in centimeters^2/second and the position units in microns measured from the metal|ceramic interface. The results appear in order of increasing temperature and time, respectively. Comments accompany these results where instructive. These results were calculated from the EPMA results of App. A using the Boltzmann-Matano methodology presented in section 3.3. These results are summarized in sections 5.1.2 and 5.2.2.

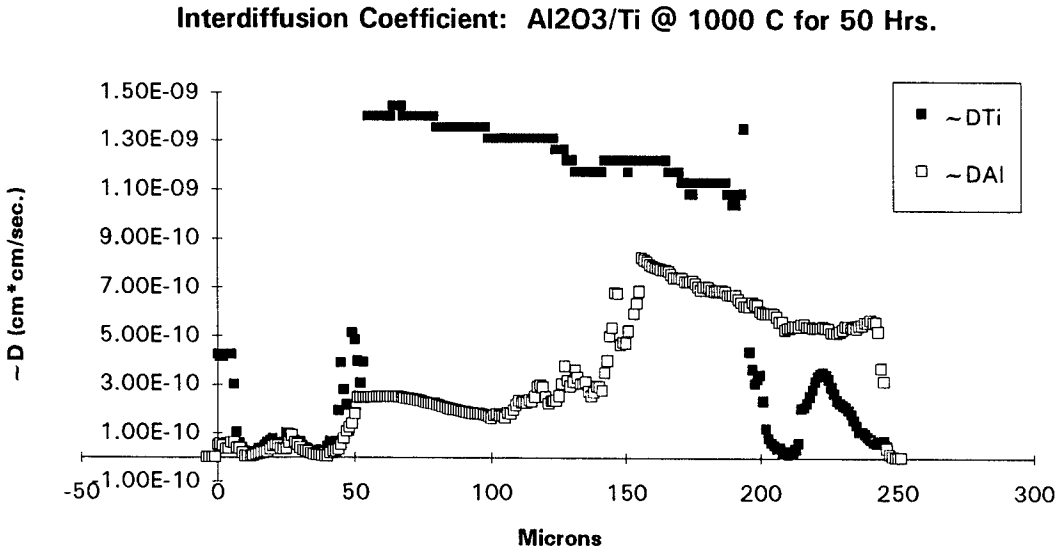

Scatter due to scatter in EPMA results and in the estimation of composition gradient (applies throughout these results).

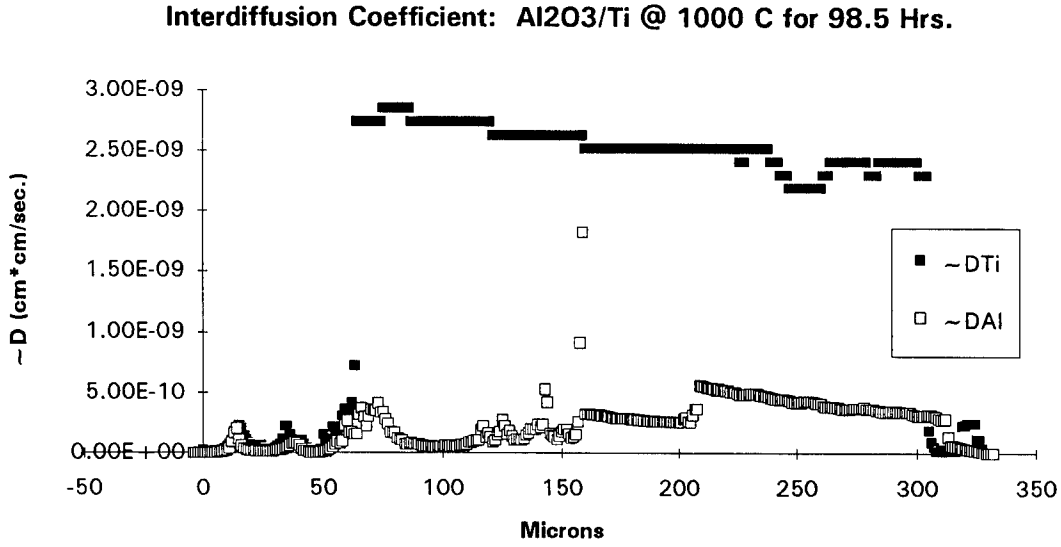

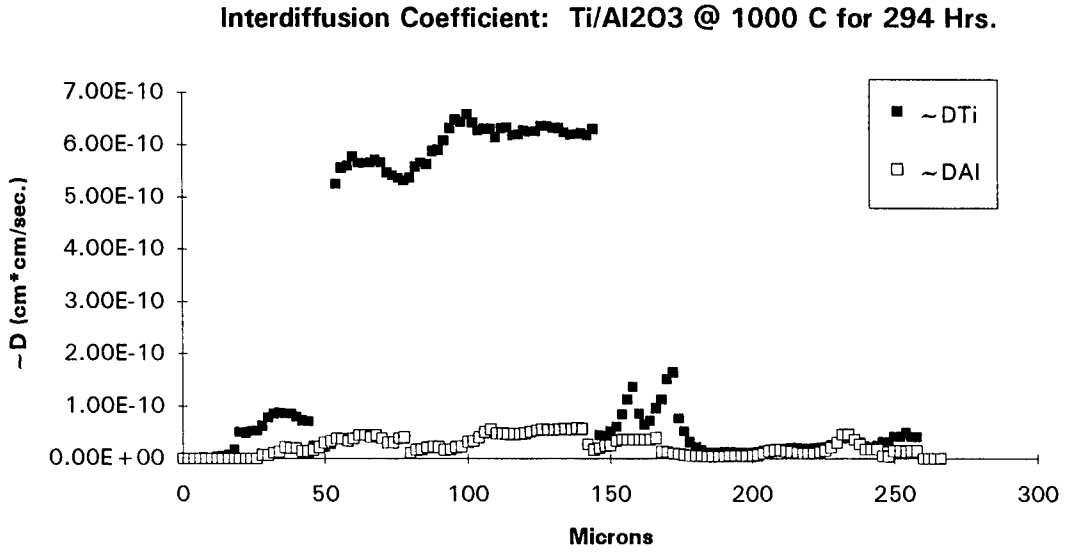
Interdiffusion Coefficient: Ti/Al2O3 @ 1000 C for 294 Hrs.
7.00E-10
6.00E-10
5.00E-10
4.00E-10
3.00E-10
2.00E-10
1.00E-10
0.00E+00
~D (cm*cm/sec.)
0
50
100
150
200
250
300
Microns
~DTi
~DAl

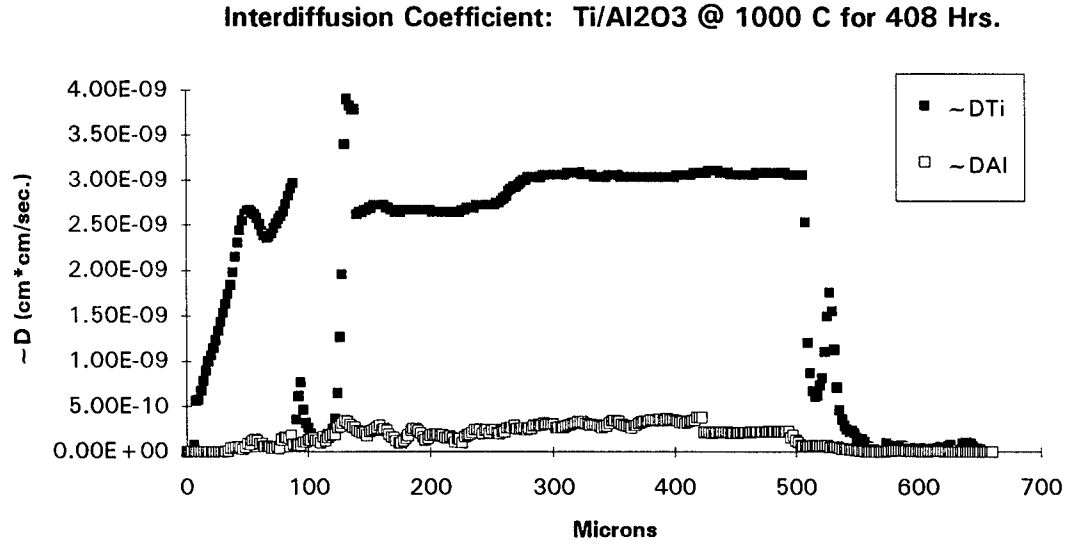
Interdiffusion Coefficient: Ti/Al2O3 @ 1000 C for 408 Hrs.
4.00E-09
3.50E-09
3.00E-09
2.50E-09
2.00E-09
1.50E-09
1.00E-09
5.00E-10
0.00E+00
~D (cm*cm/sec.)
0
100
200
300
400
500
600
700
Microns
~DTi
~DAl

Interdiffusion Coef.: Al2O3/Ti @ 1100 C for 50(A) Hrs.

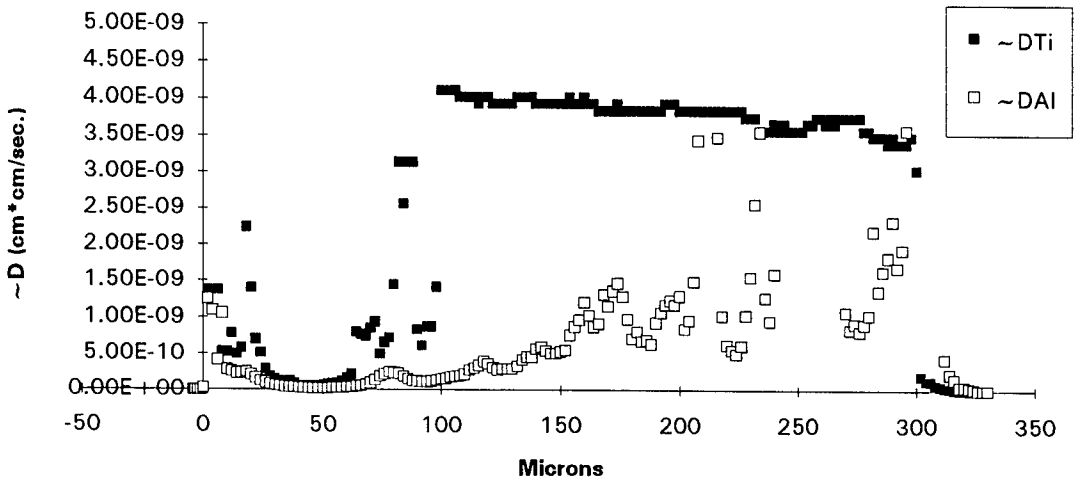

Interdiffusion Coef.: Al2O3/Ti @ 1100 C for 50(B) Hrs.

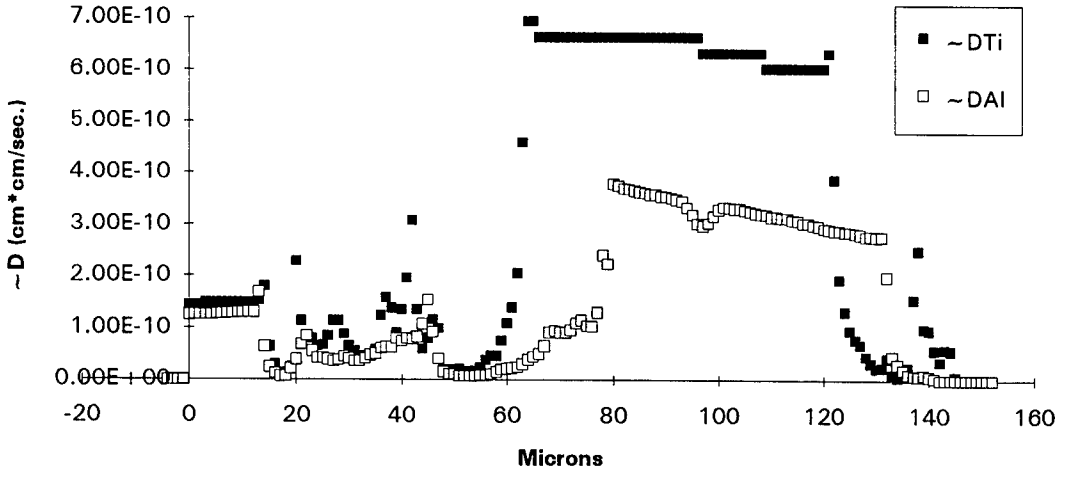

Interdiffusion Coef.: Al2O3/Ti @ 1100 C for 100(A) Hrs.

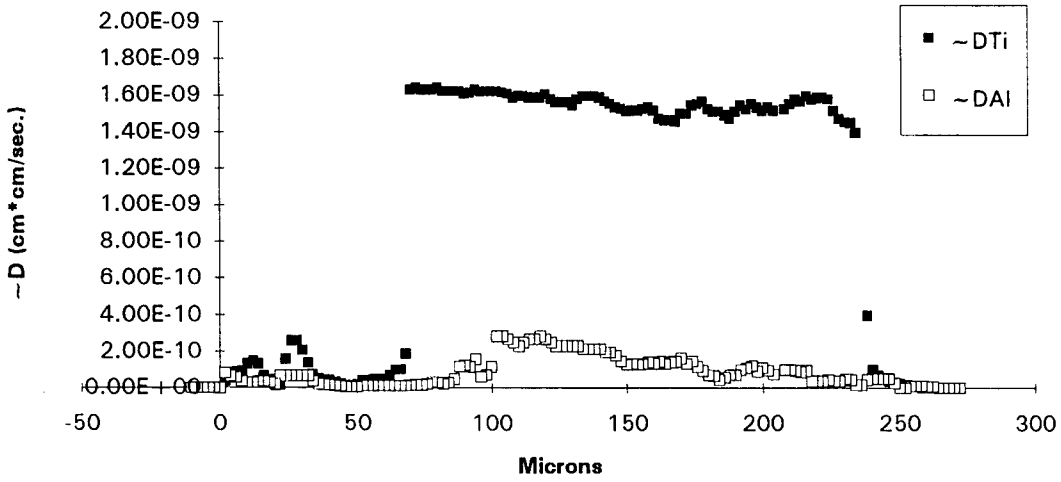

Interdiffusion Coef.: Al2O3/Ti @ 1100 C for 100(B) Hrs.

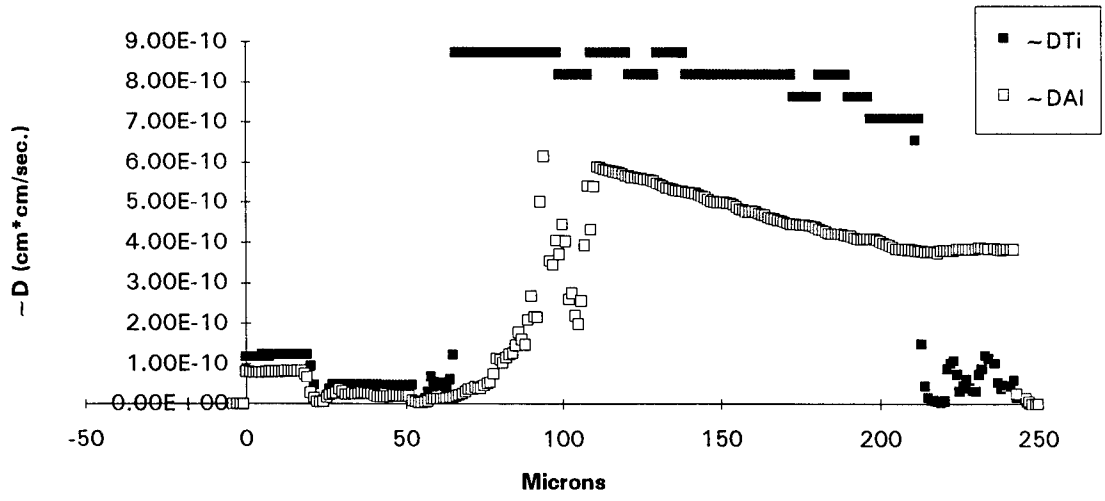

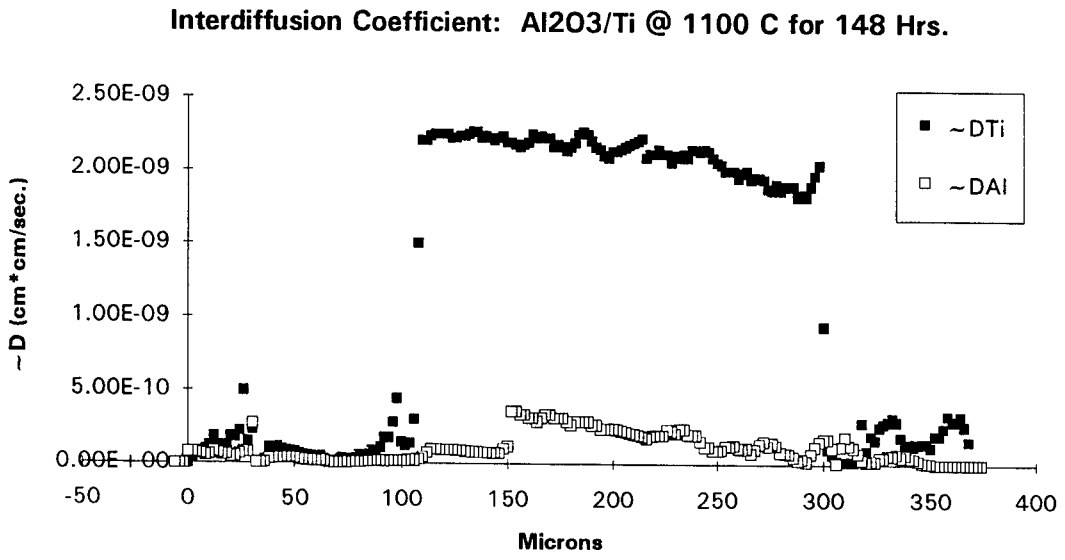
Interdiffusion Coefficient: Al2O3/Ti @ 1100 C for 148 Hrs.
2.50E-09
2.00E-09
1.50E-09
1.00E-09
5.00E-10
0.00E+00
~D (cm*cm/sec.)
-50
0
50
100
150
200
250
300
350
400
Microns
~DTi
~DAl

Diffusion Coefficients: Al2O3/Ti @ 1144 C for 25 Hrs.

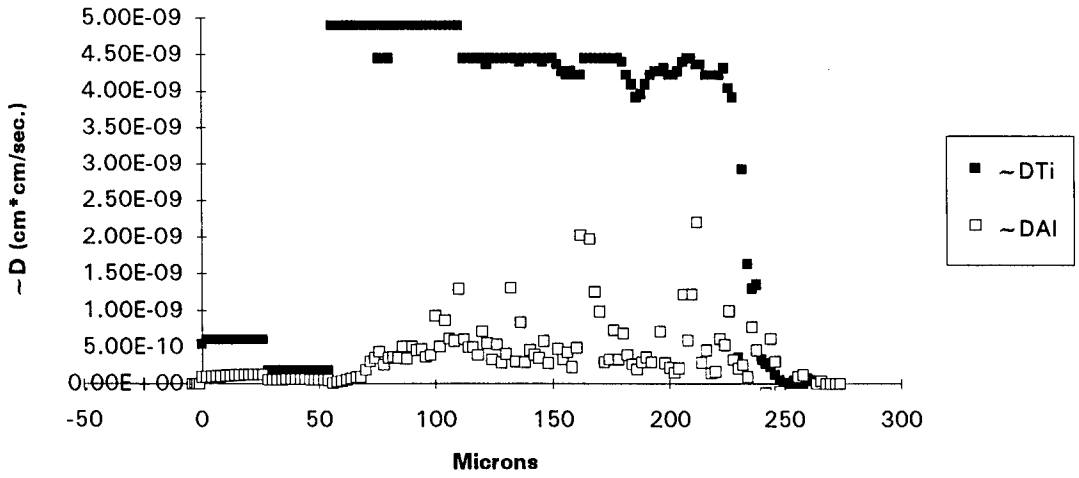

Interdiffusion Coefficients: Al2O3/Ti @ 1144 C for 50 Hrs.

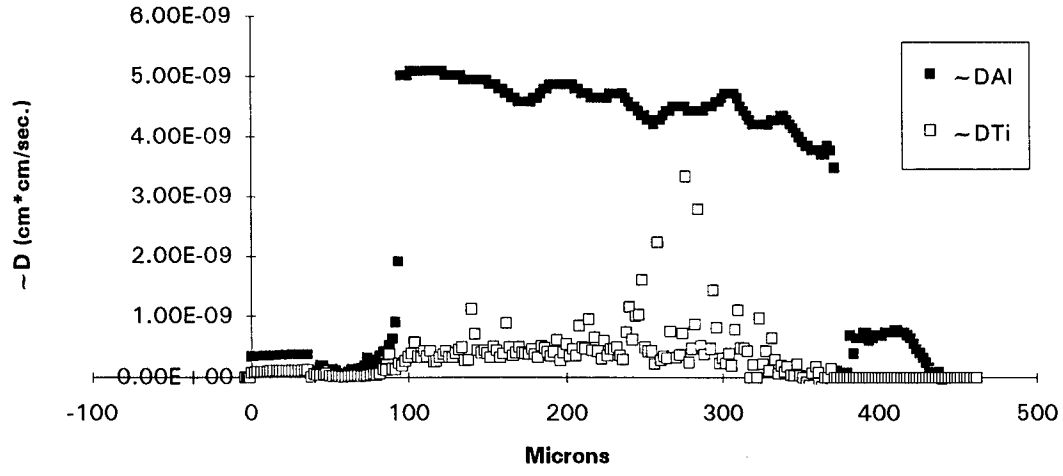

Interdiffusion Coefficient: Al2O3/Ti @ 1144 C for 75 Hrs.

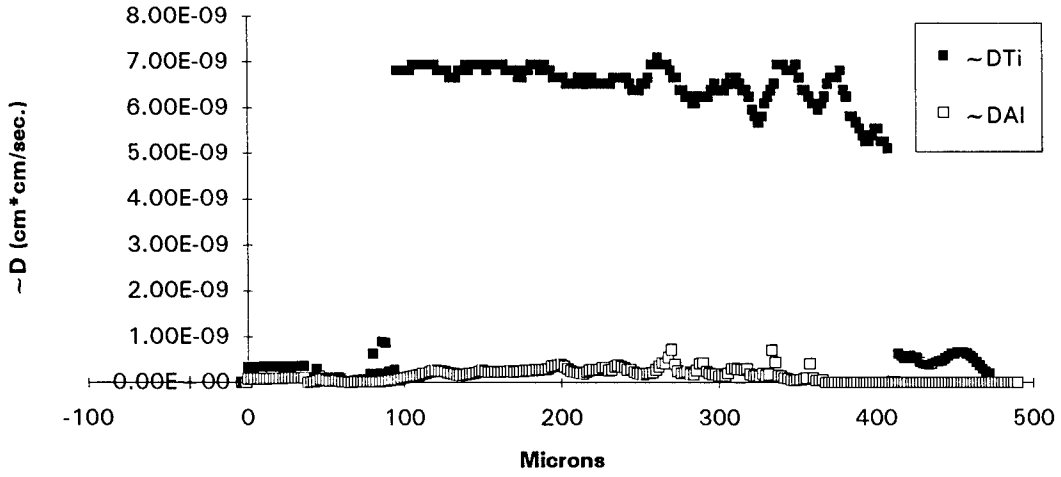

Interdiffusion Coefficient: Al2O3/Ti @ 1144 C for 100 Hrs.

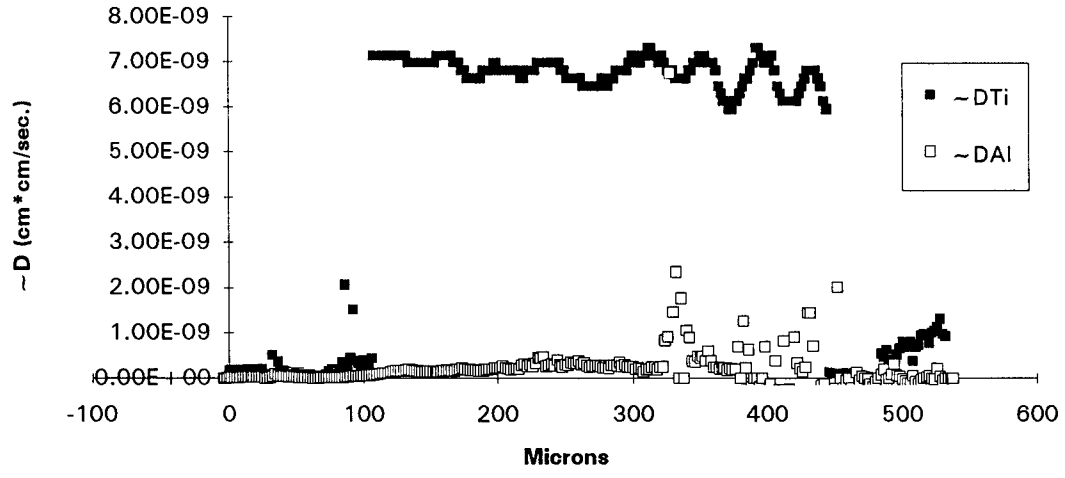

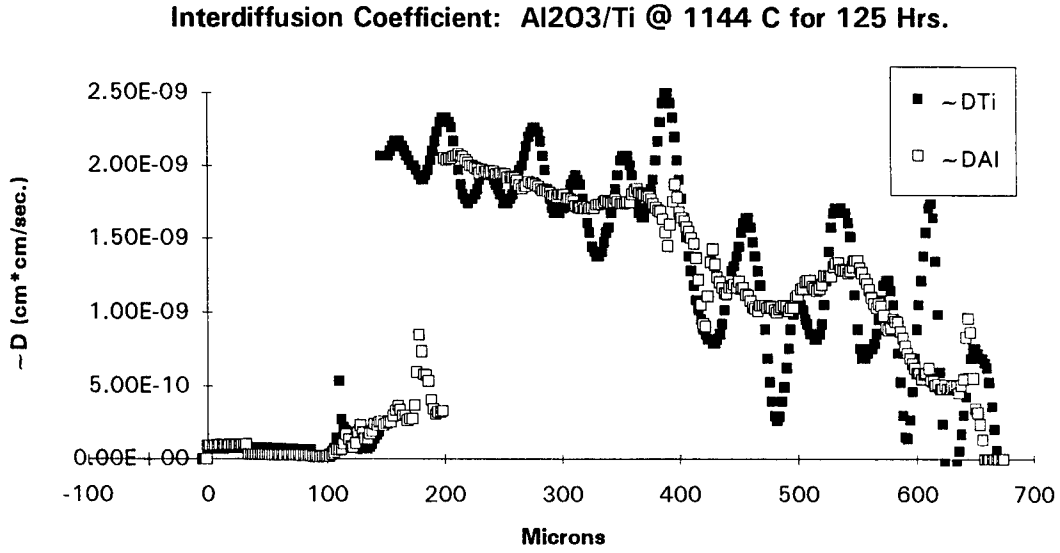
Interdiffusion Coefficient: Al2O3/Ti @ 1144 C for 125 Hrs.
~D (cm*cm/sec.)
2.50E-09
2.00E-09
1.50E-09
1.00E-09
5.00E-10
0.00E+00
-100
0
100
200
300
400
500
600
700
Microns
~DTi
~DAl

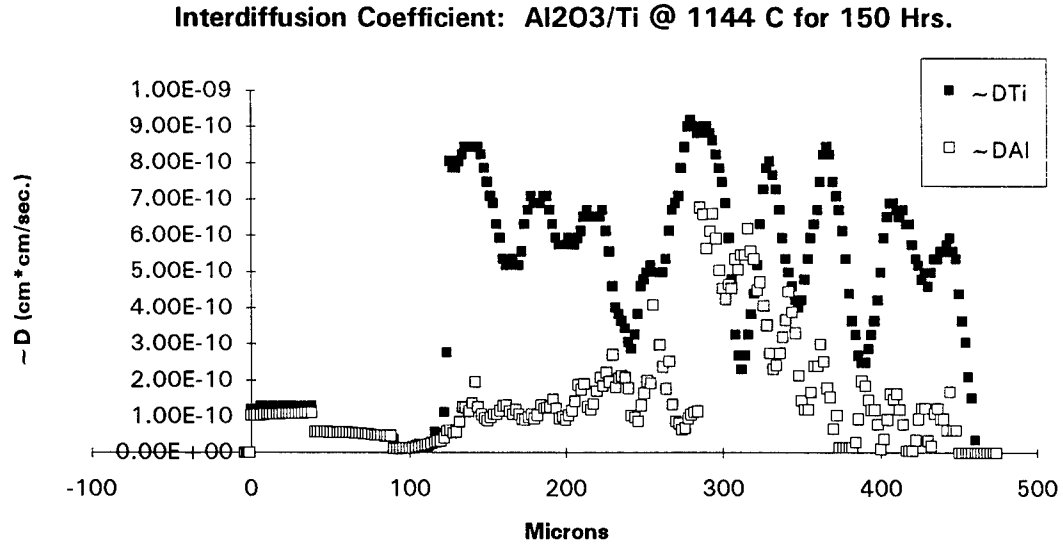
Interdiffusion Coefficient: Al2O3/Ti @ 1144 C for 150 Hrs.
~D (cm*cm/sec.)
1.00E-09
9.00E-10
8.00E-10
7.00E-10
6.00E-10
5.00E-10
4.00E-10
3.00E-10
2.00E-10
1.00E-10
0.00E+00
-100
0
100
200
300
400
500
Microns
~DTi
~DAl

Interdiffusion Coefficient: Al2O3/Ti @ 1200 C for 25 Hrs.

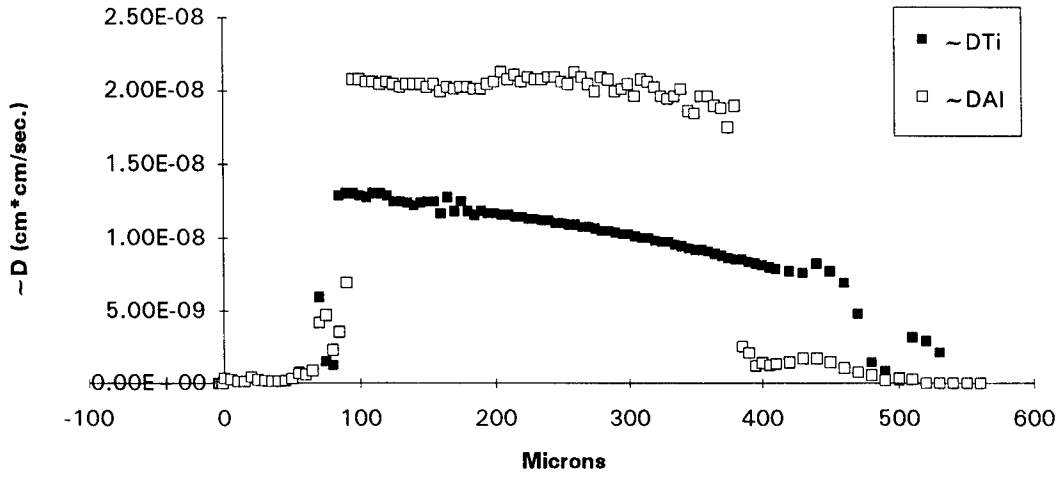

Interdiffusion Coefficient: Al2O3/Ti @ 1200 C for 50 Hrs.

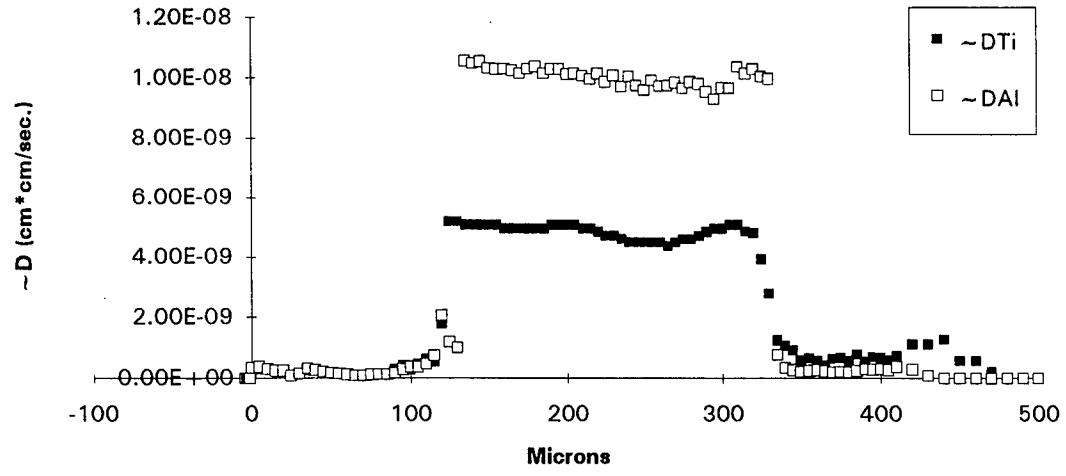

Interdiffusion Coefficient: Al2O3/Ti @ 1200 C for 75 Hrs.

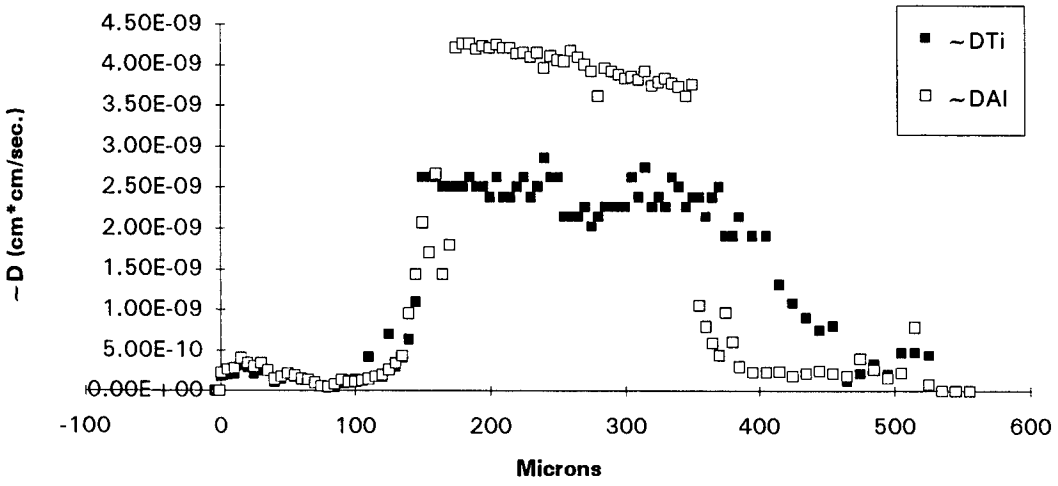

Interdiffusion Coefficient: Al2O3/Ti @ 1200 C for 100 Hrs.

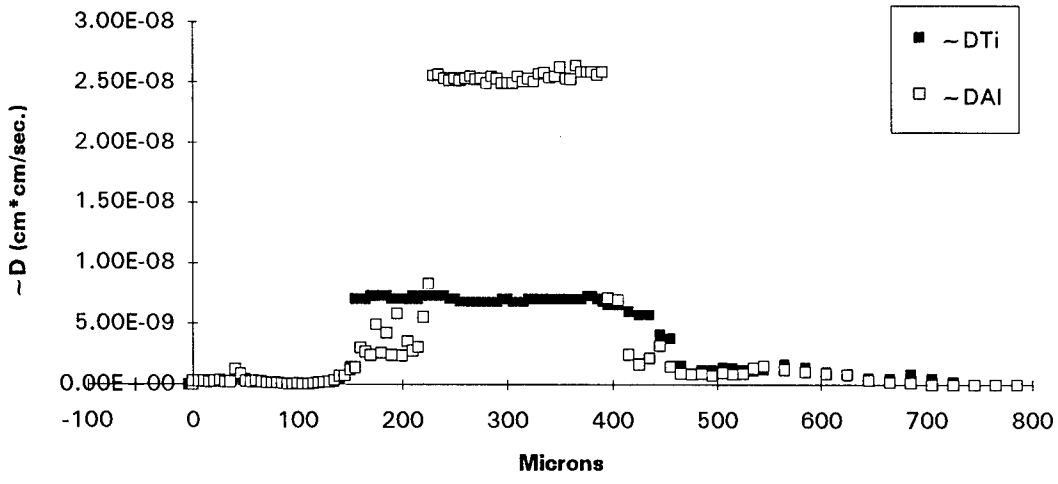

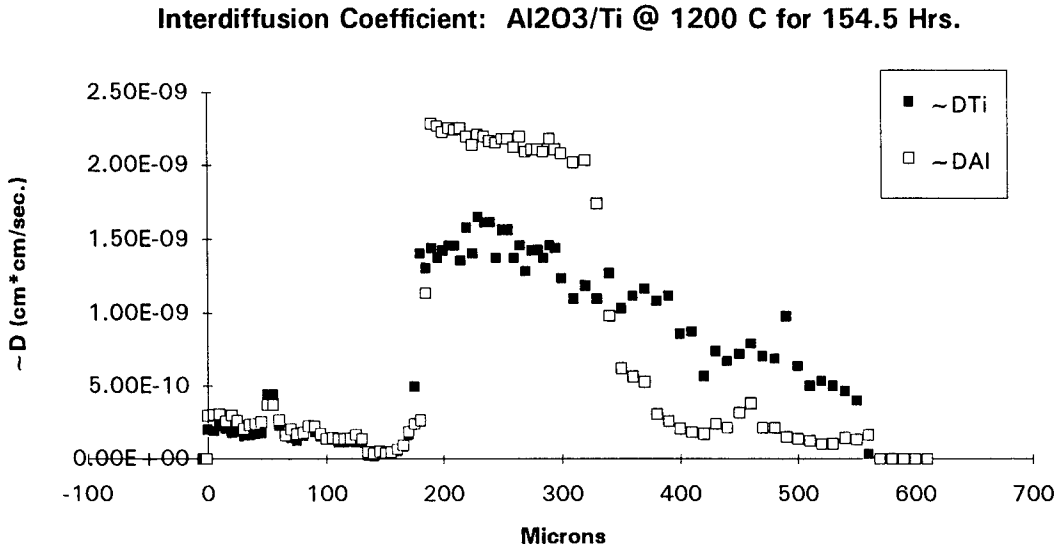
Interdiffusion Coefficient: Al2O3/Ti @ 1200 C for 154.5 Hrs.
2.50E-09
2.00E-09
1.50E-09
1.00E-09
5.00E-10
0.00E+00
~D (cm*cm/sec.)
-100
0
100
200
300
400
500
600
700
Microns
~DTi
~DAl

Interdiffusion Coefficient: Al2O3/Ti @ 1250 C for 20 Hrs.

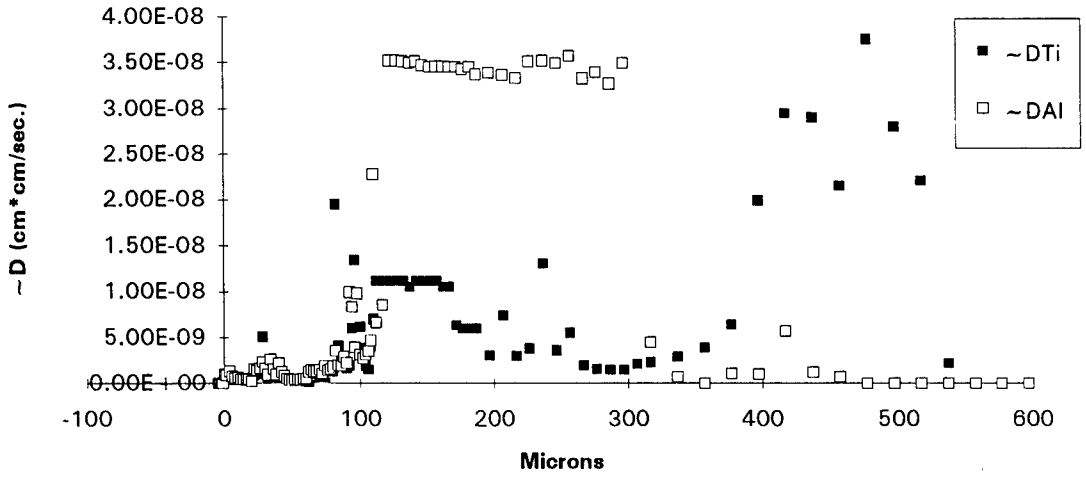

Interdiffusion Coefficient: Al2O3/Ti @ 1250 C for 30 Hrs.

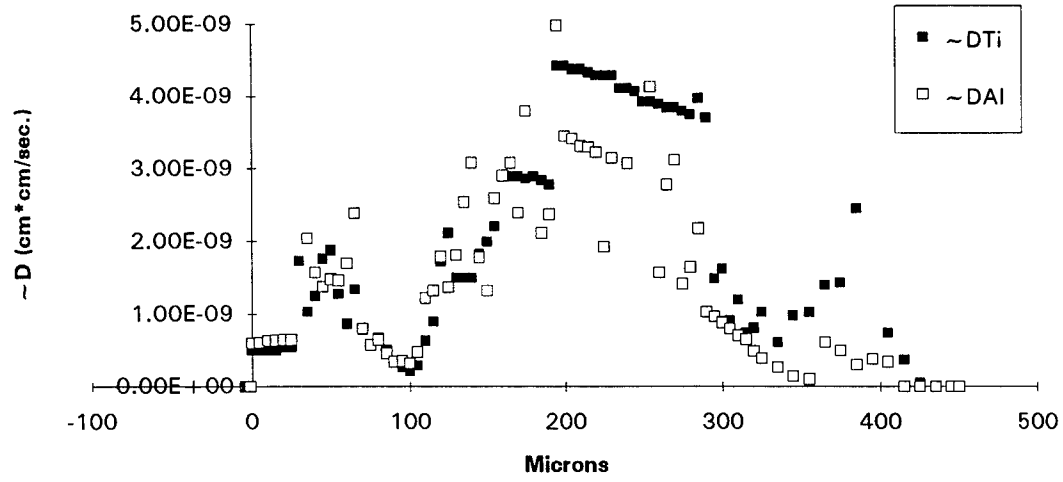

Interdiffusion Coefficient: Al2O3/Ti @ 1250 C for 50 Hrs.

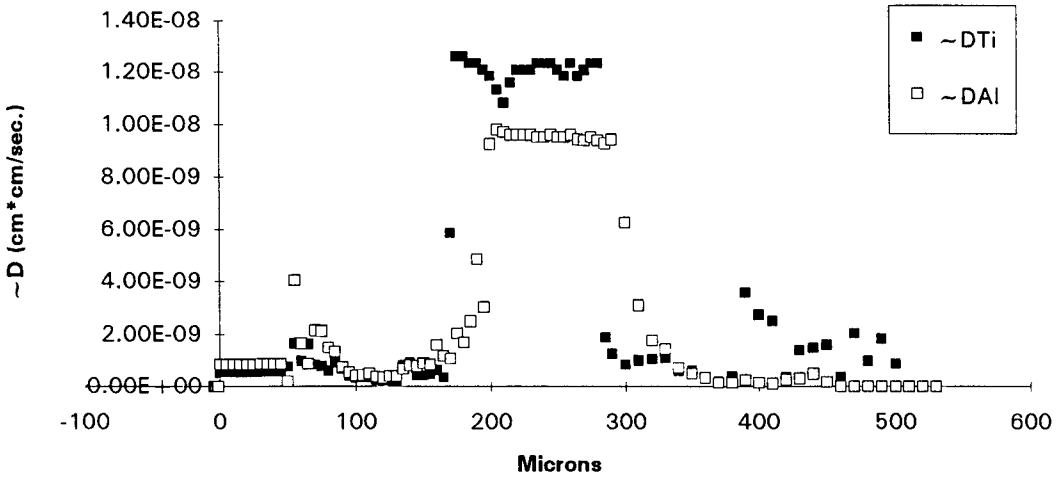

Interdiffusion Coefficient: Al2O3/Ti @ 1250 C for 70 Hrs.

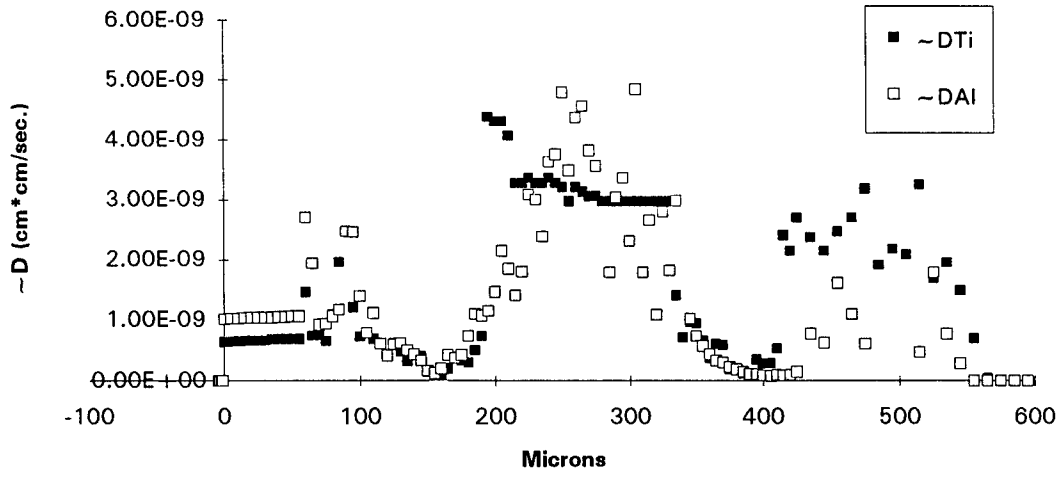

Interdiffusion Coef.: Ti3Al/Al2O3 @ 1100 C for 50 Hrs.

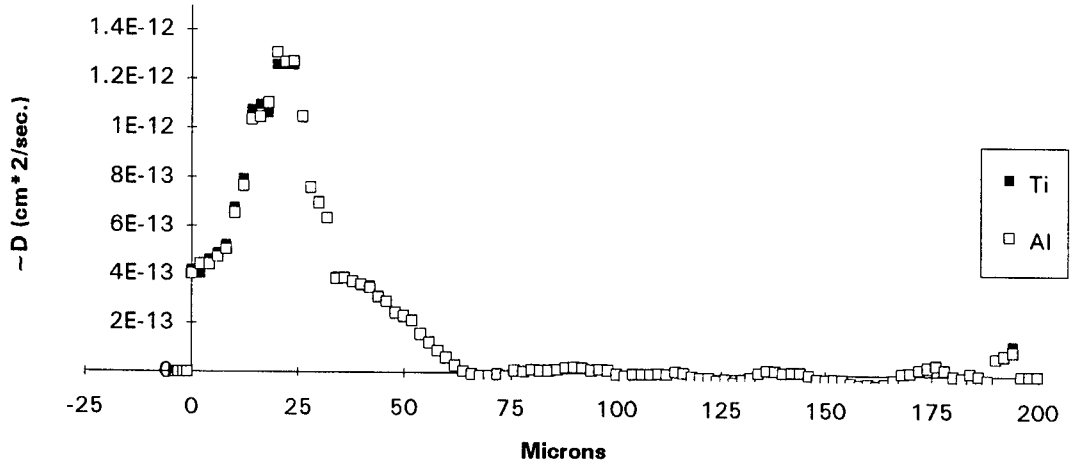

Interdiffusion Coef.: Ti3Al/Al2O3 @ 1100 C for 195 Hrs.

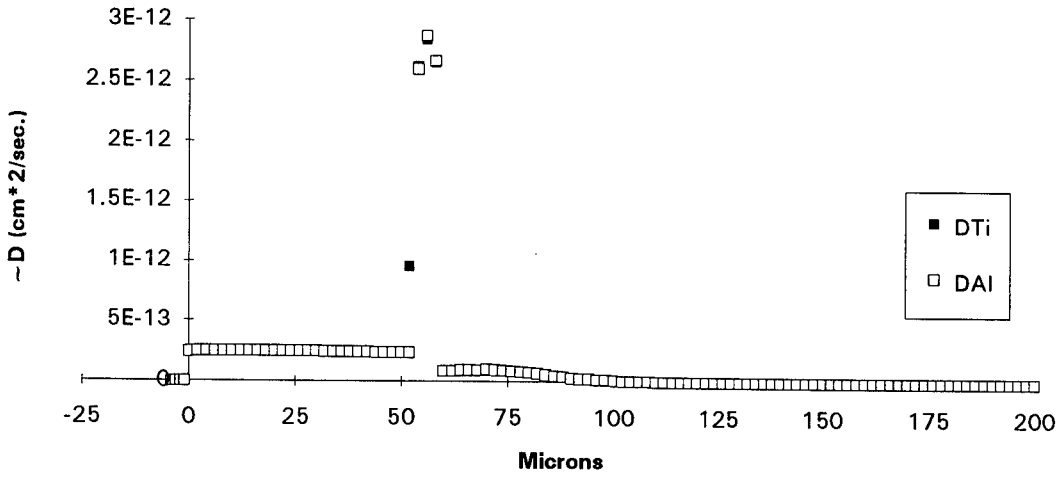

REFERENCES

[31Ons] L. Onsager, Phys. Rev., **38**, p. 2265, 1931.

[33Mat] C. Matano, Japan Phys., **8**, p. 109, 1933.

[45Ons] L. Onsager, N.Y. Acad. Sci., **46**, p. 241, 1945.

[48Dar] L. Darken, Trans. Metall. Soc. A.I.M.E., **175**, p. 184, 1948.

[51Tur] D. Turnbull, in **Atom Movements**, A.S.M., Cleveland, OH, p. 129, 1951.

[52Bum] E.S. Bumps, H.D. Kessler and M. Hansen, Trans. A.I.M.E., **196**, p. 609, 1952.

[56Wag] C. Wagner, J. Electrochem. Soc., 103, p. 571, 1956

[57Kir] J.S. Kirkaldy, Can. J. Phys., **35**, p. 435, 1957.

[58Kir] J.S. Kirkaldy, Can. J. Phys., **36**, p. 899, 1958.

[58Kir2] J.S. Kirkaldy, Can. J. Phys., **36**, p. 907, 1958.

[58Kir3] J.S. Kirkaldy, Can. J. Phys., **36**, p. 917, 1958.

[61Enc] E. Ence and H. Margolin, Trans. Metall. Soc. A.I.M.E., **221**, p. 151, 1961.

[61Gol] A.J. Goldak and J.G. Parr, Trans. Metall. Soc. A.I.M.E., **221**, p. 639, 1961.

[62Kir] J.S. Kirkaldy, Can. J. Phys., **40**, p. 208, 1962.

[63Cla] J.B. Clark, Trans. Metall. Soc. A.I.M.E., **227**, p. 1250, 1963.

[63Kir] J.S. Kirkaldy and L.C. Brown, Can. Met. Quart., **3**, p. 89, 1963.

[64Pet] P.W. Petrasek and J.W. Weeton, Trans. Metall. Soc. A.I.M.E., **230**, p. 977, 1964.

[65Day] M.A. Dayananda and R.E. Grace, Trans. Metall. Soc. A.I.M.E., **233**, p. 1287, 1965.

[68Day] M.A. Dayananda, P.F. Kirsch and R.E. Grace, Trans. Metall. Soc. A.I.M.E., **242**, p. 855, 1968.

[68Sal] M.F. Salkind, **Introduction to Interfaces in Composites**, STP452, Amer. Soc. Test. Mater., Philadelphia, PA, 1968.

[68Sok] L.F. Sokiryanski et al., Mater. Nauch-Tekh Sovesheh, 1966 (Ed.: N.P. Szhin, Izd. "Nauka": Moscow, USSR), p. 201, 1968.

[69Sok] L.F. Sokirianskii, D.V. Ignatov and A.Ya. Shinyaev, Fiz. Metal. Metalloved., **28**, p. 287, 1969.

[70Ros] C.J. Rosa, Metall. Trans., **1**,p. 2617, 1970.

[70Tik] V.I. Tikhomirov and V.I. Dyachkov, Fiz. Metal. Metalloved., **30**, p. 111, 1970.

[71Zho] S.P. Zholobou and M.D. Malev, Zh. Tekh. Fiz., **41**, p. 627, 1971.

[72Car] P.T. Carlson, M.A. Dayananda and R.E. Grace, Metall. Trans., **3**, p. 819, 1972.

[72Pou] J. Pouliquen, S. Offret and J. de Fouquet, C.R. Acad. Sci., **274**, p. 1760, 1972.

[73Rap] R.A. Rapp, A. Ezis and G.J. Yurek, Metall. Trans., **4**, p. 1283, 1973.

[73Tre] R.E. Tressler, T.L. Moore and R.L. Crane, J. Mat. Sci., **8**, p. 151, 1973.

[73van] F.J.J. van Loo and G.D. Rieck, Acta Metall., **21**, p. 61, 1973.

[73van2] F.J.J. van Loo and G.D. Rieck, Acta Metall., **21**, p. 73, 1973.

[73Yur] G.J. Yurek, R.A. Rapp and J.P. Hirth, Metall. Trans., **4**, p. 1293, 1973.

[74Met] A.G. Metcalfe, **Interfaces in Metal Matrix Composites**, Academic Press, New York, 1974.

[76Moy] T.D. Moyer and M.A. Dayananda, Metall. Trans., **7**, p. 1035, 1976.

[77Sis] R.D. Sisson and M.A. Dayananda, Metall. Trans. A, **8A**, p. 1849, 1977.

[79Che] G.H. Cheng and M.A. Dayananda, Metall. Trans. A, **10A**, p. 1415, 1976.

[79Col] E.W. Collings, Metall. Trans. A, **10A**, p. 463, 1979.

[79Day] M.A. Dayananda and C.W. Kim, Metall. Trans. A, **10A**, p. 1333, 1979.

[79Sha] S.R. Shatynski, J.P. Hirth and R.A. Rapp, Metall. Trans. A, **10A**, p. 591, 1979.

[80Lah] M.A.J.Th. Laheij, F.J.J. van Loo and R. Metselaar, Oxid. Met., **14**, p. 207, 1980.

[83Day] M.A. Dayananda, Metall. Trans. A, **14A**, p. 1851, 1983.

[83Vos] P.J.C. Vosters, M.A.J.Th. Laheij, F.J.J. van Loo and R. Metselaar, Oxid. Met., **20**, p. 147, 1983.

[84van] J.A. van Beck, P.M.T. de Kok and F.J.J. van Loo, Oxid. Met. **22**, p. 147, 1983.

[85Day] M.A. Dayananda, **Diffusion in Solids: Recent Developments** (Eds.: M.A. Dayananda and G.E. Murch), Metall. Soc. Inc., Warrendale, PA 15086, p. 195, 1985.

[85Hir] K. Hirano and Y. Iijima, **Diffusion in Solids: Recent Developments** (Eds.: M.A. Dayananda and G.E. Murch), Metall. Soc. Inc., Warrendale, PA 15086, p. 141, 1985.

[85Wri] H.A. Wriedt, Bul. Alloy Phase Diagrams, **6**, p. 548, 1985.

[86Mur] J.L. Murray, **Binary Alloy Phase Diagrams** (Eds.: T.B. Massalski, J.L. Murray, L.H. Bennett and H. Baker), **1**, A.S.M., p. 175, 1986.

[87Kir] J.S. Kirkaldy and D.J. Young, **Diffusion in the Condensed State**, The Inst. of Metals, London, 1987.

[87Mur] J.L. Murray and H.A. Wriedt, Bul. Alloy Phase Diagrams, **8**, p. 148, 1987.

[87Pie] B. Pieraggi, Oxd. Met., **27**, p. 177, 1987.

[87Val] J.J. Valencia, C. McCullough, C.G. Levi and R. Mehrabian, Scripta Metall. Mater., **21**, p. 1341, 1987.

[88Rem] F. Remy, O. Monnereau and A. Casalot, J. Solid State Chem., **76**, p. 167, 1988.

[89Day] M.A. Dayananda, Mat. Sci. Eng., **A121**, p. 351, 1989.

[89Hua] S.C. Huang and P.A. Siemers, Metall. Trans. A, **20A**, p. 1899, 1989.

[89Lin] J.C. Lin, K.J. Schulz, K.C. Hsieh and Y.A. Chang, J. Electrochem. Soc., **136**, p. 3006, 1989.

[90DeK] J.A. DeKock, Y.A. Chang, M.X. Zhang and O.Y. Chen, **Interfaces in Composites** (Eds.: C.G. Patano and E.J.H. Chen), M.R.S. Proc., 170, p. 173, 1990.

[90Sch] K.J. Schulz, X.Y. Zheng, J.C. Lin and Y.A. Chang, J. Electr. Mat., **19**, p. 581, 1990.

[91Jan] C.H. Jan, D. Swenson, X.Y. Zheng, J.C. Lin and Y.A. Chang, Acta Metall. Mater., **39**, p. 303, 1991.

[92Glo] E. Glover, Dept. Geology, Univ. Wisconsin-Madison, unpublished work.

[92Kat] U.R. Kattner, J.C. Lin and Y.A. Chang, Metall. Trans. A, **23A**, p. 2081, 1992.

[92Kaw] T. Kawabata, T. Abumiya and O. Izumi, Acta Metall. Mater., 40, p. 2557, 1992.

[92Li] X.L. Li, R. Hillel, F. Teysandier, S. Choi and F.J.J. van Loo, Acta Metall. Mater., **40**, p. 3149, 1992.

[92Zha] M.X. Zhang, K.C. Hsieh, J. DeKock and Y.A. Chang, Scripta Metall. Mater., **27**, p. 1361, 1992.

[92Zha2] M.X. Zhang, K.C. Hsieh and Y.A. Chang, **Intermetallic Matrix Composites II** (Eds.: D.B. Miracle, D.L. Anton and J.A. Graves), M.R.S. Symp. Proc., **273**,p. 103, 1992.

[93Meh] H. Mehrer, W. Sprengel and M. Denkinger, **Diffusion in Ordered Alloys** (Eds.: B. Fultz, R.W. Cahn and D. Gupta), Minerals, Metals and Materials Soc., Warrendale, PA, p. 51, 1993.

[94Cha] Y.A. Chang, R. Kieschke, J. DeKock and M.X. Zhang, **Control of Interfaces in Metal Matrix Composites** (Eds.: R.Y. Lin and S.G. Fishman), T.M.S. Symp. Proc., p. 3, 1994.

[94Hug] A. Huguet and A. Menand, Appl. Surf. Sci., **76/77**, p. 191, 1994.